
Editorial Office of *Earth's Cryosphere (Kriosfera Zemli)*
Institute of Geography, Russian Academy of Sciences
37 Vavilov str., office 22, Moscow, 117312, Russia
Editorial staff: *N.V. Arutyunyan*, *N.G. Belova, O.M. Lisitsyna, G.E. Oblogov*
Phone: 8(985) 957-10-01, e-mail: kriozem@gmail.com
Editor of the English translation: *D.E. Konyushkov*

Journal promoted by
Russian Academy of Sciences, Siberian Branch, Novosibirsk
Earth's Cryosphere Institute, Tyumen Scientific Centre SB RAS, Tyumen
Melnikov Permafrost Institute, SB RAS, Yakutsk

Editorial Manager *M.A. Trashkeeva*
Designed by *N.F. Suranova*
Typeset by *N.M. Raizvikh*

RUSSIAN ACADEMY OF SCIENCES
SIBERIAN BRANCH
EARTH'S CRYOSPHERE INSTITUTE, TYUMEN SCIENTIFIC CENTRE
MELNIKOV PERMAFROST INSTITUTE

EARTH'S CRYOSPHERE
SCIENTIFIC JOURNAL

Founded in January 1997	6 issues per year	Vol. XXVI, No. 2	March–April 2022

CONTENTS

EARTH'S CRYOSPHERE
SCIENTIFIC JOURNAL

Earth's Cryosphere, 2022, vol. XXVI, No. 2, pp. 3–19

FUNDAMENTAL ISSUES OF EARTH'S CRYOSPHERE

CLIMATE, SEA LEVEL AND GLACIATION CHANGES IN THE MARGINAL ZONE OF ANTARCTICA DURING THE LAST 50 000 YEARS

S.R. Verkulich

Arctic and Antarctic Research Institute,
Beringa str. 38, St. Petersburg, 199397 Russia; verkulich@mail.ru

The article integrates the results of half a century studies of Late Pleistocene–Holocene changes in climate, sea level, and glaciation in the marginal zone of Antarctica in order to identify the chronology, parameters, and mechanisms of these changes under the influence of global, regional, and local factors. During the interstadial (MIS 3), the natural conditions here resembled modern ones, and the sea level in some areas exceeded modern marks. The development of glaciation of the marginal zone from about 26 000 years BP went on when the temperature fell and the sea level dropped by 30–50 m. The growth of glaciation on the shelf outpaced the growth of ice on the outskirts of the continent leading to a moisture deficit in the interior regions. During the LGM, there was a thin (less than 300 m) glaciation of coastal and mountainous land areas, and a thick (more than 1000 m) glaciation on the shelf. Deglaciation of the marginal zone began about 17 000 years BP due to rising sea level and global warming. Holocene climate changes in most areas had a general trend: warming in the early Holocene to about 8000 years BP and 4000–2000 years BP, cooling 2000–1500 years BP, but also had local differences. The relative sea level rose in the regions from the Early Holocene to 8000–6000 years BP; then it fell with a decrease in speed or even with a possible rise about 2500–1300 years BP. Local differences in the amplitudes and direction of sea level changes were determined by local tectonics and dynamics of deglaciation. Deglaciation rates were high from the Early Holocene to about 7500 years BP due to warming and marine transgression and then decreased. The advance of outlet and shelf glaciers 6500 and 4500 years BP was associated with a decrease in sea level and cooling. In the period 4000–1000 years BP, outlet and shelf glaciers could also respond to changes in sea level, and ice domes expanded according to the "warming – increasing humidity – increasing snow and ice accumulation" pattern. During the Little Ice Age, moraines were created in some areas indicating a slight increase in glaciers due to cooling.

Keywords: *marginal zone of Antarctica, climate, sea level, glaciation, interstadial, last glacial maximum, Holocene, relief, Quaternary deposits, paleogeographic reconstruction*

INTRODUCTION

Marginal zone of Antarctica extends from the coast to 200–300 km inland and includes shelf and outlet glaciers and nearby islands. It differs from the glacial region within the continent by a significant influence of cyclonic activity and adjacent marine areas and, in general, by a warmer, wetter, and windy climate with increased accumulation of snow. In this zone, large irregularities of the bedrock and sea level largely determine the diversity of glaciers, borders of the continent, and presence of ice-free land areas. The mass exchange of Antarctic glaciation is the most dynamic here: ice losses account for almost 98 % of the total annual ice loss due to melt runoff, wind drift, melting at the bottom of shelf glaciers, and iceberg chipping [*Kotlyakov et al., 2003*]. Under the mutual influence of the components of the atmosphere–ocean–glacier system, the marginal zone has experienced the most rapid and large-scale restructuring of natural environments over the last 50 000 years following global climate changes, glaciations, and sea level changes. In turn, these reconstructions were important for the evolution of the Antarctic glaciation as a whole, and therefore for the global climate and the balance of water in the World Ocean.

Transformations of the marginal zone are baked in the relief and sediments of the ice-free territories (Fig. 1) – Antarctic oases [*Sokratova, 2007*]. The slope of the ice sheet is broken through by mountain oases with mean annual air temperatures (MAAT) below –20 °C. Mountain-valley oases stretch from the glacial slope to the coast. These oases are dry and windy; the MAAT is still about –20 °C, but summer temperatures in the valleys reach –1 °C. The land and sea bays of low-lying onshore oases are separated from the ocean by shelf glaciers and are bordered from the other side continental ice sheet and outlet glaciers. The MAAT in them is about –11 °C, and summer soil temperatures may be above 15 °C, air humidity is 50–55 %, and annual precipitation is less than 200 mm. The low-lying coastal oases are only partially bordered by glaciers, and the MAAT in them is about –10 °C; in the summer, mean air temperatures are up to 1 °C (often. above 10 °C); air humidity is about 60 %, and annual precipitation is 200–

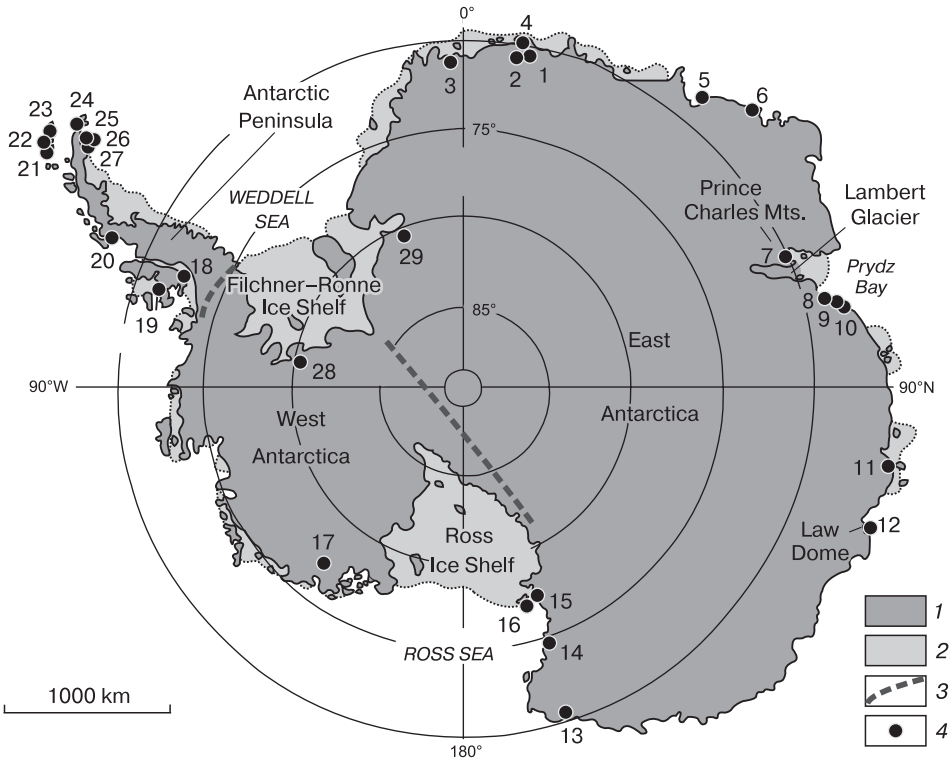

Fig. 1. Location of considered Antarctica objects.

(*1*) Ice sheets and domes, (*2*) ice shelves, (*3*) conventional boundaries between the main parts of glaciation, and (*4*) areas of the study of relief and sediments (1 – Untersee Oasis, 2 – Inzel Mountains, 3 – Robertskollen nunataks, 4 – Schirmacher Oasis, 5 – Soya Coast, 6 – Thala Hills, 7 – Amery Oasis, 8 – Larsemann Hills, 9 – Reuer Islands, 10 – Vestfold Oasis, 11 – Bunger Oasis, 12 – Windmill Islands, 13 – Little Rocks Area, 14 – Coast of Terra Nova Bay, 15 – Dry Valleys of Victoria Land, 16 – McMurdo Bay, 17 – Ridge Ford, 18 – George IV Ice Shelf, 19 – Alexander Island, 20 – Muller Ice Shelf, 21 – Livingston Island, 22 – Greenwich Island, 23 – King George Island, 24 – North of the Antarctic Peninsula, 25 – Beak Island, 26 – Vega Island, 27 – James Ross Island, 28 – Ellsworth Mountains; and 29 – Shackleton Ridge.

250 mm. In the Antarctic Peninsula, there are territories with maritime climate. In the west of the peninsula and nearby islands, the MAAT is about –3 °C; mean summer air temperatures are about 2 °C; air humidity is above 80 %, and annual precipitation reaches 600 mm on ice-free areas and is up to 1500 mm on glaciers. To the east of the ridges of the peninsula, which prevent western atmospheric transfer, the MAAT is –9 °C; summer temperatures are hardly above 0 °C, and annual precipitation is only about 150 mm.

Antarctic oases have been studied by paleogeographers for more than half a century. The accumulated data have been generalized for some parts or for the marginal zone as a whole. The issues of the Late Pleistocene–Holocene development of glaciation [*Stuiver et al., 1981; Ingólfsson et al., 1998; Anderson et al., 2002; Verkulich, 2009, 2010; Hodgson et al., 2014*], the relationships between climate changes and glaciers [*Hjort et al., 2003; Verleyen et al., 2011*], changes in sea level, and the state of the offshore zone and glaciers [*Berkman et al., 1998*] have been considered. As a rule, one or two of the main components of changes (climate, sea, glaciation) have been analyzed in these works for the period limited to the last glacial maximum (LGM) or Holocene. Russian research data are often missing in foreign publications.

The presented review includes the results of foreign and Russian paleogeographic studies in most of the ice-free Antarctic oases. In addition to the most complete presentation of data, refinement and updating of local reconstructions, this review aims to identify the course of changes in the natural environment of the marginal zone over the last 50 000 years as a whole and to determine the mechanisms and parameters of the interaction of climate, sea level, and glaciation under the influence of global, regional, and local factors.

DATA AND THEIR PALEOGEOGRAPHIC SIGNIFICANCE

Paleogeographic information on the marginal land area of Antarctica is mainly derived from the study of the relief and sediments of glacial, waterglacial, marine, lake, and ornithogenic geneses.

Evidences of glacial activity (U-shaped valleys, glacial hatching, moraines, etc.) can be found everywhere along the Antarctic periphery. Their location, morphology, and composition provide information about the extent, parameters, and stages of evolution of the glaciers. The correctness of data interpretation depends on the correctness of temporal estimates of glacial formations. Estimates of the age of moraines based on their morphology, the presence of an ice core, weathering stage, and vegetation characteristics are relative [*Adamson and Pickard, 1986; Borman and Fritzsche, 1995*]. In recent years, estimates based on measuring ^{3}He, ^{10}Be, ^{21}Ne, and ^{26}Al in stone surfaces have appeared [*Stone et al., 2003; Nicholls et al., 2019*]. Sometimes the moraines contain organic matter, the age of which indicates the time of the expansion of glaciers [*Adamson and Colhoun, 1992; Hjort et al., 2001*].

Water-glacial landforms and sediments (glaciofluvial terraces, deltas, standing water levels, and others) usually characterize the degradation of glaciers. However, in the Dry Valleys of Victoria Land, the levels of glacial lakes indicates the extent of glaciation during the LGM [*Clayton-Green et al., 1988; Hall et al., 2001*]. Organic remains in sediments allow us to date the course of deglaciation. Radiation dosimetry methods are also used for this purpose [*Gore et al., 2001; Mahesh et al., 2017*].

The occurrence, morphometry, and structure of marine formations; species composition and age of the flora and fauna in marine sediments correlate with fluctuations in relative sea level (RSL), climatic and ice conditions of sedimentation, and with changes in the boundaries of glaciers. Determination of the chronology of marine events is complicated by the need to correct radiocarbon data on marine Antarctic organics [*Gordon and Harkness, 1992*]. In addition, the wide range of depths and the diversity of habitats of marine organisms reduce the accuracy of the estimation of sea level at the time of their burial in sediments [*Ahn, 1994*].

Organic deposits accumulated in birds' nests for thousands of years are a specific data source in Antarctica [*Verkulich, 2008*]. Correlating the height and location of the nests of snow petrels (*Pagodroma nivea*) with the time of their settlement, spatial and temporal marks of the past glacial surface and the course of deglaciation processes can be reconstructed [*Ryan et al., 1992; Verkulich and Hiller, 1994*]. Adelie penguins (*Pygoscelis adeliae*) build nests above the storm-affected zone and near ice-exposed water areas, so the position and age of the nests and the intensity of nesting are indicative of sea level changes, periods of coast deglaciation, and climatic fluctuations [*Baroni and Orombelli, 1994a,b; Emslie and Woehler, 2005*]. However, paleogeographic reconstructions based on ornithogenic material are not quite reliable, because time intervals between the appearance of nesting conditions and the real nesting of the birds are unknown, and correction of radiocarbon dating is also required.

Bottom sediments of water basins represent an archive of the most detailed information about the development of the natural environment in the marginal zone of Antarctica. Lithology, granulometry, mineralogy, geochemistry of sediments inform about the regime and composition of waters, the flow of material from the catchment area, i.e., about the conditions and the course of deglaciation. The results of biogeochemical and isotopic analyses of organic matter reflect changes in the bioproductivity and regime of the reservoir, vegetation, and bird populations in the catchment area [*Hodgson et al., 2004; Wasiłowska et al., 2017*]. Diatom analysis informs about the past water exchange, chemistry, temperature, depth and ice regime of the reservoir, about the climatic conditions of sedimentation, about changes in RSL [*Whitehead and McMinn, 1997; McMinn, 2000; Verleyen et al., 2003; Roberts et al., 2004*]. Studies of mosses, shrimps, and rotifers in the sediments and pigment analysis provide data on the past dynamics and depth of the reservoir and on phototrophic communities [*Björck et al., 1991; Swadling et al., 2001; Verleyen et al., 2004*]. Dating of organic matter in sediments often provides a good chronology of paleoevents. However, paleolimnologists often meet difficulties in Antarctica because of poor knowledge of aquatic ecosystems, rarity of representative reservoirs, and the need to introduce various corrections to the results of dating.

The chronology of changes in the natural environment in the marginal zone of Antarctica is most often established using the radiocarbon (^{14}C) dating method. The correctness of dating depends on the use of various corrections of up to thousands of years [*Gordon and Harkness, 1992; Berkman and Forman, 1996*]. Most of the reconstructions considered by the author were carried out using such corrected dates. If uncorrected radiocarbon definitions were presented in original publications, the author introduced the necessary corrections in accordance with information about regional errors of radiocarbon dating and the conditions of formation and nature of the dated material.

RESULTS

The results obtained by the author and other researchers are analyzed with the aim to clarify and refine ideas about the conditions and the course of development of certain areas in the marginal zone of Antarctica.

In the area of **the Untersee oasis** (Fig. 1), the conditions of the interstadial (MIS 3) and LGM were revealed when analyzing the nesting patterns of snow petrels. In nests at 900–1300 m asl, the age of organic matter was 32 600–26 800 BP and about 17 000 BP;

in three nests in **the Inzel Mountains**, the dates of 27 100–23 000, 31 180, and 36 200 BP were determined. This suggests that birds lived on the rocks before and during the LGM [*Hiller et al., 1995*]. A comparison of the time of settlement and the height of the studied nests shows that during the LGM, the ice surface in this area rose by 250–300 m. Deglaciation began around 17 000 years ago and accelerated in 13 000–9000 BP. By about 8000 BP, birds mastered heights of 700–1150 m asl, close to the modern limits of nesting. The retreat of the glacier in the Untersee oasis 12 000–9000 BP led to the appearance of Lake Untersee [*Schwab, 1998*]. The maximum number of nests in the Untersee oasis on the slopes of **the Robertskollen** and Inzel mountains was used by birds 4000–3000 BP, probably during the warming period [*Verkulich, 2008*]. Around 2000 BP, many nests were abandoned (cooling); during the last 1500 years, birds have been actively occupying new nests (warming?). A study of bottom sediments from Lake Untersee indicates that 9000–7000 years deglaciation of this area slowed down because of climate cooling. Later, lateral moraines were deposited on slopes near the lake at the heights below 700 m asl [*Bormann and Fritzsche, 1995; Schwab, 1998*]. Their settlement by birds began around 3200 BP, which means that the glaciers grew between 7000 and 4000 BP The second group of moraine deposits near the lake reflects the fluctuations of local glaciers by tens of meters in the last hundreds of years.

In **the Schirmacher oasis** ^{14}C dating and diatom analysis of cores of frozen rocks and bottom sediments of lakes showed the presence of shallow freshwater reservoirs during MIS 3 under conditions resembling modern ones [*Verkulich et al., 2012a*]. During the LGM period, the oasis was covered by a glacier of 100–150 m in thickness [*Bormann and Fritzsche, 1995*], and even thinner over lake basins [*Mahesh et al., 2017*]. Glacial masses of the oasis on the edge of its northern steep slope met with glaciation of the shelf with a thickness of about 600 m, i.e., glacial bodies of different thicknesses developed in the oasis and on the shelf [*Verkulich et al., 2011*]. Deglaciation of the oasis began around 9000 BP [*Mahesh et al., 2017*]. Holocene conditions are reconstructed from data on the relief and lake sediments [*Bormann and Fritzsche, 1995; Schwab, 1998; Verkulich et al., 2011, 2012a*]. In addition to glacial forms, the levels of standing water–markers of the stages of development of the local lake system–can be traced in the relief. Since the beginning of the Holocene, ice melting has led to the formation of huge glacial lakes. The rapid decline of the glacial surface on the shelf led to a rapid runoff of waters from the oasis about 7000 BP, after which disjointed glaciers and large lakes remained on a larger part of the oasis. Between 7000 and 4000 BP, there was a slow melting of residual glaciers against the background of relative cooling. The warming of 4000–2000 BP led to a reduction in the area of local glaciers, the volume of lakes, and general drying of the territory. The interruption of this trend is indicated by the ridges of moraines on the edge of the glacier sheet. Their formation probably coincides with a decrease in the content of diatoms in lakes 2000–1000 and 400–150 BP.

The Soya Coast area (Lützow-Holm Bay) includes Ongul Island and peninsulas bordering a glacial slope or outlet glaciers lying in valleys extending into the bay and having a depth of about 500 m. On the Ongul Islands and the north of the Langhovde Peninsula, traces of exaration are rare; rocks are strongly weathered. There are marine deposits aged 46 000–23 000 BP. To the south, Glacial landforms are numerous, and rock weathering is weaker. Such differences may be indicative of the absence of LGM glaciation in the north of the area [*Hirakawa and Sawagaki, 1998; Miura et al., 1998a,b*], but this conclusion casts doubt. The top of ancient marine sediments is crumpled and transformed by meltwater – traces of glacier degradation. It there were no glaciation, how should we explain the compensatory elevation of the land by 20–25 m in the Holocene? It is more logical to assume that during the LGM there were both low-thick (100–200 m) glacial domes on the northern parts of the land with preserved ancient sediments under them and active glaciers of 400–500 m in thickness on the shelf. Glaciomarine sediments on the shelf have a thickness of up to 1.5 m, and the age of the oldest organic matter in them is about 14 000 BP [*Moriwaki and Yoshida, 1983*]. This confirms the erosion of the shelf by the glaciers of the LGM and indicates the beginning of deglaciation of the area around 14 000 BP. Hundreds of age determinations of fossil organic matter in sediments on the shores [*Hayashi and Yoshida, 1994; Hirakawa and Sawagaki, 1998*] allow us to construct an RSL curve: rise up to 6000–4500 BP and subsequent decline (fast 4500–3500, 2500–1500 BP, and slow 3500–2500 and about 1500 BP). A peak in dating of shells at 4000–3000 BP may mean an improvement in ice conditions, i.e., warming [*Verkulich et al., 2007*]. The warming around 4500–3500 BP is also indicated by the appearance of deltaic sediments, a signal of increased meltwater runoff [*Miura et al., 1998b*]. There are limited data on deglaciation of this area. Probably, the glaciers melted faster during the warming phase 4000–3000 BP. On the shore of the Rocky Peninsula, a push moraine of up to 10 m in height records the advance of the outlet glacier by about 200–300 m after 2000 BP with its following retreat [*Hayashi and Yoshida, 1994*].

In **the Tala Hills oasis (Enderby Land)**, studies of lake sediments [*Dolgikh et al., 2017*] indicated deglaciation no later than 11 000 BP (moraine at the base of sediments). The middle and upper layers of sediments have accumulated over the last 6500 years under harsh conditions for the development of dia-

tom flora. Favorable (warmer?) conditions for the mass development of several types of diatoms existed in the reservoir about 4000–2000 BP, when the rate of sedimentation increased.

In the region of the **Prince Charles Mountains–Lambert Glacier–Prudes Bay**, the overlap of the edges of the LGM glaciers on the bottom of Prudes Bay is recorded by linear ridges [*Leitchenkov et al., 1994*]. Massive glacial deposits were found between the ridges and the shore; the continental ice did not move into the deep part of the shelf, and sedimentation took place under the glacier shelf. Judging by the age of the sediments, the closing of part of the bay by glaciers occurred after 20 000 BP, and deglaciation began earlier than 13 800 BP [*Domack et al., 1998*]. On the slopes of the Prince Charles Mountains in the middle reaches of the Lambert outlet Glacier, moraines reflect the rise of the glacier surface by 100–120 m [*Mabin, 1991*]. In the interior of the continent, LGM moraines are developed on the slopes of nunataks up to a height of 20 m above the ice surface. The maximum increase in ice on the Lambert outlet glacier is associated with a shift to the north of the line of its overlap with the bottom of the enclosing valley [*Adamson et al., 1997*].

The Amery Oasis lies at heights of about 200 m asl at the contact of the Lambert Glacier and the shelf glacier. The absence of glacial exaration features attests to the absence of the LGM glaciation in the oasis [*Adamson et al., 1997*]. However, moraine lies at the base of Terrasovoe Lake, and the height of the moraine ridge near the lake indicates an increase in the thickness of the nearby glacier by 150 m during the LGM. The rest of the territory probably had a snow-ice cover [*Wagner et al., 2004*]. Based on the results of studying lake sediments, glaciers had already left the lake's catchment by 12 400 BP, i.e., deglaciation started even earlier. The period of 12 400–10 200 BP was marked by the cold climate, harsh ice regime of the lake, and slow deglaciation. An increase in the content of biogenic material and diatoms in sediments aged 10 200–8600 BP indicates the beginning of warming. Further, up to 6700 BP, a diatom complex developed under warm conditions, and local glaciers decreased. Cooling and, probably, the expansion of glaciers are recorded in sediments aged 6700–3600 BP. During the last 3600 years, relatively warm (3200–2400 and 1600–900 BP) and cold (2000 and 600 BP) periods are distinguished [*Wagner et al., 2004*].

The Larsemann Hills Oasis is a group of low islands and peninsulas bordered by the glacial sheet slope from the south and by an outlet glacier from the southeast. The age of organic matter at the base of bottom sediments sampled in several lakes of the oasis corresponds to MIS 3 and LGM stages. Marine sediments of MIS 3 accumulated in Lake Kirisjes when sea level rose to 8 m asl (modern topography) [*Hodgson et al., 2001, 2009*] and in Mochou Lake, up to 10 m [*Gao et al., 2020*]. The study of frozen rock cores to a depth of 11 m showed that sea water during MIS 3 reached even modern levels of about 30 m asl [*Demidov et al., 2013*]. Studies of lake sediments and glacial hatching indicated that the LGM glaciation began later than 22 000 BP and covered a larger part of the oasis; the thickness of the glaciers reached the first hundreds of meters, and their extension to the shelf was small. On the Broknes Peninsula, glaciers moved through valleys; outlet glacier affected its eastern coast. Two lake depressions in the center were covered with snow and ice fields. The variety of glacier types was determined by the local relief conditions and the diverting role of the Dålk outlet glacier [*Hodgson et al., 2001, 2005; Verleyen et al., 2005*]. The beginning of deglaciation of the oasis marks the age of lake sediments in Kirisjes Pond – 13 600 BP [*Verleyen et al., 2005*]. Changes in the accumulation of sediments under marine, freshwater, and transitional conditions allowed us to recreate the curve of RSL changes: a rise in the early Holocene until about 7000 BP; then, a drop interrupted by a small rise in 2000–1500 BP [*Verleyen et al., 2004, 2005*]. Lake sediments also provided paleoclimatic information [*Verleyen et al., 2004*]. About 13 500–11 500 BP, Kirisjes Pond was covered with ice under cold conditions. In 11 500–9500 BP, due to warming, the flow of meltwater increased, and Lake Stepped appeared. The accumulation of sediments in this lake took place under relatively cold conditions in 9500–7500 BP and under relatively warm conditions in 7500–5230 BP. In 5230–3000 BP, the climate was similar to the modern climate, except for some warming around 3800 BP. The warm conditions of 3000–2000 BP are indicated by sediments in Kirisjes Pond Pap Lagoons. Around 2000 BP, the warming was replaced by a short cooling. Diatoms in the sediments of Kirisjes Pond reflect the cooling of 760–690 and 280–140 BP. The rapid deglaciation of the oasis in the early Holocene was caused by climate warming and sea level rise [*Hodgson et al., 2005*]. Intensified ice melting under the impact of warming could take place around 6000, 4000, and 1500 BP There are no traces of glacial growth in the oasis in the Holocene, but a slowdown in deglaciation around 7500 and 3000 BC is not excluded [*Verleyen et al., 2005*].

In the area of **the Reuer Islands**, reconstructions are based on studies of bottom sediment cores from local bays [*Berg et al., 2010*]. The accumulation of material with organic residues took place about 45 000 BP at one point of core sampling and 10 000 BP at another point. The characteristics of the sediments attest to the marine non-freezing conditions in the area in MIS 3 (MIS 5?) confirming that the ice sheet during the LGM did not have a continuous distribution and depended on the topography of the shelf and land. Deglaciation of the area began about 11 200 BP and proceeded under conditions of

Early Holocene optimum until 8200 BP, when a colder stage began. Warm conditions were established in 5700–3500 BP. Then, sedimentation proceeded under colder conditions again [*Berg et al., 2010*].

The Vestfold Hills Oasis is bounded by the slope of the ice sheet on the east and by the outlet Sørsdal Glacier. Glacial hatching in two directions, the thick moraine cover in the center and west of the oasis, and moraine ridges in the center, west, and near the Sørsdal Glacier are indicative to the LGM glaciation, but the mechanism of its development is open to argument. Most of the hatches are in the east–west direction characterizing the past expansion of the glacial sheet, and the rest are associated with the Holocene onshore advance of the Sørsdal Glacier [*Adamson and Pickard, 1986*]. Other researchers considered the coincidence of the orientation of moraine ridges in the west and center of the oasis with the ridges near the Sørsdal Glacier as evidence of the extension of this glacier to the north and northwest of the oasis during the LGM [*Hirvas et al., 1993*]. The analysis of rock fragments and weathering features and data on fossil fauna in the moraines gave a new reconstruction [*Gore, 1997*]: (1) before the LGM, land areas existed in the center and in the west of the oasis, and sea bays occupied local depressions; (2) glacial sheet expanded during the LGM; (3) moraine ridges in the center of the oasis were created upon stops in the retreat of the glacial sheet; (4) rock hatching and moraine ridges near the Sørsdal Glacier mark its advance in the Late Holocene. The scenario suggested by the author of this article assumes the onshore expansion of the outlet Sørsdal Glacier that carried material from the bottom of the sea and from the weathered land surface at the beginning of the LGM. The glacial sheet carrying relatively little material and slightly eroding the surface in the eastern part of the oasis also expanded. These glaciers met in the center of the oasis and the material of future moraine ridges was concentrated at the meeting point. Then, the two glacial bodies merged: then the hatching of the western direction appeared at high levels of the oasis. The thickness of the ice could reach only 300 m [*Gore, 1997*].

The deglaciation of the oasis began 12 000–13 000 BP [*Fabel et al., 1997*], and its course was determined by changes in RSL and climate. About 7500–6500 BP, RSL reached a maximum (10–13 m asl) and then began to fall (with a slowdown in speed and even some rise in 3000–1500 BP) [*Zwartz et al., 1998*]. The oasis had relatively warm conditions in the Early Holocene, warming and humidity growth in 3500–2500 BP, cold and dry conditions in 2000–1800 BP, and then relatively cool conditions [*Fulford-Smith and Sikes, 1996; McMinn, 2000*]. By about 8000 BP, deglaciation occurred over 50 % of the oasis; in 8000–5000 BP, the retreat of the glaciers slowed down. It intensified again in the second half of the Holocene with a decrease in RSL and under relatively warm conditions. Moraines near the Sørsdal Glacier record its progress due to changes in sea level 3000–1500 BP and cooling around 2000 BP. Along the border of the glacier, ridges formed after 700 BP [*Adamson and Pickard, 1986*].

The Bunger Hills Oasis carries traces of glacial activity, but the activity of glaciers in the LGM is a matter of discussion. One of the opinions is that the oasis was covered by the sheet ice moving to the west and northwest and having a thickness of more than 500 m [*Adamson and Colhoun, 1992*]. The study of rock weathering and OSL dating of the sediments served as the basis for the conclusion about the presence of ice-free areas during the LGM period [*Gore et al., 2001*]. The dates, together with the errors of the method, fall into time intervals of about 40 000–19 000 BP and near the beginning of the Holocene. The values of ^{14}C dating of organic matter in the moraine base of bottom sediments of local lakes fall into the first interval [*Melles et al., 1994, 1997*]. There are no dates for the period 19 000–14 000 BP. Such facts indicate the presence of glacier-free territories in the area from MIS 3 to 19 000 BP and the short-term glaciation of the LGM. The variety of directions of glacial hatching contradicts the idea of the development of glaciation of the LGM only by the expansion of the glacier sheet, and the preservation of hatches is difficult to explain against the background of long-term weathering.

The thickest moraines in the west and northwest of the oasis, in the author's opinion, were formed when outlet glaciers moved to land and merged there with the glacial sheet with mass accumulation of moraine sediments in this area. Further, the movement of the ice cover depended on changes in the RSL and the subglacial relief, which created hatching in different directions. Glaciers on land were no thicker than 100 m in high areas and 300 m in depressions [*Verkulich, 2010*]; glaciers in the sea basins of the oasis had a thickness of more than 500 m [*Melles et al., 1997*]. Dating of organic sediments indicates the development biota in the reservoirs and the settlement of birds 13 550–9470 BP, the minimum time of the beginning of deglaciation [*Melles et al., 1994; Verkulich and Hiller, 1994*]. The climatic conditions of deglaciation were clarified by studying the bottom sediments in local reservoirs [*Kulbe et al., 2001; Verkulich, 2007; Berg at al., 2020*]. The RSL changes left traces on the coast up to the height of 10–11 m, as well as in the sediments of reservoirs [*Adamson and Colhoun, 1992; Verkulich et al., 2002*]; on this basis, the curve of RSL changes was constructed [*Poleshchuk and Verkulich, 2014*]. Already by 10 000–8000 BP, large areas of land and many lakes of the oasis were freed from glaciation, and oceanic waters penetrated into local bays [*Melles et al., 1997*]. With the cooling of 8000–5000 BP, the melting of glaciers on land slowed down, but due to the rise of sea level, seawater penetrated

even to the southeastern glacial margins of the oasis. From about 6000 BP, the RSL began to fall, which, against the background of cooling, led to the activation of outlet glaciers on the shores of the oasis and moraine accumulation along its western edge (6000–5000 BP). Warm conditions of 4000–2000 BP contributed to deglaciation, and by 2000 BP the boundaries of the oasis began to resemble modern ones. Then, against the background of deglaciation, the extension of the outlet Edisto glacier and the appearance of push moraine took place [*Adamson and Colhoun, 1992*] due to cooling around 2000 BP and fluctuations of the RSL [*Poleshchuk and Verkulich, 2014*].

The Windmill Islands area is bounded by the Law Dome from the north and east, and by outlet glaciers from the south. During the LGM, the northern islands were under the glacial dome, and the southern ones were eroded by outlet glaciers; the edges of the glaciers could extend into the sea for 7–15 km, the estimated ice thickness on the islands did not exceed 200 m; on the shelf, 300–400 m [*Goodwin, 1993*]. Information about the development of the area is contained in the sediments of local bays: at their base, there are organic-mineral sediments aged 46 000–26 000 BP, overlain by a moraine; above, there are glacial-marine sediments and Holocene mainly organic sediments [*Kirkup et al., 2002; Cremer et al., 2003*]. The accumulation of marine sediments in 10 500–4000 BP proceeded under relatively cold conditions; in 4000–1000 BP, conditions were generally warmer, although 2000–1700 BP the temperature began to decrease; conditions remained cold in the recent millennium [*Cremer et al., 2003*]. The RSL curve was reconstructed during the study of beaches and lake sediments: the rise in sea level up to 32 m by 6000 BP, then the decrease in sea level with a slowdown in 2500–1800 BP (in 1900–1800 BP, RSL could even rise a little) [*Goodwin, 1993; Roberts et al., 2004*]. The beginning of deglaciation in the area dates back to about 12 00 BP according to dating of organic matter in lakes and penguin rookeries [*Goodwin and Zwek, 2000*]. In the Early Holocene, the destruction of ice was facilitated by the rise of RSL, and relatively cold conditions did not prevent the development of lakes and bird nesting [*Emslie and Woehler, 2005*] until 7000 BP. With a maximum rise of RSL and cold climate of 7000–6000 BP, deglaciation slowed down. In 6000–4000 BP, the number of rookeries increased due to the beginning of the fall of the RSL, that is, the expansion of the land. The continuation of the fall of the RSL and the warming of the climate 4000–2000 BP led to a reduction in glaciation. However, at the same time, the Law Dome created moraines, because of the increased precipitation [*Goodwin, 1993*]. It was relatively cold in the area during the last 2000 years, but penguins have been actively inhabiting the islands [*Emslie and Woehler, 2005*].

In the Ross Sea–McMurdo Bay–Dry Valleys region of Victoria Land, data on LGM conditions are collected in marine basins, on the coast, in valleys, and in mountainous areas. In the Ross Sea, most of the shelf was covered by the ice sheet [*Karl, 1989; Anderson et al., 2014*]. About 20 000 BP, its boundary was found 100 km south of the edge of the continental shelf at depths of 300–500 m [*Licht et al., 1996*]. The ice sheet also closed the McMurdo Bay and entered the lower parts of the Dry Valleys in Victoria Land blocking them with ice of 200–300 m in height. From 26 000–23 000 BP, most of the valleys were free from cover glaciation; dammed lakes developed there [*Stuiver et al., 1981; Clayton-Green et al., 1988; Hall et al., 2001*]. In **the area of Terra Nova Bay**, the surface of glaciers in the mountains rose by tens of meters; in the middle parts of the valleys, by the first hundreds of meters; on the coast, by about 400 m (coastal ice strata were part of the Ross Ice Shelf). According to the dating of the shells in the moraines (37 500–25 300 BP), the glaciers that captured and moved them developed later than 25 000 BP [*Orombelli et al., 1990*]. On Ross Island near the eastern shores of the Ross Sea, the height of the ice surface reached 720 m, on the western continental margins of the Ross Sea, it was 800 to 950 m asl [*Anderson et al., 2014*]. Glaciers were somewhat thicker on **the Ford Ranges** at heights up to 950 m asl [*Stone et al., 2003*]. Data from the region confirm the presence of ice sheet on the shelf, coast, and in the mouths of mountain valleys from 25 000 BP with its maximum expansion 21 000–18 000 BP [*Stuiver et al., 1981; Clayton-Green et al., 1988; Hall et al., 2001; Anderson et al., 2002; Oberholzer et al., 2003; Stone et al., 2003*]. At the same time, the thickness of the ice sheet sharply decreased in the direction from the shelf to the continent, probably due to the interception of a significant part of the moisture of atmospheric masses by the ice shelf [*Orombelli et al., 1990*].

Deglaciation of the region began in 17 000–10 000 BP: in the Ross Sea, the retreat of the northern edge of the ice sheet began about 17 000 BP; degradation of glaciers blocking Dry Valleys dates back to 16 000–13 000 BP; penguins appeared on the shores 13 000–11 000 BP. Deglaciation in **the Little Rocks** Ford ranges started 11 000–10 000 BP [*Jordan and Wateren, 1993; Baroni and Orombelli, 1994a; Doran et al., 1994; Stone et al., 2003*]. The curve of Holocene changes in the RSL in the region is based on the study of coastal forms and penguin rookeries: sea water level reached 30–40 m around 7500 BP; then, the RSL rapidly decreased; in the last 3000 years. this process has slowed down [*Baroni and Orombelli, 1991, 1994a*]. The paleoclimate on the coast, as evidenced by the dynamics of penguin rookeries, had an optimum 4300–2900 BP; after 2900 BP there was an increase in the severity of ice conditions (cooling); in the recent millennium, the number of has increased

[*Baroni and Orombelli, 1994b*]. The study of lakes in Dry Valleys revealed the presence of warm conditions 3000–2000 BP, cold and dry conditions in the period from 2000 to 1200–1000 BP, and relatively warm and wet conditions in the recent millennium [*Smith and Friedman, 1993; Lyons et al., 1998*]. Dating of organic matter in sediments indicates rapid deglaciation of coastal areas up to 8000–7000 BP. By 7500 BP, outlet glaciers on the shores of the Terra Nova Bay retreated beyond their modern borders [*Baroni and Orombelli, 1994c; Hall et al., 2001*]. Between 5000 and 1500 BP, the edges of the glaciers moved back blocking part of the beaches; in 1200–500 BP, glaciers were smaller than modern ones, and then reached their current boundaries [*Baroni and Orombelli, 1994c*].

West Antarctica, including the **Weddell Sea, the Antarctic Peninsula,** and islands is the region with a lot of ice-free land areas. The natural conditions during MIS 3 were studied in detail on the Fildes Peninsula **of King George Island**, where marine sediments with shells, algae, bone remains, and diatoms date back to 50 000–19 000 BP. During MIS 3, the peninsula was under seawater to the level of 40 m asl and turned into an archipelago. Seawater was no colder than at present. The LGM glaciation was relatively thin, so that loose deposits of MIS 3 were preserved [*Verkulich et al., 2013, 2015*]. Shells of about 30 000 years old were found in the moraine on the coast of **Alexander Island.** They can be considered the remains of MIS 3 in the surroundings of the Antarctic Peninsula. Shells of about 34 000 years old were found in glacial deposits of **Vega and James Ross Islands** [*Clapperton and Sugden, 1982; Ingólfsson et al., 1992*].

The study of hatching and erratic boulders in the areas framing the **Filchner** and **Ronne** ice shelves indicated that the ice surface in coastal areas during the LGM was up to 400–650 m asl; on the slopes of the mountains facing the Weddell Sea, these features of glaciation can be found at heights of up 1000–1900 m asl; glaciers leaned on the bottom of the Weddell Sea at a distance of up to 800 km. The main growth of glacial masses was on the shelf [*Carrara, 1981; Waitt, 1983; Denton et al., 1992*]. Geological and geophysical studies have confirmed the development of a thick shelf ice on the western shelf of Weddell Sea, possibly, after 21 000 BP [*Elverhøi, 1981*]. The use of cosmogenic nuclides has clarified the growth of glaciers on the Weddell Sea coast; they reached the thickness of 310–650 m in the east (in the area of **Shackleton Ridge.** 800 m in the area of the **Ellsworth** mountains; at least 385 m on the western mountain margins of the Ronne Ice Shelf [*Nichols et al., 2019*]. During the LGM, glaciers of the Antarctic Peninsula and the adjacent shelf ice began to degrade approximately 18 000 BP. Deglaciation of the areas was asynchronous and depended on the subglacial topography. By the beginning of the Holocene the ice sheet approached the current configuration [*Cofaigh et al., 2014*].

The age of organic matter in sediments indicates the collapse of ice shelf in the west of the Weddell Sea before 11 270 BP [*Anderson et al., 2002*]. On the islands **of Vega, James Ross,** and **Beak**, deglaciation began 11 000–9500 BP [*Zale and Karlen, 1989; Ingólfsson et al., 1992; Sterken et al., 2012*]. On King George Island, it began at least 11 500 BP; by 9300 BP, glacier on the Fildes Peninsula had shrunk to its present size [*Verkulich et al., 2012b*]. The climate on the island was relatively warm from the beginning of the Holocene to 5300, 4000–2300 and 1400–600 BP, and cooling occurred 5300–4000, 2000–1400 BP and during the Little Ice Age (LIA) [*Verkulich et al., 2012a,b*]. The RSL was up to 19–20 m asl about 8000 BP, and then decreased (with a slowdown in 5000–4000 and 2500–1600 BP, and possibly with a slight rise 2000–1300 BP) [*Poleshchuk et al., 2016*]. On Beak Island , the study of lake sediments revealed relatively warm conditions from the Early Holocene to 6407 cal BP, then cooling to 3169 cal BP, a sharp warming of 3169–2120 cal BP, cooling 2120–543 cal BP, and then warming [*Sterken et al., 2012*]. The RSL on Beak Island after rise to a level of 15 m asl about 8000 cal BP began to decrease [*Roberts et al., 2011*].

On **Livingston Island** and the north of the Antarctic Peninsula, reconstructions of climate change and RSL are sketchy, so we will present them in the context of regional deglaciation. Until about 7000–6000 BP, the destruction of glaciers proceeded rapidly due to the rise of RSL and warming [*Zale and Karlen, 1989; Ingólfsson et al., 1992*]. The subsequent fall of the RSL and the beginning of the cold phase slowed down deglaciation, and even caused the extension of outlet and shelf glaciers that left traces on the shores of Alexander and James Ross Islands [*Ingólfsson et al., 1992; Hjort et al., 2001*]. Warming from about 4000 to 2500 BP against the background of a decrease in RSL and an increase in the area of the islands contributed to the deglaciation. However, on the James Ross Islands, the rise in temperature and humidity led to the growth of glaciers about 3000 BP [*Bjorck et al., 1996*]. Between 2000 and 1000 BP the climate of the area was, in general, colder than the modern one; this contributed to the growth of the glacier on the Fildes Peninsula [*Verkulich et al., 2012a,b*]. In the last millennium, climatic fluctuations have been frequent. The most notable was the LIA event, which caused the growth of glaciers and the extension of the edges of ice shelf and outlet glaciers [*Zale and Karlen, 1989; Domack et al., 1995; Hall, 2007*].

DISCUSSION

A comparison of reconstructions of the recent history of glaciation and deglaciation in coastal areas of Antarctica attests to some common and individual

features in the changes of climate, sea level. and glaciation–deglaciation and permits the identification of correlation and dependence of these changes on global and local factors.

Conditions of MIS 3 interstadial in the marginal zone of Antarctica

The natural conditions of MIS 3 interstadial have been reconstructed only at a few points, but their location suggests the existence of habitable land and sea spaces along the Antarctica periphery at that time. The material with the age of MIS 3 *in situ*, as well as included in the LGM sediments, confirms the presence of seawater in MIS 3 in the areas of the Soya Coast, Larsemann Hills, Rauer Islands, Bunger Oasis, Windmill Islands, Ross Sea, George IV ice shelf, Antarctic Peninsula, and its surroundings. The location of the findings indicates that the sea/glacier boundaries during MIS 3 were close to modern ones. This is confirmed by the nesting of snow petrels in the Untersee area and Inzel mountains. Feeding of birds could only be provided if the line of open ocean waters did not shift significantly to the north in comparison with the current position of the edge of the shelf ice. Studies of lake sediments, permafrost, and cosmogenic nuclides in the Schirmacher, oases, Larsemann Hills, and Bunger oases indicate the absence of a cover glaciation during MIS 3 and the presence of organic life in the lakes. For example, in the Schirmacher oasis, local conditions of the sediment accumulation in lake basins during MIS 3 were no colder than those at present [*Verkulich et al., 2012a*].

Detailed information was provided by studies of MIS 3 sediments s in situ. Paleolimnological data revealed the presence of freshwater reservoirs in the Larsemann Hills (in warm conditions) 53 000–47 000 BP, deterioration of biomass accumulation conditions by 38 000 BP, and ingression of seawater into lakes in 38 000–26 650 BP (shallow coastal zone conditions), when the RSL reached a height of about 10–12 m [*Hodgson et al., 2009; Gao et al., 2020*]. The study of cores of frozen rock from the Larsemann Hills showed that the rise of RSL in MIS 3 could reach 30 m [*Demidov et al., 2013*]. Approximately the same time interval of the MIS 3 transgression was established for sections of the Soya Coast with a rise of RSL up to 20 m [*Miura et al., 1998a*]. On King George Island, the rise of RSL in MIS 3 could reach 40 m, and most of the studied sections of marine sediments with rich flora and fauna were formed 30 000–20 000 BP [*Verkulich et al., 2013, 2015*]. The explanation for this height of the RSL at a time when the global eustatic level was about 60–70 m below modern sea level [*Lambeck et al., 2002*] is considered to be a significant increase in ice masses in the regions, which led to the deflection of the Earth's crust and, accordingly, the rise of the RSL [*Hodgson et al., 2009; Gao et al., 2020*]. However, it is quite difficult to imagine a picture of a simultaneous significant increase in glaciation of the margins of the continent and the presence of marine waters here in wider than modern borders. Such a situation, for example, is impossible for King George Island, which reduced its area and turned into an archipelago during MIS 3 [*Verkulich et al., 2013, 2015*]. The author believes that changes in the RSL depended to a large extent on regional tectonic processes that are not directly related to changes in glacial load. The considered regions are located in fault zones and other areas of tectonic activity and characterized by extreme fragmentation of the earth's surface, which indicates the probability of intense block tectonic movements.

The last glacial maximum

The period of LGM in the marginal zone of Antarctica can be estimated from minimum values of the most ancient dates of organic deposits (Fig. 2). They indicate that glaciers did not cover many mountain, coastal, island and sea areas 26 000–19 000 BP.

In low-lying areas of the coast and nearby islands, the glaciation of the LGM was relatively thin (ice thickness of 100–300 m); in the Schirmacher oasis, Larsemann Hills, Bunger Hills, and Dry Valleys of Victoria Land, there was no continuous glacial cover; part of the land in these oases was blocked only by snow and ice fields. An increase in the height of the ice cover in many areas of East Antarctica (the Untersee and Amery oases, slopes of the Prince Charles Mountains and the Terra-Nova Gulf) was less than 200–300 m. At the same time, the thickness of shelf ice during that period exceeded 500 m and even 1000 m in many areas. Deep depressions were occupied by outlet glaciers, often coming to land (the Vestfold Hills and Bunger Hills oases, Windmill Is-

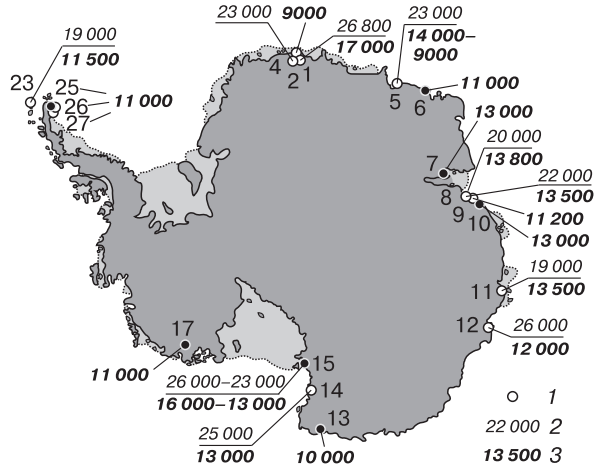

Fig. 2. Areas and time of recorded events of MIS 3 and LGM.

1 – Study areas of MIS 3 event, *2* – minimum dates of sediments before the LGM, years ago, *3* – maximum dates for postglacial events, years ago. Numbers of study sites are given in Fig. 1.

lands), or diverting continental masses of ice from land (Larsemann Hills, Ongul Island near the Soya Coast). Other areas of the shelf were blocked by thick glacial masses that made up the main part of the glaciation of the Ross and Weddell Seas, Prudes Bay, and other seas.

These features of glaciation during the LGM suggest a scenario for its development. The initiation of glaciation under cold conditions and sea level lowered by tens of meters [*Clark and Mix, 2002; Lambeck et al., 2002; Peltier, 2002*] created prerequisites for the rapid accumulation of ice masses on the drained shelf, where the line of glaciers' leaning on the bottom was shifted northward, and the water layer under the shelf glaciers was reduced. In these areas, climate cooling led to a rapid lowering of the snow line and an increase in snow accumulation in the presence of humidifying sea areas nearby. As a result, glaciers on islands and drained areas (glaciation cores) grew rapidly on the shelf, shelf glaciers thickened and began to lean on the drained bottom of shallow-water areas due to a decrease in ice melting at the bottom and an increase in accumulation on the surface. The edges of the ice sheet and outlet glaciers moved toward the shelf. Under such conditions, glaciers on the coast and in the interior of Antarctica could receive sufficient moisture supply only at the beginning of the LGM, when there were areas of open water (a source of moisture) on the shelf, and summer melting slowed down. At the same time, the drop in sea level led to an increase in ice discharge by outlet glaciers following the downward shifting of the line of glaciers to the bottom of the shelf. The further closure of the shelf by ice the spread of the shelf ice e cover to the north distanced the continental areas from the open ocean masses so strongly, that moisture shortage to feed the glaciers was established in most areas of the Antarctica. This scenario was most typical for East Antarctica, especially in the vast areas of the shallow shelf and areas of development of the system of outlet glaciers.

In West Antarctica, on the modern borders of the Filchner and Ronne ice shelves with the nearby slopes, on the western continental slopes on the border with the Ross Sea, the rise of the ice surface during the LGM was great. Assuming the above scenario of the development of the LGM, the active increase in the thickness of shelf ice and the low position of the ice sheet in these areas (at present, 1000–1500 m asl) created a situation, when shelf ice prevented ice flow from the continent, and accumulation was active at border of the shelf and continental glaciations.

Post-glacial development of the marginal zone

The beginning of deglaciation is marked by the oldest dates of the organic matter in postglacial sediments, the time of the release of rocky surfaces from under the ice and the formation of water-glacial sediments (Fig. 2). The first evidence is associated with the destruction of shelf ice in 17 000–14 000 BP, when marine sediments accumulated in bays near the Coast of Soya, in Prydz Bay, in gulfs of the Bunger Hills oasis, near the Windmill Islands, and in the McMurdo area. Snow petrels populated the Untersee oasis due to the shortening of the distance from the mountains to open ocean waters. Somewhat later (13 000–9000 BP), degradation of onshore glaciation in modern oases took place. The initial stage of deglaciation certainly depended on global changes in sea level and climate. By 14 000 BP, when the first sections of the shelf were freed from ice along Antarctica coast, sea level had already risen by 10–13 m (which is comparable with the contribution of the entire postglacial melting of Antarctic ice to sea level rise); in 12 000–10 000 BP, see level rose by 30 to 60 m [*Bentley, 1999*] causing widespread floating, disintegration, and rapid decline of glaciers. Evidences of deglaciation 16 000–14 000 BP are attributed to the period of air temperature rise recorded in ice cores. It was interrupted by a cooling of 14 000–12 500 BP (though temperatures remained higher than those during the LGM) followed by warming between 11 500 and 9000–8000 BP [*Masson et al., 2000; Jouzel et al., 2001*].

The curves ***of climate change*** in particular regions of Antarctica differ from one another in chronology and amplitude (Fig. 3), which is associated with problems of dating and time resolution of reconstructions. However, they reflect the dependence of these changes on global, regional, and local factors. The most reliable reconstructions indicate warming in the Early Holocene, up to about 8000 BP, which coincides with records in ice cores [*Masson et al., 2000*]. This is indicative of close relationship between local climate changes along Antarctic coasts and global processes: optimum of summer insolation in the Northern Hemisphere, warming of oceanic waters in the Southern Hemisphere, and changes in the atmospheric circulation [*Verleyen et al., 2003*].

The period of 8000–4000 BP was characterized by smoothing of climatic fluctuations and the proximity of climatic conditions to modern ones. According to data from ice cores, it has been warming since 6000 BP in the central regions of East Antarctica. However, on the margins of the continent, indications of a weak warming 7000–5000 BP were only found in the Larsemann Hills and Schirmacher oases. In many other areas, indications of cooling in that time were recorded. These differences seem to indicate the beginning of the regional and local conditions' influence on local climate.

For 4000–2000 BP, data on warming have been obtained almost everywhere. Ice cores produce warming peaks that are almost imperceptible in the center of East Antarctica and increase their amplitude to the edge of the ice sheet [*Masson et al., 2000*]. The in-

crease in warming from the center to the margins of Antarctica and its discrepancy with the global climatic optimum of 6000–5000 BP [*Folland et al., 1990*] indicate its dependence on regional factors.

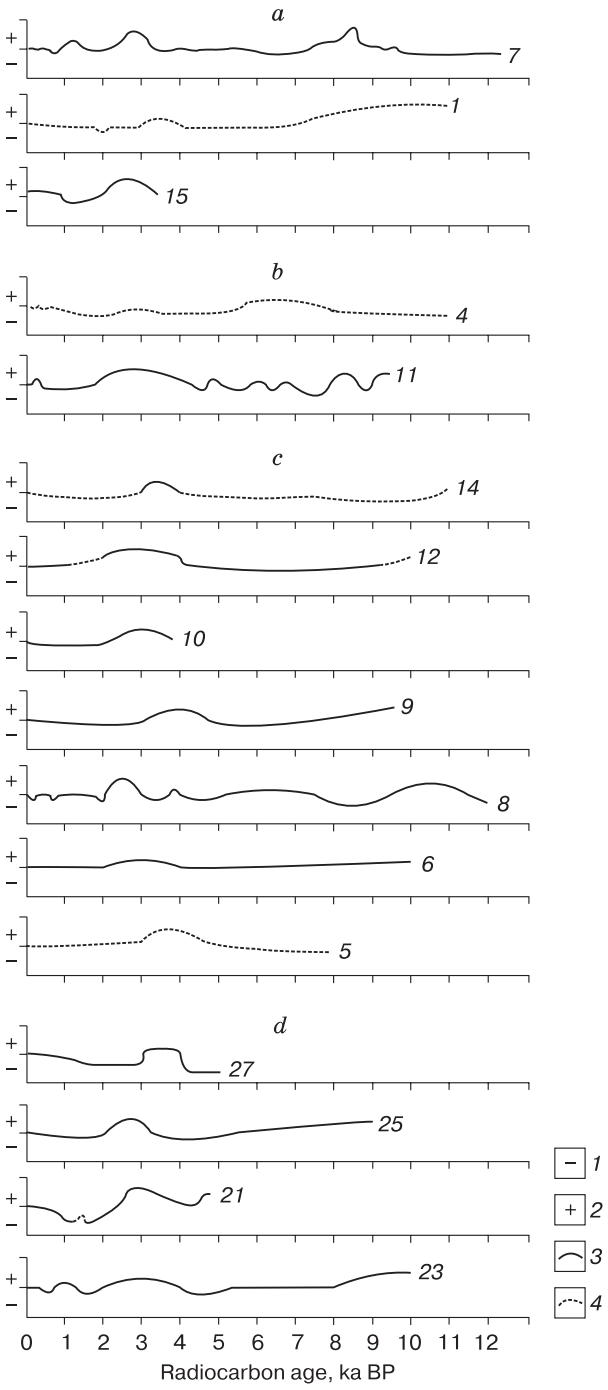

Fig. 3. Relative climate changes in the peripheral zone of Antarctica:

(*a*) mountains and mountain valleys, (*b*) onshore areas beyond ice shelf, (*c*) coastal areas, and (*d*) marine areas. *1* – Colder (drier?) climate, 2 – warmer (wetter?) climate, *3* – reliable reconstruction, and *4* – approximate reconstruction. Curve numbers denote key areas indicated in Fig. 1.

These could be changes in summer insolation in Antarctica [*Hjort et al., 1998*], oscillations of the high pressure region over the mainland [*Björck et al., 1996; Hodgson et al., 2004*], and destruction of shelf ice [*Masson et al., 2000; Verleyen et al., 2004*]. A slight warming for one of these reasons slightly changed the temperatures inside the mainland, and in coastal areas led to a reduction in sea ice cover and increased heat exchange and heat transfer, i.e., increased warming. This is confirmed by observations in the polar regions: in the depths of the continents, the amplitudes of warming are weaker than in the adjacent marine spaces [*Walsh, 2009*]. Local factors are latitude, distance from the sea, altitude and glaciated surroundings of the oases: warming is most pronounced in marine and coastal areas at relatively low latitudes.

Data on climate fluctuations over the past 2000 years allow us to identify only the traces of cooling common to most areas between about 2000 and 1500 BP. This cooling is also reflected in ice cores, i.e., it has a regional scale [*Masson et al., 2000*]. Other climatic events of the last millennium (including LIA) are difficult to find in the data from the marginal zone.

The curves of changes in the RSL (Fig. 4) demonstrate an increase in sea level from the early Holocene to maximum heights between 8000–6000 BP and the subsequent tendency for its fall. Many curves also indicate the presence of certain stages in the decrease in sea level: fast up to 3500–3000 BP, slowed

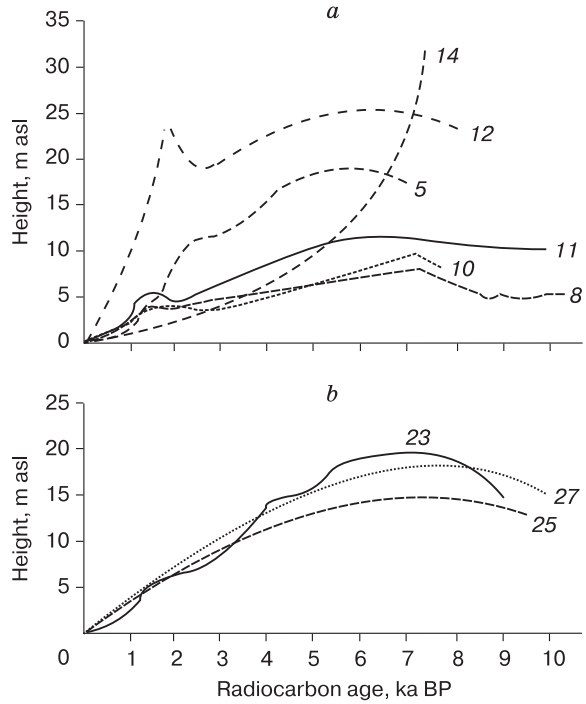

Fig. 4. Reconstructions of Holocene changes in the RSL (relative to modern absolute heights) in the peripheral zone of (*a*) East Antarctica and (*b*) West Antarctica.

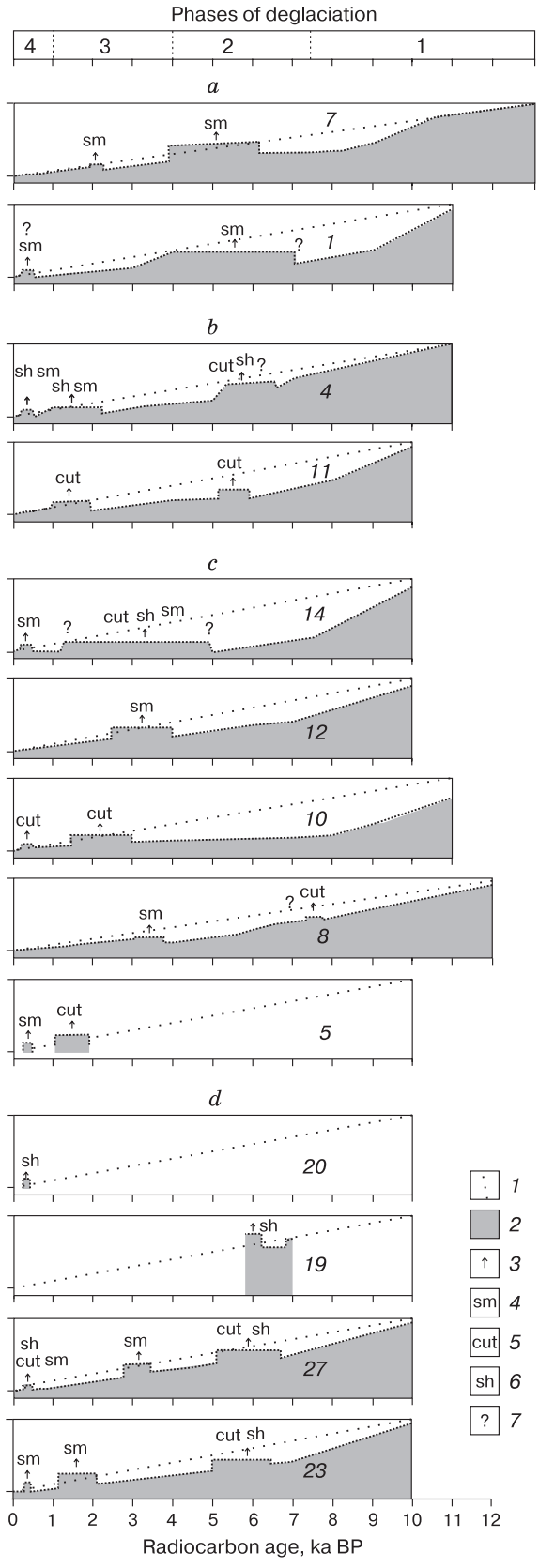

down afterwards, stopped or even replaced by sea level rise in several areas in 2500–1300 BP, and then resumed again. The rise of the RSL 1500–1400 BP was confirmed by the study of coastal bars on **Greenwich Island** [*Santana and Dumont, 2003*]. A comparison of Antarctic sea-level curves with the ideas of eustatic oscillations and the contribution of glacier melting to them [*Bentley, 1999*] reveals similarities: a rapid rise in sea level by the middle of the Holocene (although in Antarctica, the peat of this rise was 1000–1500 years earlier). The main difference between the curves is in the heights of the maximum rise of the RSL in the areas of the marginal zone of Antarctica (from 7–8 to more than 30 m). Taking into account similarity of the estimates of the thickness of the LGM glaciation for these areas, such a difference is more likely due to regional tectonic features rather than to glacioisostatic compensatory uplift of the territory. Other differences are related to the correctness of paleoreconstruction; however, they also generally reflect the relationships between global eustatic oscillations and regional tectonic movements, including local glacioisostatic movement associated with the LGM and the course of deglaciation.

A comparison of reconstructions of ***deglaciation*** in different parts of Antarctic periphery (Fig. 5) with changes in climate and sea level outlines four main phases. In the Early Holocene (the first phase), deglaciation was rapid and was related to global factors: the rise of RSL and climate warming. The phase of rapid deglaciation ended earlier (9000–8500 BP) in the mountainous oases, where it depended only on the climate. On the coast, it lasted for another 500–1500 years. Here, the rise of the RSL continued due to the predominance of the eustatic component over the rate of uplift of territories freed from glaciers: land areas were submerged, the warming effect of expanding sea areas increased, as well as ice discharge from the continent through floating outlet glaciers. On the coast, despite the relatively cold conditions since 8000 BP, relatively thin glaciers and snow–ice fields have been degrading. Ice melting in the oases was facilitated by the warming effect of growing area of glacier-free surfaces. This means that already in the first phase, the dependence of deglaciation on regional and local factors (location, glacial surroundings, local climate) was clearly manifested. By 8000–7000 BP, from 50 to 70–80 % of the area of coastal oases was freed from glaciers.

Fig. 5. Relative assessment of the course of deglaciation in the marginal zone of Antarctica.

Areas: *a* – mountainous, mountain-valley, *b* – offshore, *c* – seaside, *d* – marine. *1* – The "ideal" line for reducing the area covered by glaciers; *2* – assessment of the area covered by glaciers; *3* – the advance, the expansion of glaciers; *4* – small glaciers, glacial domes; *5* – outlet glaciers; *6* – shelf glaciers; *7* – expected events or their time limits (area numbers in Fig. 1).

In the second phase, from about 7500 to 4000 BP, deglaciation slowed down. The climate became colder and drier. In the mountainous Untersee and Amery oases, climate cooling even led to a slight increase in the area of local glaciers and snow fields. On the coast, temperatures were higher, which, together with the warming effect of the territories freed from ice, ensured a slow degradation of glaciation. Push moraines in the periphery of some oases mark the advance of shelf ice and outlet glaciers over the oases. These moraines were deposited in different times. However, everywhere, the advance of glaciers began upon lowering of sea level. Apparently, since 7500–6000 BP, glacioisostatic land uplift began to outpace eustatic sea level rise, and glaciers on the shelf grew due to cooling. Their edges rested on the rising edges of the land and created moraines. Thus, responding to global changes in general, the course of deglaciation strongly depended on the location, glacial surroundings, and local climate of the oases, as well as on differences in parameters of their glacioisostasy. As a result of the second phase, no less than 80 % of the modern area of peripheral oases was freed from glaciers, and reconstruction of local glacial systems took place.

The third phase (from about 4000 to 1000 BP) was characterized by warming 4000–2000 BP followed by cooling 2000–1500 BP and by general lowering of the RSL interrupted by a slight rise in 2500–1500 BP. In mountainous oases (where there is a minimum dependence on the influence of the ocean), warming led to a reduction in glaciation, and cooling could cause the growth of glaciers and snowfields (Amery Oasis). On the coast, along with the continuation of deglaciation, local growth of glacial domes took place between 4000 and 2000 BP because on the increase in air humidity and precipitation; such areas are known of James Ross Island and Windmill Islands. Probably, the same was the mechanism of a small growth of glaciers in the areas of the Terra Nova Bay, and the Larsemann Hills and Vestfold oases, although the chronology of these events is not quite certain, and they cannot be unambiguously linked with climate warming. Glaciation of coastal oases beyond ice shelf did not increase during that period; the local climate remained dry due to the considerable distance of these territories from the humidifying influence of ice-free ocean (ice shelves had a width of up to 100 km).

On the shores of several oases, there are indications of the advance of glaciers (push moraines) between 2000 and 1000 BP. This could be caused by climate cooling 2000–1500 BP and by fluctuations in sea level, which led to the resting of the edges of the outlet and shelf glaciers on the rising shores. Other mechanisms are also possible. For example, the advance of the outlet glacier over the land surface in the Vestfold Oasis can be explained by the retreat of the ice sheet and the cessation of its damming action on the outlet glacier [*Adamson and Pickard, 1986*]. The cooling could also contribute to the growth of glacial domes on King George Island and in the Terra Nova Bay. In general, the influence of local conditions on deglaciation increased in the third phase. By the end of this phase, the environmental conditions in the considered regions began to resemble the modern conditions, which is confirmed, for example, by the mass settlement of penguins and snow petrels that began in 2000–1000 BP [*Verkulich, 2008*].

The fourth phase started about 1000 BP with a decrease in the RSL and climatic fluctuations. The environmental conditions were generally similar to the modern ones. However, there were at least two episodes of the expansion and reduction of glaciers in some areas. The reduction of glaciers is indicated by presence of sea and lake sediments in moraines along the edges of glaciers in the Vestfold Oasis, on the shores of Terra Nova Bay, and on King George Island. Their age varies from 1200 to 700–600 BP, which makes it possible to link the retreat of glaciers with a warming of about 1000 BP, which is recorded in ice cores [*Masson et al., 2000*]. Then, the glaciers in these areas advanced again to their modern borders. Indications of the advance of glaciers by 150–500 m exist in the form of moraines with an ice core that are known on James Ross Island, the Soya Coast, and the Schirmacher and Untersee oases. The advance of ***the Muller ice shelf*** took place later (after 400 BP) [*Domack et al., 1995*]. The exact time of glaciers' growth is unknown, but most scientists associate it with the LIA.

CONCLUSIONS

The analysis, interpretation, and synthesis of the results of paleogeographic studies make it possible to update the reconstructions of climate, sea level, and glaciation changes in particular peripheral regions of Antarctica and to identify the general pattern of the development Antarctic margins over the past 50 000 years under the influence of global, regional, and local factors.

During the interstadial period (MIS 3), the boundaries of onshore glaciers and ice shelf along the Antarctic periphery, as well as the conditions of sedimentation in seas, lakes, and on land were close to modern ones. During this period, the RSL could rise to a height of up to 30 m relative to modern marks, and its changes mainly depended on regional tectonic processes that are not directly related to changes in glacial load.

The active development of glaciation during the LGM (from about 26 000 BP) in the peripheral zone of Antarctica began under conditions of a drop in sea

level by tens of meters and global cooling. The increment of glacial masses on the shelf was faster than the growth of onshore glaciers causing a shortage of atmospheric moisture supply in continental areas. During the LGM, there was a system of relatively thin (less than 300 m) glaciers on land and very thick (often, more than 1000 m) mobile ice shelves mobile in deep depressions and less mobile (anchored) on level shelf areas.

Deglaciation of the peripheral zone of Antarctica began around 17 000 BP and was not the root cause of the beginning of the planetary process of deglaciation; actually, it followed global changes in the climate and sea level.

Post-glacial climate changes in most areas had a general trend (warming in the Early Holocene until about 8000 BP and in 4000–2000 BP, cooling in 2000–1500 BP), but there were also local differences associated with factors such as latitude, altitude, features of the glacial surroundings of Antarctic oases, and distance from the sea.

Holocene curves of the RSL attest to a general rise in sea level in the Early Holocene up to maximum sea level heights in 8000–6000 BP with a subsequent tendency sea level staged drop: fast in 3500–3000 BP and slowed down afterwards (with a possible stabilization and even some rise in 2500–1300 BP in some areas). Regional differences in the amplitude of sea level changes were caused by local tectonics and deglaciation intensity.

In general, four main phases can be distinguished in deglaciation of the peripheral zone of Antarctica: from the end of the Late Pleistocene – the beginning of the Holocene to 7500 BP; from 7500 to 4000 BP; from 4000 to 1000 BP; and the last 1000 years. Deglaciation rates were high in the Early Holocene (up to about 7500 BP) due to warming and marine transgression. Then, deglaciation slowed down. The advance of the outlet and shelf glaciers in 6500–4500 BP was due to a decrease in sea level and climate cooling. In 4000–1000 BP outlet glaciers and ice shelves could react to changes in sea level, and onshore glacial domes grew according to the scheme "warming– increase in humidity–growth of snow and ice accumulation". During the LIA, push moraines were deposited in some peripheral areas of Antarctic oases attesting to a slight expansion of glaciers due to cooling. Thus, the influence of global climate and sea level changes on the development of glaciation and the environment of the Antarctic periphery was the strongest in the Early Holocene; then, it weakened simultaneously with the increasing importance of regional and local factors.

Acknowledgements. *This study was supported by the Russian Foundation for Basic Research, project no. 20-15-50236 "Expansion".*

References

Adamson, D., Colhoun, E., 1992. Late Quaternary glaciation and deglaciation of the Bunger Hills, Antarctica. Antarc. Sci. **4** (4), 435–446.

Adamson, D.A., Mabin, M.G.G., Luly, J.G., 1997. Holocene isostasy and late Cenozoic development of landforms including Beaver and Radok Lake basins in the Amery Oasis, Prince Charles Mountains, Antarctica. Antarc. Sci. **9** (3), 299–306.

Adamson, D., Pickard, J., 1986. Cainozoic history of the Vestfold Hills. In: Pickard J. (Ed.). Antarctic Oasis: Terrestrial Environments and History of the Vestfold Hills. Sydney: Academic Press Australia, p. 63–99.

Ahn, I.Y., 1994. Ecology of the Antarctic bivalve *Laternula elliptica* (King and Broderip) in Collins Harbor, King George Island: benthic environment and an adaptive strategy. In: Berkman P.A., Yoshida Y. (Eds.). Holocene environmental changes in Antarctic coastal areas (Memoirs of National Institute of Polar Research, Special issue, 50). Japan, Tokyo: NIPR, p. 1–10.

Anderson, J.B., Conway, H., Bart, P.J. et al., 2014. Ross Sea paleo-ice sheet drainage and deglacial history during and since the LGM. Quat. Sci. Rev. **100**, 31–34. doi: 10.1016/j.quascirev.2013.08.020

Anderson, J., Shipp, S., Lowe, A. et al., 2002. The Antarctic ice sheet during the last glacial maximum and its subsequent retreat history: a review. Quat. Sci. Rev. **21** (1–3), 49–70.

Baroni, C., Orombelli, G., 1991. Holocene raised beaches at Terra Nova Bay, Victoria Land, Antarctica. Quat. Res. **36**, 157–177.

Baroni, C., Orombelli, G., 1994a. The retreat of the Antarctic Ice Sheet from the Ross Sea continental shelf and the Holocene diffusion of Adelie penguins in Victoria Land. Terra Antarctica **1**, 151–152.

Baroni, C., Orombelli, G., 1994b. Abandoned penguin rookeries as Holocene palaeoclimatic indicators in Antarctica. Geology **22**, 23–26.

Baroni, C., Orombelli, G., 1994c. Holocene glacier variations in the Terra Nova Bay area (Victoria Land, Antarctica). Antarc. Sci. **6** (4), 497–505.

Bentley, M.J., 1999. Volume of Antarctic ice at the Last Glacial Maximum, and its impact on global sea level change. Quat. Sci. Rev. **18**, 1569–1595.

Berg, S., Melles, M., Gore, D., Verkulich, S. et al., 2020. Postglacial evolution of marine and lacustrine water bodies in Bunger Hills. Antarc. Sci. **32** (2), 107–129. doi: 10.1017/S0954102019000476

Berg, S., Wagner, B., Crèmer, H. et al., 2010. Late Quaternary environmental and climate history of Rauer Group, East Antarctica. Palaeogeogr. Palaeoclimatol. Palaeoecol. **297**, 201–213. doi: 10.1016/j.palaeo.2010.08.002

Berkman, P.A., Andrews, J.T., Björck, S. et al., 1998. Circum-Antarctic coastal environmental shifts during the Late Quaternary reflected by emerged marine deposits. Antarc. Sci. **10** (3), 345–362.

Berkman, P.A., Forman, S.L., 1996. Pre-bomb radiocarbon and the reservoir correction for calcareous marine species in the Southern Ocean. Geophys. Res. Lett. **23**, 363–366.

Björck, S., Hakansson, H., Zale, R. et al., 1991. A Late Holocene lake sediment sequence from Livingston Island, South Shetland Islands, with paleoclimatic implications. Antarc. Sci. **3** (1), 61–72.

Björck, S., Olsson, S., Ellis-Evans, C. et al., 1996. Late Holocene palaeoclimatic records from lake sediments on James Ross Island, Antarctica. Palaeogeogr. Palaeoclimatol. Palaeoecol. **121**, 195–220.

Bormann, P., Fritzsche, D., 1995. The Schirmacher Oasis, Queen Maud Land, East Antarctica, and its surroundings. Germany, Gotha: Justus Perthes Verlag, p. 171–206.

Carrara, P., 1981. Evidence for a former large ice sheet in the Orville Coast-Ronne Ice Shelf area, Antarctica. J. Glaciol. **27**, 487–491.

Clapperton, C.M., Sugden, D.E., 1982. Late Quaternary glacial history of George VI Sound area, West Antarctica. Quat. Res. **18**, 243–267.

Clark, P.U., Mix, A.C., 2002. Ice sheets and sea level of the Last Glacial Maximum. Quat. Sci. Rev. **21**, 1–7.

Clayton-Green, J.M., Hendy, C.H., Hogg, A.G., 1988. Chronology of a Wisconsin age proglacial lake in the Miers Valley, Antarctica. New Zealand J. Geol. Geophys. **31**, 353–361.

Cofaigh, C., Davies, B.J., Livingstone, S.J. et al., 2014. Reconstruction of ice-sheet changes in the Antarctic Peninsula since the Last Glacial Maximum. Quat. Sci. Rev. **100**, 87–110. doi: 10.1016/j.quascirev.2014.06.023

Cremer, H., Gore, D., Melles, M., Roberts, D., 2003. Palaeoclimatic significance of late Quaternary diatom assemblages from southern Windmill Islands, East Antarctica. Palaeogeogr. Palaeoclimatol. Palaeoecol. **195**, 261–280.

Demidov, N.E., Verkulich, S.R., Zanina, O.V. et al., 2013. Terminal moraine and lacustrine-lagoon deposits in the section of Quaternary deposits of the Larsemann Hills oasis, East Antarctica. Probl. Arktiki Antarktiki 3 (**97**), 79–90 (in Russian).

Denton, G.H., Bockheim, J.G., Rutford, R.H., Andersen, B.G., 1992. Glacial history of the Ellsworth Mountains, West Antarctica. Geol. Soc. Am. Memoirs, **170**, 403–432.

Dolgikh, A., Alexandrin, M., Konstantinov, E., et al., 2017. Radiocarbon age of the Holocene deglaciation in the Thala Hills oasis, East Antarctica. In: Abstracts 1st Int. Workshop on Antarctic Permafrost, Periglacial Processes and Soils (ANTPAS) "From an Expert Group to a Research Program", Varese, Italy, 4–6 October 2017, p. 14.

Domack, E.W., Ishman, S.E., Stein, A.B. et al., 1995. Late Holocene advance of the Müller Ice Shelf, Antarctic Peninsula: sedimentological, geochemical and palaeontological evidence. Antarc. Sci. **7** (2), 159–170.

Domack, E., O'Brien, P., Harris, P. et al., 1998. Late Quaternary sediment facies in Prydz Bay, East Antarctica and their relationship to glacial advance onto the continental shelf. Antarc. Sci. **10**, 234–244.

Doran, P.T., Wharton, R.A., Lyons, W.B., 1994. Paleolimnology of McMurdo Dry Valleys, Antarctica. J. Paleolimnol. **10**, 85–114.

Elverhøi, A., 1981. Evidence for a late Wisconsin glaciation of the Weddell Sea. Nature **295**, 641–642.

Emslie, S.D., Woehler, E.J., 2005. A 9000-year record of Adelie penguin occupation and diet in the Windmill Islands, East Antarctica. Antarc. Sci. **17** (1), 57–66.

Fabel, D., Stone, J., Fifield, L.K., Cresswell, R.G., 1997. Deglaciation of the Vestfold Hills, East Antarctica: preliminary evidence from exposure dating of three subglacial erratics. In: Ricci C.A. (Ed.). The Antarctic Region: Geological Evolution and Processes. Proc. Seventh Int. Symp. on Antarctic Earth Sciences (Siena, 1995), Italy, Siena: Terra Antarctica Publ., p. 829–834.

Folland, C.K., Karl, T.R., Vinnikov, K.Y., 1990. Observed climate variations and change. Climate Change, the IPCC scientific assessment. WMO/UNEP. Great Britain, Cambridge, Cambridge University Press, p. 201–238.

Fulford-Smith, S.P., Sikes, E.L., 1996. The evolution of Ace Lake, Antarctica, determined from sedimentary diatom assemblages. Palaeogeogr. Palaeclimatol. Palaeoecol. **124**, 73–86.

Gao, Y., Yang, L., Mei, Y. et al., 2020. Ice sheet changes and GIA – induced surface displacement of the Larsemann Hills during the last 50 kyr. J. Geophys. Res.: Solid Earth. **125**. doi: 10.1029/2020JB020167

Goodwin, I.D., 1993. Holocene deglaciation, sea-level change, and the emergence of the Windmill Islands, Budd Coast, Antarctica. Quat. Res. **40**, 70–80.

Goodwin, I.D., Zweck, C., 2000. Glacio-isostasy and glacial ice load at Law Dome, Wilkes Land, East Antarctica. Quat. Res. **53**, 285–293.

Gordon, J.E., Harkness, D.D., 1992. Magnitude and geographic variation of the radiocarbon content in Antarctic marine life: implications for reservoir corrections in radiocarbon dating. Quat. Sci. Rev. **11**, 697–708.

Gore, D.B., 1997. Last glaciation of Vestfold Hills: extension of the East Antarctic ice sheet or lateral expansion of Sørsdal Glacier. Polar Record **33** (184), p. 5–12.

Gore, D., Rhodes, E., Augustinus, P. et al., 2001. Bunger Hills, East Antarctica: ice free at the Last Glacial Maximum. Geology **29**, 1103–1106.

Hall, B.L., 2007. Late-Holocene advance of the Collins Ice Cap, King George Island, South Shetland Islands. The Holocene **17** (8), 1253–1258.

Hall, B.L., Denton, G.H., Overturf, B., 2001. Glacial lake Wright, a high-level Antarctic lake during the LGM and early Holocene. Antarc. Sci. **13** (1), 53–60.

Hayashi, M., Yoshida, Y., 1994. Holocene raised beaches in the Lützow-Holm Bay region, East Antarctica. In: Berkman P.A., Yoshida Y. (Eds.). Holocene environmental changes in Antarctic coastal areas. Memoirs of Natl. Inst. Polar Res., special iss. 50, Tokyo, NIPR, p. 49–84.

Hiller, A., Hermichen, W.-D., Wand, U., 1995. Radiocarbon-dated subfossil stomach oil deposits from petrel nesting sites: novel paleoenvironmental records from continental Antarctica. Radiocarbon **37** (2), 171–180.

Hirakawa, K., Sawagaki, T., 1998. Radiocarbon dates of fossil shells from raised beach sediments along the Soya Coast, East Antarctica – a report on a geomorphological survey during JARE-35 (1993–94). Antarc. Record **42**, 151–167.

Hirvas, H., Nenonen, K., Quilty, P., 1993. Till stratigraphy and glacial history of the Vestfold Hills area, East Antarctica. Quat. Int. **18**, 81–95.

Hjort, C., Bentley, M.J., Ingólfsson, O., 2001. Holocene and pre-Holocene temporary disappearance of the George VI Ice Shelf, Antarctic Peninsula. Antarc. Sci. **13** (3), 296–301.

Hjort, C., Björck, S., Ingólfsson, O., Möller, P., 1998. Holocene deglaciation and climate history of the northern Antarctic Peninsula region: a discussion of correlations between the Southern and Northern Hemispheres. Annals Glaciol. **27**, 110–112.

Hjort, C., Ingólfsson, O., Bentley, M.J., Björck, S., 2003. The Late Pleistocene and Holocene glacial and climate history of the Antarctica Peninsula region as documented by the land and lake sediment records – a review. Antarc. Res. Ser. **79**, 95–102.

Hodgson, D.A., Doran, P.T., Roberts, D., McMinn, A., 2004. Paleolimnological studies from the Antarctic and Subantarctic islands. In: Pienitz R., Douglas M.S.V., Smol J.P. (Eds.), Long-term environmental change in Arctic and Antarctic lakes. The Netherlands, Springer, p. 419–474.

Hodgson, D.A., Graham, A.G.C., Roberts, J.R. et al., 2014. Terrestrial and submarine evidence for the extent and timing of the last glacial maximum and the onset of deglaciation on the maritime-Antarctic and sub-Antarctic islands. Quat. Sci. Rev. **100**, 138–158.

Hodgson, D.A., Noon, P.E., Vyverman, W. et al., 2001. Where the Larsemann Hills ice-free through the Last Glacial Maximum? Antarc. Sci. **14** (4), 440–454.

Hodgson, D.A., Verleyen, E., Sabbe, K. et al., 2005. Late Quaternary climate-driven environmental change in the Larsemann Hills, East Antarctica, multi-proxy evidence from a lake sediment core. Quat. Res. **64**, 83–99.

Hodgson, D.A., Verleyen, E., Vyverman, W. et al., 2009. A geological constraint on relative sea level in Marine Isotope Stage 3 in the Larsemann Hills, Lambert Glacier region, East Antarctica (31366–33228 cal yr BP). Quat. Sci. Rev. **28**, 2689–2696.

Ingólfsson, Ó., Björck, S., Hjort, C., Smith, R.I.L., 1992. Late Pleistocene and Holocene glacial history of James Ross Island, Antarctic Peninsula. Boreas **21,** 209–222.

Ingólfsson, Ó., Hjort, C., Berkman, P.A. et al., 1998. Antarctic glacial history since the Last Glacial Maximum: an overview of the record on land. Antarc. Sci. **10** (3), 326–344.

Jordan, H., van der Wateren, F.M., 1993. The lakes of Little Rocks, North Victoria Land, Antarctica – consequences for the deglaciation of the Rennick Valley. Geologis. Jahrbuch **47**, 371–388.

Jouzel, J., Masson, V., Cattani, O. et al., 2001. A new 27 ky high resolution East Antarctic climate record. Geophys. Res. Lett. **28** (16), 3199–3202.

Karl, H.A., 1989. High-resolution seismic reflection interpretations of some sediment deposits, Antarctic continental margin: focus on the western Ross Sea. Marine Geol. **85**, 205–223.

Kirkup, H., Melles, M., Gore, D.B., 2002. Late Quaternary environment of southern Windmill Islands, East Antarctica. Antarc. Sci. **14**, 385–394.

Kotlyakov, V.M., Zakharov, V.G., Moskalevsky, M.Yu., Khromova, T.E., 2003. Assessment of the structure, regime and evolution of glaciers in the marginal zone of Antarctica. Materialy Glyatsiologich. Issled. **95**, 135–140 (in Russian).

Kulbe, T., Melles, M., Verkulich, S., Pushina, Z., 2001. East Antarctic climate and environmental variability over the last 9400 years inferred from marine sediments of the Bunger Oasis. Arct. . Antarc. Alp. Res. **33** (2), 223–230.

Lambeck, K., Yokoyama, Y., Purcell, T., 2002. Into and out of the last glacial maximum: sea level changes during oxygen isotope stages 3 and 2. Quat. Sci. Rev. **21** (1–3), 343–360.

Leitchenkov, G., Stagg, H., Gandiukhin, V. et al., 1994. Cenozoic seismic stratigraphy of Prydz Bay (Antarctic). Terra Antarctica **1**, 395–397.

Licht, K.J., Jennings, A.E., Andrews, J.T., Williams, K.M., 1996. Chronology of late Wisconsin ice retreat from the western Ross Sea, Antarctica. Geology **24** (3), 223–226.

Lyons, W.B., Tyler, S.W., Wharton, R.A. et al., 1998. A Late Holocene desiccation of Lake Hoare and Lake Fryxell, McMurdo Dry Valleys, Antarctica. Antarc. Sci. **10** (3), 247–256.

Mabin, M.C.G., 1991. The glacial history of the Lambert Glacier – Prince Charles Mountains area and comparisons with the record from the Transantarctic Mountains In: Gillieson D., Fitzsimons S. (Eds.). Quaternary research in Australian Antarctica: future directions. Special Publ. 3. Canberra, Australian Defence Force Academy, p. 15–23.

Mahesh, J.B.., Warrier, A., Mohan, K.R. et al., 2017. Response of Sandy Lake in Schirmacher Oasis, East Antarctica to the glacial-interglacial climate shift. J. Paleolimnol. **58**, 275–289. doi: 10.1007/s10933-017-9977-8

Masson, V., Vimeux, F., Jouzel, J. et al., 2000. Holocene climate variability in Antarctica based on 11 ice-core isotopic records. Quat. Res. **54**, 348–358.

McMinn, A., 2000. Late Holocene increase in sea ice extent in fjords of the Vestfold Hills, eastern Antarctica. Antarc. Sci. **12** (1), 80–88.

Melles, M., Kulbe, T., Verkulich, S. et al., 1997. Late Pleistocene and Holocene environmental history of Bunger Hills, East Antarctica, as revealed by fresh-water and epishelf lake sediments. In: Ricci C.A. (Ed.). The Antarctic Region: Geological Evolution and Processes. Proc. 7th Int. Symp. on Antarctic Earth Sciences (Siena, 1995), Italy, Sien, Terra Antarctica Publ., p. 809–820.

Melles, M., Verkulich, S.R., Hermichen, W.-D., 1994. Radiocarbon dating of lacustrine and marine sediments from the Bunger Hills, East Antarctica. Antarc. Sci. **6** (3), 375–378.

Miura, H., Maemoku, H., Igarashi, A. et al., 1998a. Late Quaternary raised beach deposits and radiocarbon dates of marine fossils around Lutzow-Holm Bay. Tokyo: National Inst. Polar Res., 46 p.

Miura, H., Moriwaki, K., Maemoku, H., Hirakawa, K., 1998b. Fluctuations of the East Antarctic ice-sheet margin since the last glaciation from the stratigraphy of raised beach deposits along the Sôya Coast. Ann. Glaciol. **27**, 297–301.

Moriwaki, K., Yoshida, Y., 1983. Submarine topography of Lützow-Holm bay, Antarctica. Memoirs of the National Inst. Polar Res. **28**, 247–258.

Nichols, K.A., Goehring, B.M., Balco, G. et al., 2019. New Last Glacial Maximum ice thickness constraints for the Weddell Sea Embayment, Antarctica. The Cryosphere **13**, 2935–2951. doi: 10.5194/tc-13-2935-2019.

Oberholzer, P., Baroni, C., Schaefer, J.M. et al., 2003. Limited Pliocene/Pleistocene glaciation in Deep Freeze Range, northern Victoria Land, Antarctica, derived from in situ cosmogenic nuclides. Antarc. Sci. **15** (4), 493–502.

Orombelli, G., Baroni, C., Denton, G.H., 1990. Late Cenozoic glacial history of the Terra Nova Bay region, Northern Victoria Land, Antarctica. Geograf. Fisica Dinamica Quat. **13**, 139–163.

Peltier, W.R., 2002. On eustatic sea level history: last glacial maximum to Holocene. Quat. Sci. Rev. **21** (1–3), 377–396.

Poleshchuk, K.V., Verkulich, S.R., 2014. Reconstruction of Holocene relative sea-level changes in the Bunger oasis region (East Antarctica). Probl. Arktiki Antarktiki 2 (**100**), 15–24 (in Russian).

Poleshchuk, K.V., Verkulich, S.R., Ezhikov, I.S., Pushina, Z.V., 2016. Postglacial relative sea level change at Fildes Peninsula, King George Island (West Antarctic). Led i Sneg **56** (1), 92–103 (in Russian). doi: 10.15356/2076-6734-2016-1-93-102

Roberts, D., McMinn, A., Cremer, H. et al., 2004. The Holocene evolution and palaeosalinity history of Beall Lake, Windmill Islands (East Antarctica) using an expanded diatom-based weighted averaging model. Palaeogeogr. Palaeoclimatol. Palaeoecol. **208**, 121–140.

Roberts, S.J, Hodgson, D.A., Sterken, M. et al., 2011. Geological constraints on glacio-isostatic adjustment models of relative sea-level change during deglaciation of Prince Gustav Channel, Antarctic Peninsula. Quat. Sci. Rev. **30**, 3603–3617. doi: 10.1016/j.quascirev.2011.09.009

Ryan, P.G., Steele, W.K., Siegfried, W.R. et al., 1992. Radiocarbon dates of snow petrel regurgitations can reveal exposure periods for nunataks in Antarctica. South African J. Sci. **88**, 578–580.

Santana, E., Dumont, J.F., 2003. Coastal morphology of a fast uplifting coast: characteristics and implications, the Antarctic Peninsula, Greenwich Island, South Shetland. In: 9th Int. Symp. Antarctic Earth Sciences (September 8–12, 2003, Programme and Abstracts). Germany, Potsdam, Terra Nostra, p. 285–286.

Schwab, M.J., 1998. Reconstruction of the Late Quaternary climatic and environmental history of the Schirmacher Oasis and the Wohlthat Massif, East Antarctica. (Berichte zur Polar- und Meeresforschung 545). Germany, Bremerhaven, Alfred-Wegener-Institute für Polar- und Meeresforschung, 128 p.

Smith, G.I., Friedman, I., 1993. Lithology and paleoclimatic implications of lacustrine deposits around Lake Vanda and Don Juan Pond, Antarctica. Antarc. Res. Ser. **59**, 83–94.

Sokratova, I.N., 2007. Antarctic oases: history and meaning of the term. Led i Sneg **103**, 25–29 (in Russian).

Sterken, M., Roberts, S.J., Hodgson, D.A. et al., 2012. Holocene glacial and climate history of Prince Gustav Channel, northeastern Antarctic Peninsula. Quat. Sci. Rev. **31**, 93–111. doi: 10.1016/j.quascirev.2011.10.017

Stone, J.O., Balco, G.A., Sugden, D.A. et al., 2003. Holocene deglaciation of Marie Byrd Land, West Antarctica. Science **299**, 99–102.

Stuiver, M., Denton, G., Hughes, T., Fastook, J., 1981. History of the Marine Ice Sheet in West Antarctica during the last glaciation: a working hypothesis. In: Denton G.H., Hughes T. (Eds.). The Last Great Ice Sheets. USA, New York: John Wiley and Sons, p. 319–436.

Swadling, K.M., Dartnall, H.J., Gibson, J.A., 2001. Fossil rotifers and the early colonization of an Antarctic lake. Quat. Res. **55**, 380 –384.

Verkulich, S.R., 2007. Reconstruction of Holocene climate changes in the marginal zone of East Antarctica based on the study of bottom sediments of lakes and sea bays. Izvest. Ross. Akad. Nauk, Ser. Geogr., No. 4, 38–43 (in Russian).

Verkulich, S.R., 2008. Organic sediments in nests of penguins and snow petrels – evidence of the conditions and progress of deglaciation of the marginal zone of Antarctica. Izvest. Russk. Geogr. O-va, No. 3, 16–21 (in Russian).

Verkulich, S.R., 2009. Conditions and regime of the last deglaciation in the edge zone of Antarctica. Kriosfera Zemli (Earth's Cryosphere), **13** (2), 73–81 (in Russian).

Verkulich, S.R., 2010. The last glacial maximum in the marginal zone of Antarctica: synthesis of paleogeographic data. Led i Sneg 50 (4), p. 91–100 (in Russian).

Verkulich, S.R., Dorozhkina, M.V., Pushina, Z.V. et al., 2013. Interstadial conditions (MIS 3) and glaciation patterns of the last glacial maximum on King George Island (West Antarctica). Led i Sneg, No. 1 (**121**), 111–117 (in Russian).

Verkulich, S., Hiller, A., 1994. Holocene deglaciation history of the Bunger Hills revealed by C-14 measurements on stomach oil deposits in show petrel colonies. Antarc. Sci. **6** (3), 395–399.

Verkulich, S.R., Melles, M., Pushina, Z.V., Hubberten, H.-W., 2002. Holocene environmental changes and development of Figurnoye Lake in the southern Bunger Oasis, East Antarctica. J. Paleolimnol. **28**, 253–267.

Verkulich, S.R., Pushina, Z.V., Dorozhkina, M.V. et al., 2015. Characterization of environmental conditions of the interstadial (MIS 3) deposits formation in King George Island (West Antarctica) based on the study of fossil diatom assemblages. Probl. Arktiki Antarktiki, No. 4 (**106**), 109–119 (in Russian).

Verkulich, S.R., Pushina, Z.V., Sokratova, I.N. et al., 2007. Changes in sea level and glacial isostasy on the Antarctic coast in the Holocene. Mater. Glyatsiol. Issled. **102**, 161–167 (in Russian).

Verkulich, S.R., Pushina, Z.V., Sokratova, I.N., Tatur, A., 2011. Changes in glaciation of the Schirmacher oasis (East Antarctica) since the end of the Late Neopleistocene. Led i Sneg, 51 (2), 116–121 (in Russian).

Verkulich, S.R., Pushina, Z.V., Tatur, A. et al., 2012a. Environmental changes and diatom flora in the Schirmacher oasis (East Antarctica) at the end of the Late Neopleistocene and in the Holocene. Probl. Akrtiki Antarktiki, No. 2 (**92**), 27–42 (in Russian).

Verkulich, S.R., Pushina, Z.V., Tatur, A. et al., 2012b. Holocene environmental changes in Fildes Peninsula, King George Island (West Antarctica). Probl. Arktiki Antarktiki, No. 3 (**93**), 17–27 (in Russian).

Verleyen, E., Hodgson, D.A., Milne, G. A. et al., 2005. Relative sea-level history from the Lambert Glacier region, East Antarctica, and its relation to deglaciation and Holocene glacier readvance. Quat. Res. **63**, 45–52.

Verleyen, E., Hodgson, D.A., Sabbe, K., Vyverman, W., 2004. Late Quaternary deglaciation and climate history of the Larsemann Hills (East Antarctica). J. Quat. Sci. **19** (4), 361–375.

Verleyen, E., Hodgson, D.A., Sabbe, K. et al., 2011. Post-glacial regional climate variability along the East Antarctic coastal margin – evidence from shallow marine and coastal terrestrial records. Earth Sci. Rev. **104**, 199–212.

Verleyen, E., Hodgson, D.A., Vyverman, W. et al., 2003. Modelling diatom responses to climate induced fluctuations in the moisture balance in continental Antarctic lakes. J. Paleolimnol. **30**, 195–215.

Wagner, B., Cremer, H., Hultzsch, N. et al., 2004. Late Pleistocene and Holocene history of Lake Terrasovoje, Amery Oasis, East Antarctica, and its climatic and environmental implications. J. Paleolimnol. **32**, 321–339.

Waitt, R.B., 1983. Thicker West Antarctic ice sheet and peninsula ice cap in late Wisconsin time – sparse evidence from northern Lassiter Coast. Antarc. J. of US, **18** (5), 91–93.

Walsh, J.E., 2009. A comparison of Arctic and Antarctic climate change, present and future. Antarc. Sci. **21** (3), 179–188.

Wasiłowska, A., Tatur, A., Pushina, Z. et al., 2017. Impact of the "Little Ice Age" climate cooling on the maar lake ecosystem affected by penguins: a lacustrine sediment record, Penguin Island, West Antarctica. The Holocene, **27** (8), 1115–1131. doi: 10.1177/0959683616683254

Whitehead, J., McMinn, A., 1997. Use of benthic diatom assemblages from the Vestfold Hills for paleodepth analysis. Marine Micropaleontol. **29**, 301–318.

Zale, R., Karlen, W., 1989. Lake sediment cores from the Antarctic Peninsula and surrounding islands. Geografiska Annaler, **71 A**, 211–220.

Zwartz, D., Bird, M., Stone, J., Lambeck, K., 1998. Holocene sea level change and ice-sheet history in the Vestfold Hills, East Antarctica. Earth Planet. Sci. Lett. **155**, 131–145.

Received August 18, 2021
Revised November 29, 2021
Accepted February 26, 2022

Translated by S.B Sokolov

EARTH'S CRYOSPHERE
SCIENTIFIC JOURNAL

Earth's Cryosphere, 2022, vol. XXVI, No. 2, pp. 20–33

SURFACE AND GROUND WATERS IN TERRESTRIAL PERMAFROST REGION

FLOODPLAIN TALIK WIDTHS IN RELATION TO RIVER CATCHMENT AREAS AND CHANNEL TYPES

V. M. Mikhailov

North-Eastern Permafrost Research Station, Melnikov Permafrost Institute,
Siberian Branch of the Russian Academy of Sciences,
Portovaya str. 16, Magadan, 685000 Russia; vmmikhailov@gmail.com

Data on the width of floodplain taliks in river valleys of the mountainous areas in the northeast of Russia and adjacent areas of the Far East were gathered and organized. The investigated region extends from the Arctic coast to the southern limits of the continuous permafrost area. To assess talik widths, satellite images of high resolution from the *Google Earth* service and previously established indicative landscape features were applied. The catchment areas at downstream ends of the chosen 340 representative river sections varied from less than 10 to more than 200 000 km^2; talik widths, from 41 to 4100 m. The rivers were subdivided into four channel types according to the degree of channel branching based on the previous studies confirming that the floodplain taliks were formed only by braided rivers on coarse-grained alluvium. The studied sites are generally evenly distributed both over the territory and according to the selected channel types. The changes in talik widths from marginal coastal to central continental river basins in relation to the channel type are discussed in this paper. The parameters of the empirical power-law dependence of the talik width on the catchment area of the river are calculated. The results obtained allow us to estimate the range of variation in the talik zone width on floodplain in dependence on the given river catchment area and determine the most probable minimum value of this parameter. In future, this approach in combination with field research will contribute to the improvement of remote sensing data interpretation.

Keywords: *permafrost, floodplain taliks, talik width, river catchment areas, river channel types, interpretation of remote sensing data*

INTRODUCTION

Studies into the development and distribution of thawed zones in permafrost and methods for indicating taliks and estimating their size are among the traditional and important fields of geocryological research. For a long time, floodplain taliks remained the least studied. The term floodplain talik was first used in the monograph by I.A. Nekrasov [*1967*], though data on talik zones occupying the entire width of floodplains and even nearby sections of terraces had been mentioned earlier mentioned by A.I. Kalabin [*1960*] and V.M. Ponomarev [*1960*].

The monograph [*Mikhailov, 2013*] considers the history of the pertinent research in detail and sets out an integral concept that links all the previous studies.

The core mechanism for the development of floodplain taliks is intensive heat and water exchange between river and groundwater flows. The groundwater is mainly concentrated in a powerful filtration flow covering the entire zone of channel reformations and directed along the slope of the valley.

Water exchange happens due to the mismatch between the direction of this flow and flows in the river branches and channels. The most obvious examples are the straightening of the bends of the channels by the flows and inter-flow filtration.

The river water is the main heat source in the talik–river system, since it is a natural receiver of the solar energy, and filtered water is a perfect heat carrier from the channel to the alluvium.

An important single factor theoretically capable of ensuring the development of taliks even under otherwise unfavorable conditions is high permeability of channel alluvium. This factor exceeds by an order of magnitude the values that until recently have been cited in the hydrogeological references as the maximum possible values amounting to hundreds of meters per hour. In mountainous areas, this factor is associated with multi-branching because of the highly gravelly nature of the bedrock prevailing in the river basin (according to the size of rock fragments forming at the first stages of weathering) [*Mikhailov, 2011*]. In water flows, these fragments roll down to boulders and gravel, whereas the content of fine-grained fractions remains small. In this paper we exclusively discuss multi-branched rivers flowing within mountain structures.

It follows that the floodplain talik is an integral, genetically unified formation. Therefore, attempts to identify within it an under-channel talik, proper floodplain talik, and, possibly, terrace talik are mean-

ingless from a hydrogeological point of view [*Mikhailov, 2013, p. 42*].

The high permeability of alluvium also provides for an abundance of tree species that require aeration of the root layer: in the floodplains that require aeration of the root layer: chosenia and poplars. According to the works of I.A. Nekrasov [*1967*] and V.R. Alekseev [*1968*] such forest stands have served as a common and actually a single indicator of floodplain taliks for a long time.

Information about the size of floodplain taliks is still scattered. Their width varies from a few tens of meters in low-order valleys [*Zelenkevich, 1964; Mikhailov, 2013*] up to several kilometers near high-water rivers [*Vtyurin, 1964; Nekrasov, 1967*]. This is associated with insufficient and extremely uneven knowledge of the permafrost zone. However, there are two more important factors: (1) the availability of only black and white aerial photographs of a scale, as a rule, no larger than 1:40,000 and (2) application of a single criterion for remote interpretation of the talik boundaries.

Nowadays, possibilities for interpretation are larger due to availability of color satellite *Google Earth* imagery. It allows one to distinguish between deciduous and mixed forest stands more confidently. This commonly used feature is also supplemented with the possibility to trace channel branching, which is also important for interpretation of talik zones. The "trinity" of floodplain taliks, branching rivers, and poplar-chosenia forest stands was first noted by G.N. Egorova [*1983*]. In addition, separate areas of the earth's surface in *Google Earth* are captured with a very high resolution (up to 0.35 m), which makes it possible to detect taliks in the valleys of small streams.

The goal of this paper is to find out the nature and degree of connection between the transverse dimensions of the floodplain taliks, stream discharge, and types of multi-branch channels. The results obtained should contribute to the improvement of methods for interpreting talik zones in river valleys and determining accurate territorial estimates of their distribution. The explored river valleys are located in the northeast of Russia and in adjacent regions of the Far East. Branched river channels often predominate in the east of Russia; hence, floodplain taliks are common in permafrost areas. In other parts of the permafrost zone of Russia, branching channels and taliks are rather rare.

THEORETICAL BASIS

Terminology. Some of the used terms have ambiguous interpretations in the scientific literature. In such cases, formulations adopted from a number of options with links to primary sources are given in a reference dictionary [*Timofeev, 1981*]. They are as follows:

Floodplain: (1) the lowest periodically flooded part of the river valleys (*p. 116*) and (2) surface or strip of relatively flat land adjacent to the riverbed and formed or being formed by the river (*p. 117*).

Floodplain talik is a thawed zone, which is formed "directly under the channel, on the floodplain, or, in some cases, within river terraces" [*Nekrasov, 1967, p. 18*].

Channel: (1) the entire width and length of the river during the low-water season (according to V.I. Dal' dictionary of Russian language); (2) part of the valley bottom, where river flow takes place during the low-water season (*p. 160*). River channel is entirely located within the floodplain..." [*Voskresensky, 1985, p. 75*].

Branching channel is the channel of the river divided into several branches forming a complex network of small merging and diverging arms (*p. 160*).

Terraces are relatively horizontal areas located at different heights above the modern bottom of the valley (*p. 183*).

Transverse dimensions of taliks and indication of their boundaries. As follows from the concise description given in the introductory part, floodplain taliks are distributed within the zone of highly permeable sediments. Its minimum width coincides with the width of channel branching zone, where deposition of fine-grained material is prevented by frequent erosion and redeposition. Beyond this zone, episodic washout of alluvium occurs as a result of seasonal displacement of peripheral branches and arms. The presence of taliks under accumulative terraces (apparently as residual formations) indicates that permeability of sediments can be sustained for a long time by high velocities of groundwater flows in preferential flow zones. However, permafrost may also exist on floodplains (that are sometimes hypsometrically hardly distinguishable from the adjoining low terraces). Despite a relatively small transverse dimension of the branching zone, it plays the role of the key "reference" indicator of the talik and its boundaries, because the are occupied by the geobotanical indicator of taliks is even smaller. Thus, within a key area (2 × 2 km) subjected to a detailed survey on the Kolyma River floodplain, poplar-chosenia and mixed forest stands occupied only about 30 % of the territory [*Mikhailov, 2013*], whereas a larger part of the talik was under relatively high larch forest with an insignificant admixture of other species. Similar forest stands are quite confidently distinguished on satellite images compared to suppressed low forests on permafrost soils, and, therefore, can attributed to geobotanical indicators. A similar role belongs to the willows inhabiting the newly formed areas of low floodplain.

The foregoing does not cover all the possibilities and difficulties of delimiting areas of talik and permafrost distribution in river valleys. Specific features are characteristic of the floodplains of small streams,

Fig. 1. The Yama River branch disconnected in the upper reaches from the nearest large channel and fed by a seepage flow (upstream from point 338, see appendix, sheet l).

where branching may not be clearly expressed. Specific features are also characteristic of terraces composed of thawed sediments [*Mikhailov, 2013*].

Quite often, unambiguous interpretation of satellite images is impossible without additional field studies. In the present paper, such situations are usually excluded from consideration.

Taliks and the main characteristics of river channels. The most detailed studies of branched river channels in Russia are mainly based on the classification of channel branching, which includes 11 varieties [*Chalov, 2017, 2019*]. However, they do not consider the width of the zone of channel transformation.

It seems that the width of the channel transformation zone is directly dependent on the number of branches and channels in the cross section of the valley. Quantitative indicator is called the braiding index or braiding intensity in the foreign reference. Such indices, their comparability, and their variability in dependence on the hydrological conditions are discussed in detail in [*Egozi and Ashmore, 2008*],

These indices differ from one another and significantly depend on water levels. It is concluded that measurements should be carried out at several water levels to obtain representative results. This makes it quite challenging to apply quantitative estimates when using satellite data. In floodplain taliks with intense filtration flows the situation is complicated by the fact that the concept of an active branch (channel) becomes indefinite.

In secondary arms and channels, water discharge can decrease downstream up to complete disappearance of surface water flow (water flow becomes absorbed into the alluvium). Vice versa, a channel with

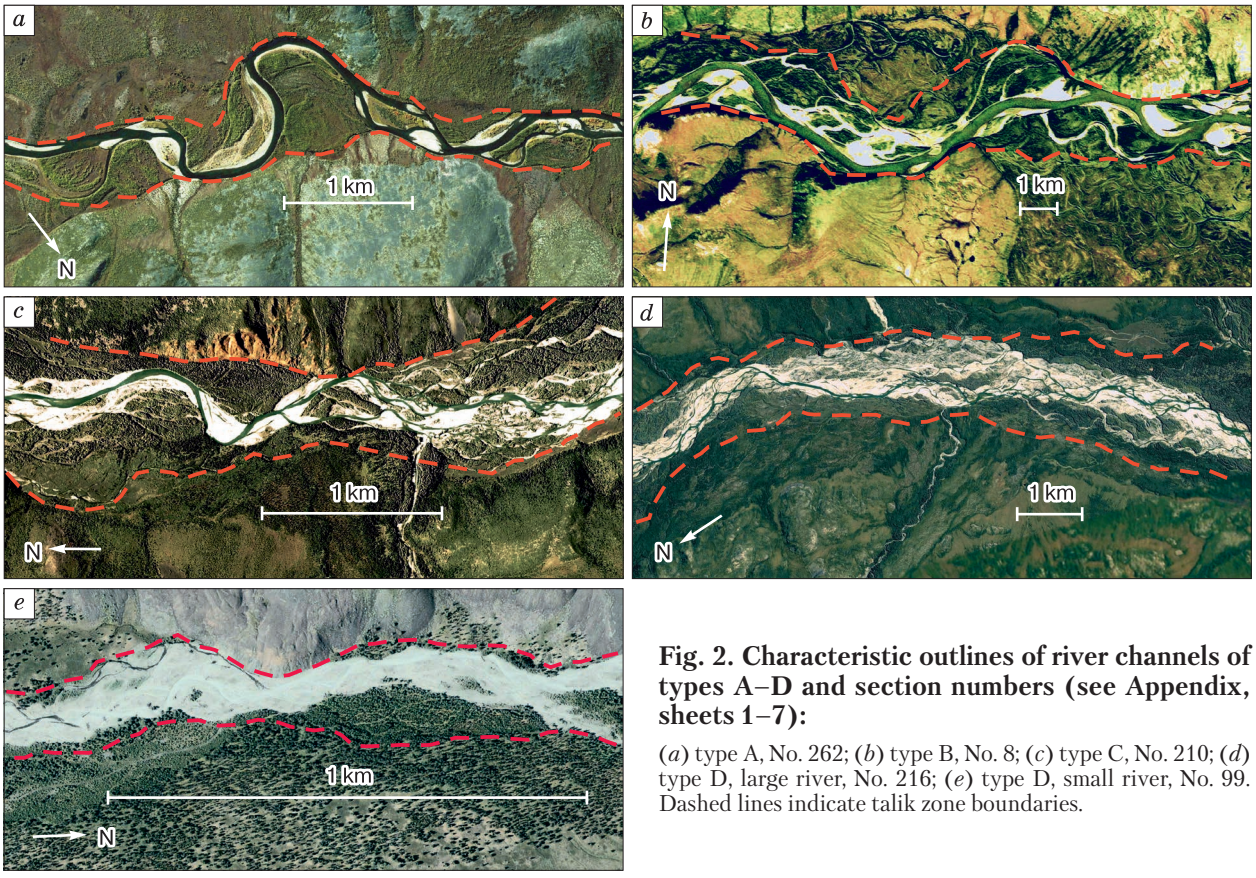

Fig. 2. Characteristic outlines of river channels of types A–D and section numbers (see Appendix, sheets 1–7):

(*a*) type A, No. 262; (*b*) type B, No. 8; (*c*) type C, No. 210; (*d*) type D, large river, No. 216; (*e*) type D, small river, No. 99. Dashed lines indicate talik zone boundaries.

an increasing discharge downstream can appear "out of nowhere" due to groundwater seepage (Fig. 1). Often, there is a combination of both phenomena. It is obvious that when the water level in the river changes, such channels can become completely dry or merge together with larger channels. In many small streams, secondary channels are partially or even completely closed and shaded by forest stands.

A rational alternative to the use of still imperfect quantitative methods is a visual assessment of branching intensity with a division into a number of well-distinguishable types. This approach was used to determine the sinuosity coefficient of river channels. In the study [*Chebotarev, 1975*], 9 types of channels forming 12 characteristic patterns were described. The intensity of river braiding can be found by comparing the actual channel pattern with these characteristic patterns and choosing closest pattern.

Examples of branching channel patterns, characteristic for the four identified types (A–D) are shown in Fig. 2 (branching index increases from A to D). Two examples are given for type D: the largest river and a stream of minimum discharge required for talik development. Figures 2, *c* and 2, *d* demonstrate a complexity of various branch combinations.

Considering the above challenges, it does not make sense to apply quantitative estimates; they are considered impractical for the foreseeable future. In addition, it remains unclear what numerical criteria should be used to distinguish between channel branching types even with the most scrupulous and correct calculations of the branching indices. That is, a quantitative approach is just as subjective as a qualitative description.

MATERIALS AND METHODS

To measure the width of the taliks, sections of branching rivers and streams with the length of about 10–30 times larger than the expected talik width (depending on the degree of homogeneity of the site) were studied. However, the choice was limited to those small areas where Google Earth satellite images have a resolution of up to 0.35 m, allowing to distinguish even separate shrubs. For large rivers with catchment areas of more than 20 000 km^2, resolution of 5–7 m (which is quite common for *Google Earth* service) is usually sufficient for delineation of taliks.

A total of 340 sites were selected in three large areas: catchments of the Indigirka and Kolyma rivers in their upper and middle reaches and river catchments near the seas of the Pacific and Arctic basins. The latter are further called marginal rivers, because the central mountainous part of the northeast of Russia belongs to large catchments of the Indigirka and Kolyma rivers.

Table 1. **Distribution of the studied areas by types of channels and river basins, %**

Basin	Total number of studied sites	Type of channel			
		A	B	C	D
Marginal	122	15 / 28	30 / 37	27 / 46	28 / 51
Kolyma	120	26 / 48	46 / 41	17 / 28	11 / 19
Indigirka*	98	16 / 24	45 / 32	18 / 28	21 / 30
Total number of sites	**340**	**67**	**135**	**71**	**67**

Note: Numerator indicates the percent of the given type of channel in the basin, and denominator shows the percent of the given basin in the total number of sites with this type of channel.

* Including 8 sites from adjacent basins of the Yana (7) and Lena (1) rivers.

Quite often, sites on the same watercourse with a shift downstream were selected. The approach used is consistent with the principles of constructing a random sample. First, the criterion of high-resolution of *Google Earth* images is, in fact, irrelevant to the purposes of this paper. Second, the types of channels, even in the nearby sections of the rivers, are not actually interconnected. For example, incised channels can be replaced by the free development of channel deformations, and vice versa*. The same is true for the width of the thawed zones. Specific data about the studied sites are given in the appendix. Generalized data are given in Table 1.

The catchment area (*F*) is used as the main characteristic of the river. It is further used to estimate river discharge, or, more precisely, the average maximum flow, which has the greatest impact on the reshaping of the river channel during the year. Previously, a close relationship between these values was established, and the parameters of this dependence remain unchanged throughout the entire territory of the northeast of Russia [*Mikhailov, 2014*]. The measurements of *F* in the outlet sections of the selected areas were made using topographic maps. The plots were grouped according to *F* values arranged in a uniform logarithmic scale as follows:

F, km^2	<20	20–200	200–2000	2000–20 000	20 000–200 000
Share of plots, %	5.3	38	24	24	9.1

Method for determining transverse dimensions of thawed zones requires explanation. According to theoretical concepts, taliks usually occupy the entire zone of channel transformation affected by intense

* A bright example is the Kolyma River valley in the area of Sugoi bend (64°09′ N, 154°27′ E) with deeply incised channel, whereas upstream and downstream sections are characterized by branching channels.

filtration flow. According to the results of field studies [*Kalabin, 1960; Ponomarev, 1960; Mikhailov, 2013*], taliks may extend beyond this zone and occupy not only the entire floodplain but also low terraces. The applied method is based on the principle of "not exaggerating" the area of taliks. The boundaries of talik zones were drawn predominantly along the lines delineating the zones of channel branching with the following adjustments:

1. Sections of rivers with large floodplain islands with a possible presence of permafrost were excluded from the plots selected for measurements. In particular, the most water-abundant areas in the Kolyma River valley with vast islands and numerous lakes of presumably thermokarst origin were excluded from the list of study objects.

2. The areas beyond the channel branching zone, where the vegetation cover significantly differed from that on the adjacent territories and unequivocally indicated the thawed zone, were incorporated into floodplain taliks. In particular, these were the areas with an increased density of forest stands and wide distribution of deciduous species.

3. If the nature of the vegetation cover changed sharply near the channel in the opposite direction, in case of rare occurrence or absence of forest stands, then the borders of the talik were drawn mainly along the shoreline or parallel to it with a slight deviation. Based on physical considerations, a minimum graphic interpolation was allowed, where the boundary line was broken (upon junction or disjunction of channels or in places of the sharpest turns).

4. The channel flow of the small streams at the low water level may be interrupted, sometimes for a considerable length, due to the infiltration of channel waters into highly permeable soil (Fig. 2, *d*). In such cases, the zone of the most intense channel deformations is marked by freshly deposited alluvium, which is clearly indicated by light color on the satellite images.

Next, the thawed area, its length along the axial line and the average width B were measured. The dependence $B(F)$ was approximated by the formula commonly applied in analogous cases [*Park, 1977*]:

$$B = \alpha F^{\beta}, \quad (1)$$

where α and β are dependence parameters; F is the catchment area, km^2; and B is the average width, m. The coefficient of determination R^2 was used to assess the degree of correlation.

RESULTS AND DISCUSSION

As can be seen from Table 1, the selected sites are more or less evenly distributed over the main basins and types of channels. However, the analysis of generalized data allows us to trace certain trends. Most of the intensely branching rivers of types C and D belong to marginal (coastal) areas (47 and 51 %, respectively), whereas types A and B predominate in continental parts. Almost a half of 216 watercourses of the two basins belong to the more branched type B. Thus, in general, the degree of channel branching and the associated width of taliks decrease from the marginal areas of the region to its central parts, although this trend is not clearly pronounced.

The results of statistical data processing are presented in Figs. 3 and 4 and in Tables 2 and 3. Figure 3 shows dependence graphs built (1) separately for each of the selected areas and types of channels (12 in total). However, the approximating lines lie so close to one another other that it is challenging to distinguish them even in color. Thus, Fig. 3 shows the region occupied by all these lines together, except for three extreme lines clearly defining area boundaries. For similar reasons, Table 2 shows only the extreme values of the dependence parameters.

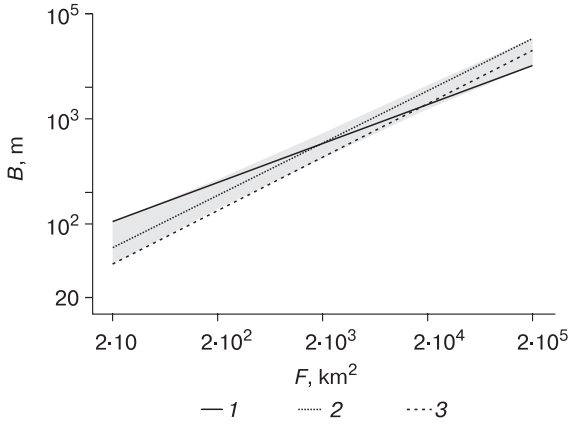

Fig. 3. The dependence of the average width of the talik zones from the catchment area $B(F)$ in the logarithmic coordinate system:

(*1, 2*) Indigirka basin, types C and D, respectively; (*3*) Kolyma basin, type B. The area where all approximating lines of the $B(F)$ lie is shown by flood fill.

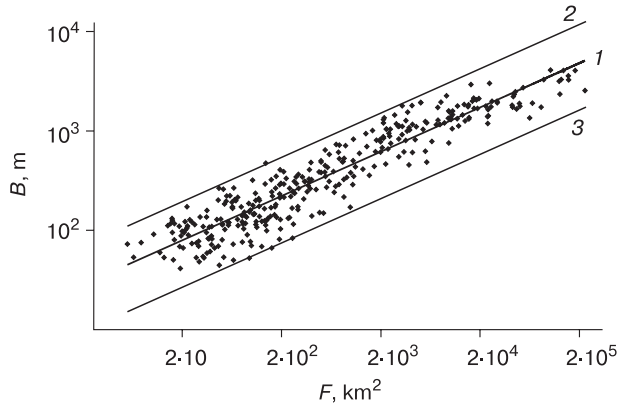

Fig. 4. Field of points (values F and B) for all considered sections:

(*1*) approximating dependence $B(F)$; (*2, 3*) upper and lower envelopes

The dependence between characteristics *B* and *F*, as estimated by R^2, turned out to be much closer than expected from theoretical concepts, despite the heterogeneity of the studied samples and their small volumes. In this case, the ranges of values β and especially α (Table 2) do not fully reflect the actual picture, which is more adequately represented by the graph (Fig. 3). Figure 3 indicates that the variations in the desired value *B* are mainly determined by parameter β, which varies within relatively narrow limits. The role of parameter ά in the given case is rather "technical", since it significantly affects *B* only beyond the considered range of catchment areas.

A clear representation of the statistically justified variations in the width of talik zones depending on the type of channel in each of the three basins is given in Table 3. It follows that the maximum values of *B* correspond to types C and D and the minimum values of *B,* to types A and B. For almost all values of *F*, except for the smallest streams, the largest transverse dimensions of taliks are confined to marginal basins.

Thus, despite the unconditional dominance of the flow size factor, the other two factors – the type of the channel and the marginal or continental type of the basin–play a significant role. If the first trend is theoretically expected (though weaker than expected), the second one requires additional investigation.

Figure 4 shows the area of all points considered for sections with an approximation line *B*(*F*) obtained by calculation (β = 0.4455, α = 20.8), and two lines parallel to it, which represent the top (α = 52.8) and lower (α = 7.08) enveloping the above area. The approximating line basically displays averaged widths of taliks near rivers of various discharges. However, it should be emphasized that we consider not the most probable value of *B*, but its most probable lower estimate. As noted above, measurements of the talik width are based on the principle of "no exaggeration". Therefore, the values of *B* obtained from statistical calculations are often significantly lower than the actual values. The two examples are provided below.

1. The Buyunda River in the Seimchan–Buyunda basin with a catchment area of 20,700 km^2 (point No. 77, Appendix, p. l). Earlier, an inner delta with an area of more than 200 km^2 and a talik of comparable size were formed in this place. In that period, the river split into numerous small channels. At present, the branching zone of the river has significantly decreased and corresponds to type B. According to the modern landscape features, the width of the talik zone does not exceed 1.7 km, which is less than the results of calculations by formula (1). By substituting the value α = 52.8 corresponding to the upper envelope of the area of points, *B* increases up to 4.4 km. The established width of the talik in the central part of the delta (along the highway) is 14 km [*Mikhailov and Bantsekina, 2001*]. However, at the upstream part of the delta, the talik width is limited by a relatively narrow branching zone (lightly more than 1 km). Downstream, talik areas are interspersed with expanding permafrost areas and then narrow down to the branching zone again. The talik zone within the inner delta is about 26 km long, and its average width does not go beyond the upper envelope in Fig. 4.

2. The Kubaka Creek, studied in detail over a 21-km-long segment [*Mikhailov and Ukhov, 1999*], where catchment area increases from 56 to 131 km^2 (outlet gate coordinates 63°40′08″ N, 159°58′34″ E). The channel is of type A. According to the landscape features, the maximum width of the talik (within a short segment) is 200 m. Calculations using formula (1) give *B* = 151 m. According to the results of instrumental measurements, the width of the talik varies from 140 to 510 m weakly correlating with *F*. The average value is about 330 m. According to G.N. Egorova [*1983*], geosystems, characteristic for the creek floodplain, are widespread in the basin of the Omolon River. This allows us to argue that a similar underestimation of the width of the talik is not an exception, but rather common, at least for one type of landscape. The key factor of talik development is the initiation of valleys along fault zones with increased fracturing of rocks [*Mikhailov and Ukhov, 1999*]. This allows us to assume that such extremely broad taliks are quite common in other river basins of the northeast of Russia. However, substituting into formula (1) the coefficient α calculated for the upper envelope, we obtain an ave-

Table 2. **Maximum and minimum of parameters of dependence (1) and corresponding sample sizes (*n*) by channel types and studied basins**

Parameter	Values max/min	Channel type	Basin	*n*
α	33.4 / 11.0	D B	Indigirka Kolyma	20 55
β	0.500 / 0.404	B A	Kolyma Marginal	55 18
R^2	0.963 / 0.826	D A	Indigirka Indigirka	20 16

Table 3. **Variations in *B* values calculated according to formula (1) for a number of fixed values of *F* in accordance with approximations of the dependence *B*(*F*) (Fig. 3)**

F, km^2	*B*, m max/min	Type of channel	Basin
20	126 / 50	C B	Indigirka Kolyma
200	316 / 166	C A, B	Marginal Indigirka, Kolyma
2000	832 / 457	C A	Marginal Indigirka
20 000	2290 / 1320	C, D A	Marginal Indigirka
200 000	6310 / 3470	C, D B, C	Marginal Indigirka

rage talik width of 384 m, which is even larger than the average value obtained by instrumental measurements.

So, the whole set of studied objects clearly reflects the diversity of transverse dimensions of floodplain taliks. Their *B* values with big probabilities lie within the limits outlined in Fig. 3 by lower and upper envelopes of the point area. In relation to the lower envelope, this statement is based on the applied method. The limiting position of the upper envelope is not just as obvious. Nevertheless, the latter was demonstrated using the above example of two taliks of outstanding transverse dimensions.

The data obtained also indicate the absence of the influence of climatic conditions on the size of floodplain taliks. Two regions most unfavorable for their development are the vicinity of the "cold pole" with the most severe winters and the Arctic coast with short and cold summers. The Agayakan River belongs to the first region, whereas the Ekiatap River belongs to the second region (nos. 3 and 331, respectively, see Appendix). According to the measurements, the widths of floodplain taliks of these rivers are greater than the values calculated by formula (1) by 15 and 27 %, respectively.

CONCLUSIONS

For the first time, statistically representative data on the width of floodplain taliks in river valleys within the region of their maximum abundance in the northeast of Russia and nearby areas obtained from the results of interpretation of remote sensing data on 340 valley sites are systematized. The sample used for the calculations represents the most diverse climatic conditions for the permafrost zone. Drainage areas of rivers in outlets of the selected sites vary widely, covering the entire range of floodplain talik areas from <20 to >200 thousand km^2. At the same time, they are quite evenly distributed over three large areas and among the distinguished types of river channels. The lower and upper limits of the transverse dimensions of thawed zones are 41.1 and 4100 m. Almost for the entire range of catchment areas, except for the smallest values, the minimum and maximum values of *B* at a fixed parameter *F* differ by less than tw times. The statistical dependence of the characteristics under consideration is approximated by a power function, and the parameters of this dependence are determined.

The width of taliks displays a tendency for a decrease from marginal coastal basins to central parts of mountain structures and directly depends on the degree of river channel branching. These tendencies are generally expressed quite distinctly. The results of the study indicate that it is possible to estimate the limits of variation in the width of thawed zones in river valleys for a given catchment and to determine the most probable minimum values of talik width. In the future, this approach in combination with field studies will contribute to the improvement of interpretation of remote sensing data. On this basis, it is planned to carry out the zoning of the northeast of Russia and adjacent territories according to the distribution of floodplain taliks and corresponding landscapes in river valleys.

References

Alekseev, V.R., 1968. On the role of geobotanical maps when studying frozen grounds. Dokl. Inst. Geogr. Sibiri i Dal'nego Vostoka, **17**, 20–26 (in Russian).

Chalov, R.S., 2017. Channel Processes (Riverbed Science). Moscow: INFRA-M, 569 p. (in Russian).

Chalov, R.S., 2019. On the morphological diversity and classification of braided river channels. Geomorfologiya, No. 3, 3–18 (in Russian).

Chebotarev, A.I., 1975. General General Hydrology (Land Waters). Leningrad: Gidrometeoizdat, 544 p. (in Russian).

Egorova, G.N., 1983. Morpholithosystems and the Landscape SPattern (by the example of the Omolon River Basin). Vladivostok: Izd. DVNTs Akad. Nauk SSSR, 164 p. (in Russian).

Egozi, R., Ashmore, P., 2008. Defining and measuring braiding intensity. Earth Surf. Process. Landf. **33** (13), 2121–2138.

Kalabin, A.I., 1960. Permafrost and hydrogeology of the northeast of the USSR. Tr. Vses. Nauchno-Issled. Inst.-1, vol. 18, 469 p. (in Russian).

Mikhailov, V.M., 2011. Morphodynamics of river channels in mountainous countries and lithology of bedrock. Geomorfologiya, No. 4, 11–21 (in Russian).

Mikhailov, V.M., 2013. Floodplain Taliks of the Russian Northeast. Novosibirsk: "Geo" Publ. House, 244 p. (in Russian).

Mikhailov, V.M., 2014. Variations and assessments of mean maximum water discharge in rivers of the Russian northeast. Byull. Sev.-Vost. Nauchn. Ts. Ross. Akad. Nauk, No. 2, 21–26 (in Russian).

Mikhailov, V.M., Bantsekina, T.V., 2001. Ground-filtration talik in the continental delta of the Buyunda River (Seymchan-Buyunda Depression). Kriosfera Zemli [Earth's Cryosphere], **V** (2), 20–28 (in Russian).

Mikhailov, V.M., Ukhov, N.V., 1999. Peculiarities of geocryological and groundwater regimes of the large floodplain talik in the Omolon River basin and accompanying landscape indicators. Kriosfera Zemli [Earth's Cryosphere], **III** (3), 50–58 (in Russian).

Nekrasov, I.A., 1967. Taliks in River Valleys and Regularities of Their Distribution on the Example of the Anadyr River Basin. Moscow: Nauka, 140 p. (in Russian).

Park, C.C., 1977. World-wide variations in hydraulic geometry exponents of stream channels: an analysis and some observations. J. Hydrol. **33** (1–2), 133–146.

Ponomarev, V.M., 1960. Groundwater in the Area of Deep Permafrost. Moscow: Izd. Akad. Nauk SSSR, 200 p. (in Russian).

Timofeev, D.A., 1981. Terminology of Fluvial Geomorphology. Moscow: Nauka, 1981, 268 p. (in Russian).

Voskresensky, S.S., 1985. Geomorphology of Placers. Moscow: Izd. Mosk. Gos. Univ., 204 p. (in Russian).

Vtyurin, B.I., 1964. Geocryological conditions of the Markovo Depression. In: Geocryological Conditions of the Western Siberia, Yakutia, and Chukotka. Moscow: Nauka, p. 115–133 (in Russian).

Zelenkevich, A.A, 1964. Hydrogeological structures and waterbearing complexes in the northeast of the USSR. In: Materials on the Geology and Mineral Deposits of the Northeast of the USSR, **17**, 200–208 (in Russian).

Received August 25, 2020
Revised December 18, 2021
Accepted January 18, 2022

Translated by E.S. Shelekhova

Appendix. **Data on the studied sites. Sheet 1**

No.	Name of watercourse	Geographic coordinates, N. Lat.–E. Long.	Catchment area, km^2	Talik width, m	Channel type
1	2	3	4	5	6
1	Agan	60°20′35″–150°54′02″	58.3	121	B
2	Agan	60°19′16″–150°56′31″	82.4	115	B
3	Agayakan	67°11′36″–135°40′56″	7630	1280	D
4	Adycha	67°11′36″–135°40′56″	55 000	2720	B
5	Amguema	67°53′22″–177°43′34″	26 700	1990	D
6	Anadyr	65°31′52″–168°52′54″	16 400	2920	D
7	Anadyr	64°52′00″–168°36′17″	47 300	2920	B
8	Anadyr	64°47′06″–169°28′44″	50 500	1660	B
9	Apuka	60°58′29″–170°27′33″	9780	1590	C
10	Apukavayam	61°01′31″–170°32′06″	5880	1210	C
11	Arga-Tirekhtyakh	66°31′02″–143°08′54″	560	348	D
12	Arga-Tirekhtyakh	66°32′25″–143°15′38″	555	642	D
13	Arkagala	63°14′30″–146°46′33″	506	382	D
14	Arkagala	63°08′30″–146°54′44″	831	487	D
15	Arkagala	63°02′29″–146°57′39″	1062	502	D
16	Arman	60°42′46″–150°38′56″	843	492	B
17	Arman	60°35′44″–150°39′38″	1070	825	D
18	Arman	60°32′45″–150°37′56″	1460	696	C
19	Arman	60°27′04″–150°32′22″	2090	678	B
20	Arman	60°13′35″–150°16′51″	2480	886	C
21	Arman	60°09′01″–150°15′53″	3030	1110	C
22	Arman	60°07′39″–150°14′19″	3100	1120	C
23	Arman	60°00′11″–150°16′45″	3620	1270	C
24	Arman	60°44′11″–150°13′46″	4170	1800	D
25	Arman	59°40′01″–150°09′18″	7590	1720	D
26	Achaivayam	61°01′24″–170°32′30″	3900	1080	B
27	Ayan-Tyryakh	62°25′17″–147°41′16″	14 300	1260	A
28	Ayan-Tyryakh	62°18′33″–147°44′22″	24 100	1400	A
29	Ayan-Tyryakh	62°50′32″–146°34′52″	4610	1100	B
30	Ayan-Tyryakh	62°44′17″–146°45′39″	12 300	1120	A
31	Bol. Anyui	66°45′02″–164°49′35″	16 920	1990	C
32	Balagannakh	65°46′19″– 145°47′10″	163	221	B
33	Balagannakh	65°42′14″–145°40′44″	81.2	76	A
34	Balagannakh	65°46′05″–145°42′32″	136	124	A
35	Balygychan	63°51′28″–154°15′54″	17 400	2140	B
36	Nameless	66°03′47″–164°44′41″	33.4	53	B
37	Nameless	63°17′17″–146°56′29″	21	95	B
38	Nameless	64°54′02″–143°50′29″	16.4	50	B
39	Nameless	64°54′05″–143°47′58″	25.2	74	B
40	Nameless	64°59′48″–143°38′57″	15.9	131	D
41	Nameless	65°00′14″–143°39′55″	16.8	117	C
42	Nameless	65°00′51″–143°40′10″	15.4	104	C
43	Nameless	65°05′05″–143°47′15″	14.4	111	C
44	Nameless	65°05′04″–143°47′46″	7.76	75	D
45	Nameless	65°06′27″–143°48′42″	6.52	53	D
46	Nameless	65°07′42″–143°39′06″	5.64	73	D
47	Nameless	65°21′47″–143°39′16″	50.8	80	A
48	Nameless	65°23′06″–143°41′13″	35.8	59	A
49	Nameless	65°25′43″–143°56′12″	20.6	66	B
50	Nameless	62°26′02″–155°32′38″	9	104	B
51	Nameless	62°26′36″–155°33′20″	15	108	A

Appendix, contined. Sheet 2

1	2	3	4	5	6
52	Nameless	62°31′53″–155°31′32″	40	82	C
53	Nameless	62°32′57″–155°32′24″	30	69	B
54	Nameless	62°38′21″–155°49′01″	28	563	D
55	Nameless	62°46′04″–155°49′05″	49	129	C
56	Nameless	60°15′58″–151°46′08″	40	109	B
57	Nameless	60°08′42″–151°46′59″	16	127	B
58	Belaya	65°31′54″–173°17′37″	44 700	2330	B
59	Belichan	63°01′48″–147°14′53″	128	123	A
60	Berelekh	63°35′27″–146°56′54″	917	341	B
61	Berelekh	63°28′25″–147°01′44″	1080	350	B
62	Berelekh	63°24′48″–146°05′38″	1230	595	B
63	Berelekh	63°21′40″–147°56′34″	1330	412	A
64	Berelekh	63°18′28″–147°17′20″	1550	357	A
65	Berelekh	63°18′40″–147°27′01″	1830	806	A
66	Berelekh	63°18′20″–147°40′00″	2540	750	B
67	Berelekh	62°58′08″–148°03′21″	5390	1040	B
68	Berelekh	62°28′52″–147°41′48″	9810	756	A
69	Berelekh	63°37′54″–146°56′34″	709	277	B
70	Bol. Keperveem	67°51′55″–166°13′49″	2790	1440	B
71	Bol. Peledon	65°31′23″–168°50′04″	3770	1540	B
72	Burgagchan	66°00′06″–164°44′15″	408	139	B
73	Burgagchan	66°01′26″–164°44′26″	488	151	B
74	Burgagchan	66°05′07″–164°42′07″	860	216	B
75	Burgagchan	66°12′21″–164°41′59″	2270	464	A
76	Burgagchan	66°17′16″–164°43′51″	3890	455	B
77	Buyunda	62°28′49″–153°26′48″	20 700	1590	C
78	Bergendya	60°39′06″–150°23′14″	138	293	A
79	Bergendya	60°38′01″–150°27′25″	271	310	A
80	Velikaya	63°53′37″–175°34′30″	25 200	3010	B
81	Vost. Khandyga	62°31′59″–135°37′49″	9950	1550	B
82	Vostochnyi	60°34′56″–150°51′52″	37.4	82	C
83	Gedan	60°12′51″–150°15′53″	482	387	B
84	Gedan	60°17′05″–149°59′30″	178	350	B
85	Goluboi	62°25′25″–155°42′05″	67	287	A
86	Dalnii	66°14′24″–161°40′11″	295	173	D
87	Debin	62°29′14″–149°41′27″	3460	616	B
88	Delyankir	63°48′50″–145°34′40″	3070	830	B
89	Dzhagun	62°46′46″–155°30′28″	40	88	B
90	Dzhana	54°41′00″–135°08′55″	3950	1020	B
91	Dich	60°28′55″–150°40′14″	26.9	114	B
92	Dondychan	60°31′48″–150°52′12″	89.6	136	A
93	Dondychan	60°34′10″–150°51′37″	105	145	A
94	Dukcha	59°42′53″–150°53′18″	120	174	B
95	Eemyu	63°40′00″–145°38′26″	2010	613	A
96	Elvat	66°04′25″–161°33′56″	86.8	140	A
97	Ermolaich	61°38′37″–144°45′56″	63.8	191	C
98	Eropol	65°15′23″–168°38′26″	10 700	1590	C
99	Echenka	65°03′28″–143°47′16″	10.4	91	D
100	Echenka	65°05′00″–143°47′22″	21.9	102	D
101	Echenka	65°06′54″–143°47′36″	73	215	C
102	Echenka	65°09′44″–143°41′30″	103	319	B
103	Echenka	65°10′23″–143°39′02″	212	389	C
104	Igandya	60°35′10″–150°23′01″	159	323	C

Appendix, contined. Sheet 3

1	2	3	4	5	6
105	Igandya	60°36′21″–150°24′27″	195	406	B
106	Igandya	60°38′15″–150°29′06″	506	486	C
107	Igandya	60°42′05″–150°34′35″	556	448	C
108	Igandya	60°42′43″–150°38′15″	612	582	C
109	Indigirka	66°26′03″–143°09′11″	127 000	3170	C
110	Indigirka	66°28′45″–143°08′32″	157 000	3580	D
111	Indigirka	64°31′34″–143°00′26″	83 500	1730	D
112	Indigirka	64°11′08″–142°02′07″	51 100	1770	C
113	Indigirka	63°28′02″–142°47′54″	24 500	1420	B
114	In'yali	65°14′28″–143°07′58″	3310	917	C
115	Inya	59°24′48″–144°54′03″	19 700	2120	C
116	Iran	62°00′54″–155°40′08″	17.0	80	C
117	Iregin'ya	65°25′03″–144°00′44″	161	669	B
118	Kadykchan	60°02′36″–150°45′39″	64.9	172	A
119	Kakhovka	62°38′36″–155°00′36″	114	107	B
120	Kegali	64°26′43″–161°09′08″	10 600	1050	B
121	Kedon	65°37′37″–159°23′55″	10 300	1300	B
122	Ken'elichi	61°40′04″–144°49′23″	345	310	D
123	Ken'elichi	61°41′02″–144°45′57″	225	333	C
124	Kipchistan-Tirekhtyakh	65°51′03″–143°51′05″	504	501	D
125	Kipchistan-Tirekhtyakh	65°48′55″–145°52′39″	299	365	A
126	Kipchistan-Tirekhtyakh	65°37′01″–143°51′21″	108	146	A
127	Kipchistan-Tirekhtyakh	65°38′17″–143°55′22″	180	135	B
128	Kipchistan-Tirekhtyakh	65°40′31″–144°01′08″	296	161	B
129	Kirik	60°09′35″–151°51′19″	111	200	B
130	Kolyma	62°07′51″–148°23′06″	42 600	1813	B
131	Kolyma	62°45′19″–152°33′23″	104 000	4100	A
132	Kolyma	62°54′25″–152°28′18″	129 000	2340	A
133	Kolyma	63°07′44″–152°32′03″	133 000	3290	B
134	Kolyma	63°57′05″–154°04′47″	140 000	4050	B
135	Kolyma	64°03′47″–154°26′27″	158 000	3260	B
136	Kolyma	64°22′27″–154°10′55″	184 000	4050	B
137	Kolyma	64°42′15″–153°35′12″	231 000	2540	A
138	Kontrand'ya	63°15′28″–146°56′20″	66.6	266	D
139	Kontrand'ya	63°12′22″–146°49′21″	194	212	D
140	Kuvet	69°14′16″–175°00′56″	4220	1160	D
141	Kulu	61°52′13″–147°25′21″	10 300	1310	B
142	Kulu	62°17′27″–147°29′12″	15 600	1320	B
143	Kuob	64°55′21″–143°44′50″	97.9	160	B
144	Kuobakh-Baga	64°56′52″–143°46′49″	81.3	140	B
145	Kuobakh-Baga	64°54′45″–143°40′31″	241	265	C
146	Kyrchan	62°24′22″–155°08′16″	73	129	B
147	Kyrchan	62°21′02″–155°04′06″	117	77	C
148	Ken	62°40′06″–155°29′07″	66	72	B
149	Ken	62°39′39″–155°30′42″	39	61	B
150	Kyuente	63°44′25″–142°14′42″	43 800	2220	D
151	Kyurbelyakh	64°26′06″–143°57′21″	214	216	B
152	Kyurbelyakh	64°25′36″–143°56′46″	176	265	A
153	Kyurbelyakh	64°22′31″–143°55′40″	143	99	A
154	Kyurbelyakh	64°17′34″–143°51′49″	112	122	B
155	Lev. Kuobakh-Baga	64°54′03″–143°49′13″	79.3	172	B
156	Lev. Kuobakh-Baga	64°53′48″–143°51′07″	51.4	116	A
157	Lev. Kuobakh-Baga	64°54′25″–143°43′11″	119	208	B

Appendix, contined. Sheet 4

1	2	3	4	5	6
158	Lev. Intakh	64°46′50″–143°59′53″	32.7	109	B
159	Lev. Intakh	64°47′01″–143°58′56″	22.8	110	B
160	Lev. Kyrchan	62°23′53″–155°13′01″	19.0	41	B
161	Lev. Omchikchan	62°13′19″–155°46′47″	197	217	A
162	Lev. Omchikchan	62°12′32″–155°44′19″	143	126	C
163	Lev. Tirekhtyakh	64°48′59″–143°40′05″	35.8	158	B
164	Lesistaya	61°10′08″–151°18′31″	121	138	A
165	Leshii	65°24′24″–143°52′23″	25.3	121	D
166	Leshii	65°25′46″–143°55′23″	42.7	66	B
167	Lyukinde	66°09′09″–143°40′39″	52.3	259	D
168	Lyukinde	66°08′37″–143°40′05″	46.4	201	C
169	Lyunkindala	65°00′28″–143°38′43″	18.8	110	C
170	Magadaven	60°31′44″–150°58′42″	56.6	222	C
171	Magadaven	60°34′46″–150°51′54″	136	165	D
172	Magadaven	60°35′57″–150°39′57″	393	263	D
173	Main	64°09′43″–171°02′08″	18 600	2050	C
174	Mal. Anyui	68°08′52″–163°19′43″	43 100	1740	D
175	Mal. Anyui	68°11′12″–163°40′34″	30 000	1990	D
176	Maltan	60°45′26″–151°45′30″	450	257	C
177	Maya	54°29′55″–134°37′29″	15 300	1750	C
178	Maykan	60°05′22″–151°44′53″	1005	380	A
179	Mikurde	66°06′22″–164°40′04″	995	171	A
180	Mitrei-Ongontakh	65°08′44″–144°00′07″	107	146	D
181	Molandzha	65°08′38″–160°43′03″	4490	816	A
182	Moma	66°26′24″–143°11′38″	30 200	1920	B
183	Morozov	60°05′30″–150°50′56″	70	199	A
184	Mukul’chan	60°39′12″–150°22′49″	104	178	C
185	Myaundzha	63°01′46″–147°14′52″	386	306	A
186	Myaundzha	63°01′50″–147°14′15″	514	264	C
187	Myaundzha	63°00′42″–146°58′31″	1050	288	A
188	Myaundzha	63°00′25″–147°03′42″	686	241	B
189	Naledнyi	65°38′15″–143°55′32″	87.5	117	B
190	Nankala	60°19′14″–150°56′50″	45.0	128	A
191	Nankala	60°17′03″–150°56′24″	53.8	184	A
192	Nachal’nyi	62°37′36″–155°53′16″	23.0	171	B
193	Nachal’nyi	62°38′27″–155°48′48″	23.0	106	C
194	Nachal’nyi	62°38′25″–155°47′01″	19.0	69	C
195	Nachal’nyi	62°38′37″–155°46′27″	10.0	75	B
196	Nevskii	62°20′30″–155°41′15″	156	138	C
197	Nevskiiй	62°17′48″–155°30′09″	111	114	C
198	Nelkandya	60°12′35″–150°40′48″	140	503	D
199	Nelkandya	60°17′02″–150°56′44″	55.8	196	D
200	Nelkandya	60°16′30″–150°55′32″	110	236	D
201	Neponyatnyi	62°31′06″–155°31′20″	172	143	B
202	Neponyatnyi	62°32′02″–155°29′48″	128	69	A
203	Nera	64°33′44″–143°23′34″	24 400	1640	B
204	Nera	64°31′25″–143°38′38″	24 200	1190	A
205	Nera	63°48′36″–145°35′23″	6610	783	C
206	Nera	63°51′50″–145°28′26″	9680	1340	C
207	Neryuchi	61°54′58″–147°16′12″	2140	874	B
208	Nimfa	62°28′40″–155°41′05″	33.0	54	D
209	Nosagchan	61°06′38″–151°17′25″	366	244	B
210	Nukh	60°14′35″–151°45′14″	756	610	C

Appendix, contined. Sheet 5

1	2	3	4	5	6
211	Oktyabrina	62°47′07″–155°49′16″	38.0	107	B
212	Oktyabrina	62°46′32″–155°44′28″	20.0	88	A
213	Oktyabrina	62°47′28″–155°50′29″	94.0	186	C
214	Oktyabrina	62°50′28″–155°56′33″	140	113	C
215	Oktyabrina	62°51′06″–156°02′19″	382	328	A
216	Ola	60°06′36″–151°45′42″	2190	1350	D
217	Oloi	66°28′07″–159°29′55″	23 100	1780	C
218	Oloi	65°40′52″–162°18′08″	15 700	1360	C
219	Oloichan	66°14′43″–161°34′46″	1120	435	C
220	Omolon	66°37′39″–159°31′22″	88 700	3280	C
221	Omchikchan	62°20′45″–155°41′33″	767	290	A
222	Omchikchan	62°24′50″–155°41′48″	856	326	A
223	Omchikchan	62°33′11″–155°51′15″	1736	439	B
224	Omchikchan	62°36′23″–155°54′30″	1785	618	B
225	Orlovka	66°47′20″–164°49′05″	2440	947	B
226	Orlovka	66°50′42″–164°57′19″	1990	819	B
227	Okhota	59°24′07″–143°00′40″	19 100	1680	C
228	Palatka	60°05′06″–150°55′00″	258	167	A
229	Pegtymel’	69°37′57″–174°12′20″	17 600	1680	D
230	Pekarnyi	62°28′40″–149°37′05″	262	247	D
231	Peschanaya	63°17′01″–177°59′37″	266	240	D
232	Pikas’vayam	61°57′46″–172°46′39″	2300	1040	D
233	Prav. Kuobakh-Baga	64°59′29″–143°41′40″	64.8	167	C
234	Prav. Kuobakh-Baga	64°58′53″–143°47′58″	35.4	136	C
235	Prav, Tiretyakh	64°51′06″–143°41′01″	67.8	203	B
236	Prav. Omchikchan	62°10′38″–155°47′02″	236	132	D
237	Prav. Omchikchan	62°06′44″–155°41′24″	66.0	50	A
238	Prav. Omchikchan	62°06′07″–155°37′03″	48.0	45	B
239	Prav. Omchikchan	62°09′28″–155°30′23″	23.0	90	C
240	Prav. Tadleoan*	64°42′27″–179°38′14″	177	181	D
241	Prav. Erucha	61°48′13″–144°53′56″	59.3	120	D
242	Pritochnyi	60°12′33″–150°40′16″	47.3	265	A
243	Propushchennyi	60°33′16″–150°30′39″	29.5	78	A
244	Propushchennyi	60°30′42″–150°32′03″	54.2	102	B
245	Pryamoi	66°12′23″–164°42′17″	197	103	D
246	Pryamoi	66°11′54″–164°45′21″	192	81	A
247	Razin	64°38′02″–143°47′59″	51.1	114	B
248	Razin	64°38′56″–143°45′18″	24.0	128	B
249	Razin	64°39′31″–143°44′27″	13.2	53	A
250	Sartang	65°17′38″–132°52′48″	3725	997	D
251	Svetlyi	60°46′15″–150°31′13″	30.5	136	C
252	Svetlyi	60°44′19″–150°40′48″	61.0	222	C
253	Sev. Pekul’neveem	65°33′19″–173°31′18″	574	271	D
254	Seimkan	60°02′30″–149°11′53″	2900	1180	D
255	Seimchan	62°55′39″–152°27′42″	3600	803	D
256	Sol’veig	62°25′35″–155°46′41″	85.0	152	A
257	Sol’veig	62°23′19″–155°51′28″	46.0	69	A
258	Srednii	66°03′14″–164°45′13″	95.6	53	B
259	Srednii	66°03′23″–164°46′18″	52.8	54	A
260	Sugoi	64°14′52″–154°30′58″	26 100	1750	D
261	Sugoi	62°33′59″–155°59′36″	5680	624	A
262	Sugoi	62°40′17″–155°56′31″	5880	485	D
263	Suntar	63°20′19″–141°44′16″	7990	1160	D

Appendix, contined. Sheet 6

1	2	3	4	5	6
264	Suruktakh	65°20′00″–132°50′19″	610	310	D
265	Sukhoi	60°43′35″–150°39′22″	16.0	95	C
266	Tagargacha	64°31′43″–143°45′53″	338	207	B
267	Tagargacha	64°35′58″–143°36′20″	274	236	A
268	Tamnar	65°38′15″–143°24′32″	21.5	122	B
269	Tap	62°01′58″–155°44′06″	193	232	C
270	Tap	62°03′07″–155°48′55″	213	292	D
271	Tap	62°00′52″–155°59′08″	286	295	B
272	Taskan	62°45′02″–150°47′40″	8850	1200	D
273	Takhtayama	60°14′38″–154°44′46″	5110	1927	D
274	Tverdyi	64°37′03″–143°51′40″	29.9	48	B
275	Tingkalakh	65°06′24″–133°00′49″	863	5360	D
276	Tirekh	61°11′36″–151°17′42″	12.0	69	A
277	Tirekhtyakh	67°33′57″–137°08′33″	1430	938	D
278	Tikhon-Yuryakh	66°00′00″–145°23′20″	673	390	B
279	Tikhon-Yuryakh	65°54′03″–145°28′52″	552	385	A
280	Tikhon-Yuryakh	65°39′55″–145°25′19″	266	115	A
281	Tikhon-Yuryakh	65°38′33″–145°24′47″	243	134	A
282	Tangakhchan	60°30′15″–150°28′05″	20.1	98	B
283	Tangakhchan	60°30′34″–150°31′34″	35.3	95	A
284	Tangakhchan	60°29′44″–150°33′36″	95.8	153	B
285	Trezor	62°51′58″–155°46′20″	40.0	72	B
286	Trezor	62°51′27″–155°52′29″	197	128	A
287	Tymtei	63°47′05″–145°39′14″	4220	607	D
288	Tyry	62°21′58″–135°49′39″	14 000	1840	D
289	Tetemveem	67°49′44″–165°53′57″	3070	549	D
290	Teuterendzh	62°19′25″–155°01′26″	100	70	B
291	Teuteredhzek	62°20′08″–155°00′00″	261	80	B
292	Ugulan	60°27′06″–155°11′08″	2150	1200	C
293	Uda	54°40′01″–135°08′34″	46 000	2470	D
294	Uzelok	62°20′48″–155°02′18″	147	132	B
295	Ukelayat (Ugulan)	61°44′31″–173°30′11″	2150	1300	D
296	Ukelayat	61°57′17″–172°45′28″	3320	1790	D
297	Ulu-Tumul	65°06′37″–132°57′21″	405	324	D
298	Ul'beya	59°22′41″–144°25′12″	13 500	1450	D
299	Ul'ya	58°52′01″–141°50′00″	15 500	1830	D
300	Ulyagan	65°18′26″–160°47′24″	2010	778	B
301	Urak	59°17′39″–142°50′27″	10 700	1460	D
302	Utesnyi	60°31′53″–150°40′17″	36.8	83	A
303	Uchyugei-Yuryakh	64°45′43″–143°38′58″	91.0	90	A
304	Faraon	60°15′08″–149°43′20″	193	287	D
305	Final'nyi	60°30′01″–150°34′47″	58.9	112	A
306	Finish	60°33′40″–150°39′47″	73.6	112	A
307	Khasyn	60°09′37″–151°02′56″	199	296	B
308	Khasyn	60°07′40″–150°58′47″	283	344	B
309	Khasyn	60°05′36″–150°55′04″	327	344	B
310	Khasyn	60°04′55″–150°54′00″	588	430	C
311	Khasyn	60°05′18″–150°49′33″	718	731	B
312	Khasyn	60°03′22″–150°43′42″	892	710	B
313	Khasyn	60°03′55″–150°42′10″	773	720	C
314	Khasyn	60°02′06″–150°41′41″	1670	1010	A
315	Khasyn	59°44′28″–150°17′28″	3330	1110	A
316	Khatachan	60°17′46″–149°23′12″	346	310	B

Appendix, contined. Sheet 7

1	2	3	4	5	6
317	Khatys-Yuryakh	65°18′42″–143°47′40″	81.1	122	B
318	Khatys-Yuryakh	65°19′59″–143°39′13″	121	200	B
319	Kheta	61°06′23″–151°20′22″	773	525	C
320	Khilgalin	60°07′10″–150°13′35″	386	407	A
321	Khudzhakh	63°47′26″–145°39′49″	2390	658	D
322	Chalbyga	60°00′36″–150°32′41″	400	481	B
323	Chapchik	62°27′47″–155°40′43″	535	149	D
324	Chapchik	62°29′18″–155°36′06″	375	282	B
325	Chapchik	62°30′40″–155°32′05″	174	173	B
326	Charky	66°50′20″–137°02′33″	7330	1150	D
327	Chelomdzha	59°51′55″–148°12′50″	12 000	1780	D
328	Egelyakh	64°28′15″–143°51′57″	250	219	B
329	Egelyakh	64°24′39″–143°46′31″	158	169	B
330	Egelyakh	64°20′14″–143°38′22″	64.2	171	B
331	Ekiatap	69°07′21″–179°01′49″	5690	1240	D
332	Ekityki	67°40′02″–178°46′05″	10 300	1380	D
333	El’gi	64°16′28″–142°05′57″	68 200	1905	B
334	El’gi	64°18′25″–141°52′25″	64 100	1349	B
335	Emtegei	62°58′35″–146°52′34″	2160	847	A
336	Enmyvaam	66°16′52″–173°31′55″	11 900	1326	D
337	Yablon’	65°23′11″–168°32′21″	9280	2254	D
338	Yama	59°50′32″–153°18′04″	12 200	1550	D
339	Yana	59°46′27″–149°12′01″	8160	1946	D
340	Yana	60°22′47″–148°28′06″	2520	1040	C

* Western Hemisphere.

Earth's Cryosphere, 2022, vol. XXVI, No. 2, pp. 34–41

FLUORIDE DISTRIBUTION IN SUBPERMAFROST GROUNDWATER IN CENTRAL YAKUTIA

N.A. Pavlova, S.V. Fedorova

Melnikov Permafrost Institute, Siberian Branch of the Russian Academy of Sciences, Merzlotnaya str. 36, Yakutsk, 677010 Russia; na-pavlova@yandex.ru

We studied the distribution of fluoride (F^-) in fresh and moderately mineralized waters of subpermafrost aquifers in Central Yakutia. We analyzed the data archive of 296 water samples collected by the Melnikov Permafrost Institute staff members during hydrochemical surveys between 1984 and 2019. The average fluoride concentrations varied between 5 and 10 mg/L. Highest concentrations (up to 15.5 mg/L) were determined in waters of the terrigenous aquifers over the crystalline basement. The sources of fluoride can likely be the various fluorine-bearing minerals of aluminosilicate rocks. The high fluoride concentrations in these aquifers are associated with geochemistry (alkaline medium and sodium bicarbonate water type) resulting from cryogenic metamorphism of rocks. Lowest concentrations (0.4–0.8 to 2–3 mg/L) were found in subpermafrost water samples collected from boreholes near the Lena River channel. These low concentrations indirectly indicate the presence of open taliks under the channel and the infiltration of stream water into the subpermafrost aquifers.

Keywords: *artesian basin of Yakutia, subpermafrost water, permafrost, low groundwater circulation zone, chemical composition, fluoride*

INTRODUCTION

Surface waters are the main source of fresh drinking water in the continuous permafrost area of Central Yakutia. Waters of hydrogenous taliks, as well as subpermafrost waters are less commonly used. Concentration of fluoride is one of the water quality indicators. The optimal concentration lies within the range of 0.5–1.0 mg/L, while the maximum allowable concentration cannot exceed 1.2–1.5 mg/L [*Fordyce et al., 2007; Ozsvath, 2009; Donskikh, 2013; WHO, 2017; Yousefi et al., 2019*]. Long-term consumption of water with high fluoride concentration (>1.5 mg/L) has a toxic effect on the musculoskeletal, neuroendocrine, and cardiovascular systems, while the low concentrations (<0.5–0.6 mg/L) lead to the development of dental caries [*Brindha and Elango, 2011; Donskikh, 2013*].

Fluorine enters water solutions from rocks, in which it is normally present as a component of sellaite (MgF_2), fluorite or fluorspar (CaF_2), cryolite (Na_3AlF_6), and fluorapatite ($Ca_5(PO_4)_2F$) minerals. The fluorine abundance in the lithosphere is estimated at 400–800 mg/kg [*Vernadsky, 1955; Yanin, 2007*]. The highest content of fluorine is in granites: 500 to 1400 mg/kg [*Krauskopf and Bird, 1995*], 810 mg/kg on the average [*Wedepohl, 1969*]. Its content reaches 330 mg/kg in calcareous rocks, sands, and sandstones and is up to 610 mg/kg in clays and shale [*Grigoriev, 2009*]. The concentration of fluoride in ocean water is approximately 1.3 mg/L [*Turekian, 1972; Bordovsky and Ivanenkov, 1979; Gordeev, 1983*]. The range of fluoride concentrations is wide in fresh and slightly saline natural waters: from trace amounts in river water to 16 mg/L and higher in underground aquifers [*Gordeev, 1981; Kraynov and Shvets, 1987; Shvartsev et al., 2007; Anichkina, 2016*]. Normal fluoride concentrations in natural waters are often exceeded in tropical climate [*Shvartsev et al, 2007; Brindha and Elango, 2011; Subba Rao, 2017; Malago et al., 2017*]. Evaporative concentration, ion exchange, and technogenic groundwater pollution by wastewaters from various sources (chemical, rubber, electrical industry, non-ferrous and ferrous plants, mechanical engineering, as well as coal-fired power plants) are the main processes that lead to the formation of fluoride-rich waters) [*Kraynov and Shvets, 1987; Shvartsev et al., 2007; Yanin 2007*].

Data on fluoride concentrations in fresh groundwaters in permafrost areas are rather scarce and mainly concern water in the zone of free water exchange. It is known that the fluoride concentration in the groundwater of West Siberian artesian basin lies within sanitary standards [*Beshentsev, 2013*]. The prevailing concentration of 0.2–0.6 mg/L is observed in the spring water of Chita region with isolated permafrost distribution [*Zamana et al., 2011*]. The average fluoride concentration of 0.1–0.3 mg/L is found in supra-permafrost waters of arctic and subarctic regions of Russia, Alaska, and Canada [*Shvartsev, 1978*], while in mountainous fluorine-bearing provinces it can reach 0.7 mg/L [*Kraynov and Shvets, 1987*]. The concentration of fluorine varies from trace amounts to 0.4 mg/L in fresh groundwater of the Aldan Highland (East Siberia) with discontinuous permafrost [*Filimonova, 1977*]. Elevated concentrations of fluoride (up to 2.7 mg/L) have only been documented in water samples extracted from exploration-al boreholes in river valleys over large tectonic faults.

Earlier, the analysis of fluoride concentrations in subpermafrost groundwater confined to the zone of impeded water exchange in was conducted by N.P. Anisimova and T.M. Golovanova [*Anisimova, 1958, 1981; Anisimova and Golovanova, 1972*]. These

works pointed out the significant (one-order magnitude) differences in fluoride concentrations that could be observed within groundwater of the same aquifer. It was also found that the concentration of fluoride in subpermafrost groundwater increases with an increase in waster alkalinity and the concentration of sodium bicarbonates.

At present, there is a large amount of data on fluoride concentrations in groundwater of Central Yakutia, which requires the synthesis and analysis. The aim of this study is probability assessment of finding elevated fluoride concentrations within aquifers of this region.

MATERIALS AND METHODS

Main sources of information for this study were legacy hydrochemical data collected in Central Yakutia by staff members of the Melnikov Permafrost Institute, Siberian Branch of the Russian Academy of Sciences in 1984–2019 and data from repositories of various geological organizations. To characterize the chemistry of subpermafrost aquifers and the concentration of fluoride in them, data on 296 water samples were analyzed. Most of the samples (153 samples) were obtained in the city of Yakutsk and its vicinities. Nowadays, there are about 50 deep water wells providing technical water supply to various enterprises. Water treatment systems including defluorination of subpermafrost water and its use for drinking purposes are installed on several of these drilled wells. Less studied are fresh and slightly saline (<3 g/L) subpermafrost waters of the Lena–Aldan (134 samples) and Lena–Vilyui (nine samples) interfluves. Hydrochemical data from samples of lake and river water (183 samples) were also considered for fluoride concentration assessment in surface waters.

Water samples with the total mineralization of less than 3 g/L were considered while processing the results of chemical analyses. Fluoride concentrations in water were determined by potentiometric method. Before 2000, an electrode system consisting of a fluoride selective electrode and a silver chloride reference electrode. Later, an ion-selective single-crystal lanthanum fluoride membrane electrode was applied.

NATURAL CONDITIONS OF CENTRAL YAKUTIA

Study area is located within the Central Yakutian accumulative plain with absolute heights ranging between 200 and 400 m asl in the middle reaches of the Lena River and its tributaries Aldan and Vilyui. Snowmelt and rainwater are the main sources of river discharge. The contribution of groundwater is only about 13–17 % [*Dzhamalov et al., 2012*]. In rivers, the content of total dissolved solids (TDS) during the summer usually does not exceed 0.05–0.4 g/L; the chemical composition is dominated by bicarbonate and magnesium and calcium ions; the reaction is neutral. In winter, the TDS contents increases up to 0.3–0.7 g/L under the lack of atmospheric precipitation, and the chemical composition turns to chloride-bicarbonate with mixed cations [*Anisimova and Pavlova, 2014*]. In low-water winter conditions, the TDS content in the Vilyui and Aldan rivers is 0.1–0.2 g/L higher compared to that in summer without changes in dominating ions. In winter, small rivers/streams do normally freeze to the bottom. Average fluoride concentrations in these streams do not significantly differ from average concentrations in rivers beyond the permafrost zone and do not reach optimal levels for drinking purposes.

Lakes of various geneses are widespread in the study area. Ionic composition of freshwater lakes is of the bicarbonate calcium–magnesium or magnesium-calcium types [*Anisimova, 1981*]. Slightly saline (1–3 g/L) lake waters are dominated by bicarbonates among anions, and by sodium and magnesium among cations. Water pH varies from neutral to strongly alkaline values; fluoride concentration, from 0.2 to 1.1 mg/L reaching 1.7–2.3 mg/L in closed thermokarst and erosional-thermokarst lakes.

In terms of hydrogeology, the area belongs to the Yakutsk artesian basin, the sedimentary cover of which consists of terrigenous-carbonate deposits of Paleozoic and Mesozoic ages. In general, the sedimentary cover deposits lie gently with an inclination towards the inner part of the basin. Sediment thickness reaches 1–4 km and more decreasing in to 538–890 m the area of Yakutsk arch uplift [*Balobaev et al., 2003*]. The territory is underlain by continuous permafrost with the average thickness of 300–450 m reaching the maximum of 885 m within the Buotama–Amga interfluve [*Balobaev et al., 2003*]. A significant decrease in permafrost thickness and appearance of open taliks can only be observed under the Lena River channel, its main tributaries, and under several lakes.

Under the regional cryogenic aquiclude, there are subpermafrost aquifers with hydrological regimes depending on the long-term climatic changes. Nowadays, permafrost is being thawed from the bottom [*Balobaev, 1991*]. Most of researchers explain the low water pressure and low salinity of subpermafrost waters in the central part of the artesian basin by the uplift of permafrost base [*Kononova, 1973; Romanovskii, 1983; Shepelev et al., 1984; Balobaev et al., 2003*]. The composition of trace elements in subperamfrost waters is relatively stable. Fluorine is one of the constantly occurring elements.

SUBPERMAFROST WATERS AND FLUORIDE DISTRIBUTION

In Central Yakutia, subpermafrost waters occur within the Archean formations of the crystalline basement and aquifers of the sedimentary cover com-

posed of carbonate rocks of the Upper Proterozoic (Vendian) and Cambrian, as well as terrigenous Jurassic and Cretaceous deposits (Fig. 1).

Archean basement rocks consist of biotite gneisses, granite-gneisses, and crystalline schist. These are located at depths of 560–589 m in the central part of Yakutsk arch uplift and at a depth of 1022 m in the Amga trough [*Balobaev et al., 2003*]. The water content in the basement rocks is relatively low. The TDS content in the basement groundwater is 4.0–4.3 g/L; the ionic composition is dominated by sulfate or sulfate–bicarbonate anions and sodium cations. There is no information about the fluoride concentrations in these waters, except for a single borehole drilled on the floodplain of the Lena River. In this borehole, the concentration of fluoride in groundwater of Archean rocks is 2.2 mg/L. However, this value can possibly be not representative, because the borehole is close to the open talik under the Lena River channel. Northward, in the area of the Yakutsk arch uplift, the concentration of fluoride in groundwater of Archean and Lower Jurassic aquifers reaches 8.8–9.0 mg/L.

The Vendian and Lower Cambrian rocks are represented by fractured dolomites and dolomitic limestones bituminous to varying degrees. These rocks were studied in the southern part of Central Yakutia up to the latitude of Yakutsk. They are located at depths ranging from 285 to 520 m. The TDS content in the groundwater of these aquifers is 3.5–4.4 g/L; in the chemical composition, sulfate or bicarbonate–chloride anions and sodium cations predominate; less often, there is mixed cation composition; the reaction is neutral or slightly alkaline; fluoride concentrations vary from 1.7 to 4.4 mg/L.

The Middle Cambrian deposits are widespread within the northern flank of the Aldan anteclise, except for the Yakutsk uplift, where Jurassic deposits overlie Archean formations [*Balobaev et al., 2003; Shepelev and Makogonova, 2010*].

The Middle Cambrian aquifer is composed of limestones, marls, and dolomites. It has been found while drilling at depths ranging from 180 to 422 m. The TDS content in the groundwater of this aquifer is within 0.9–1.9 g/L. The fluoride concentration in bicarbonate and chloride–bicarbonate water with neutral or slightly reaction varies within 3.4–8.8 mg/L (Figs. 2 and 3). Less often, the Middle Cambrian deposits contain bicarbonate–sulfate water with mixed composition of cations, neutral reaction, and fluoride concentration of 1.3–2.2 mg/L.

In Yakutsk, aquifers associated with terrigenous Jurassic and Cretaceous rocks have been studies rela-

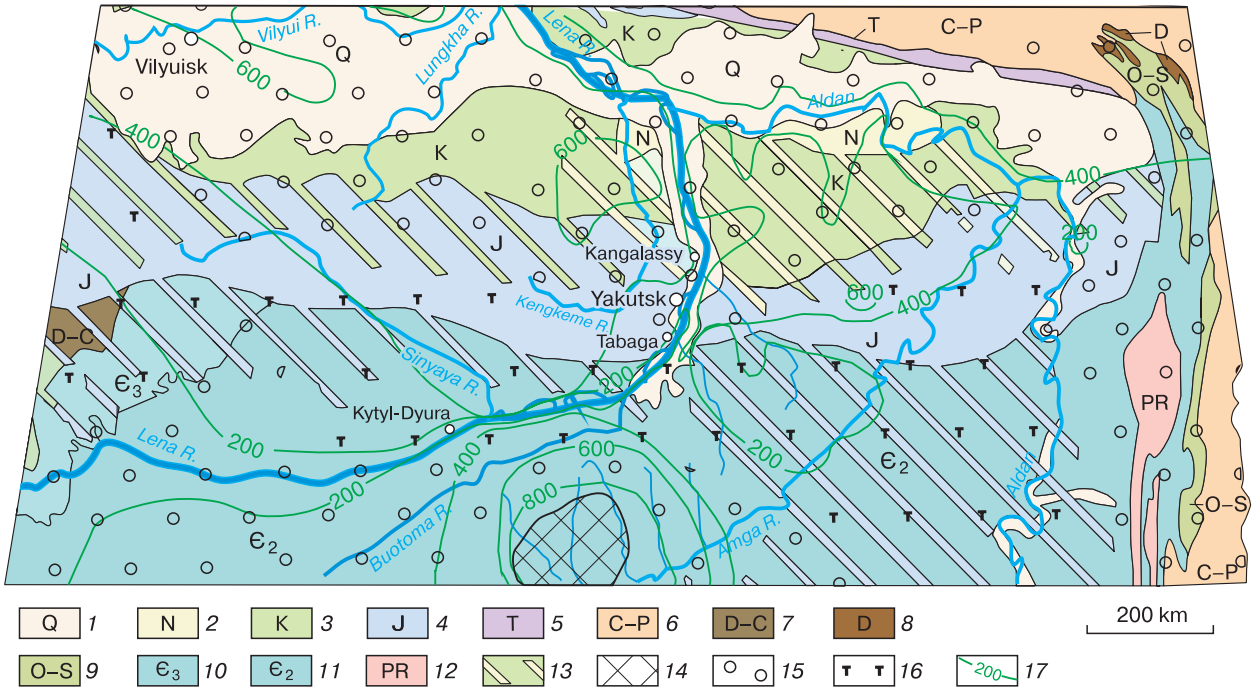

Fig. 1. Schematic hydrogeological map of the study area (modified after [*Efimova and Zaitsev, 1970*; *Melnikov and Tolstikhin, 1983; Balobaev et al., 2003; Semenov and Zheleznyak, 2018*].

Aquifers within: (*1*) Quaternary, (*2*) Neogene, (*3*) Cretaceous, (*4*) Jurassic, (*5*) Triassic, (*6*) Carboniferous and Permian, (*7*) Devonian and Carboniferous, (*8*) Devonian, (*9*) Ordovician and Silurian, (*10*) Upper Cambrian, (*11*) Lower Cambrian, and (*12*) Upper Proterozoic deposits; (*13, 14*) sediment complexes that do not contain gravity water in the liquid phase: (*13*) frozen aquifers (the color of narrow bands corresponds to the age of the frozen complex, and the background color corresponds to the age of the first aquifer from the surface), (*14*) absence of subpermafrost water in the basin's sedimentary cover; TDS content: (*15*) <1 g/L, (*16*) 1–3 g/L; (*17*) isolines of the thickness of the cryogenic aquiclude.

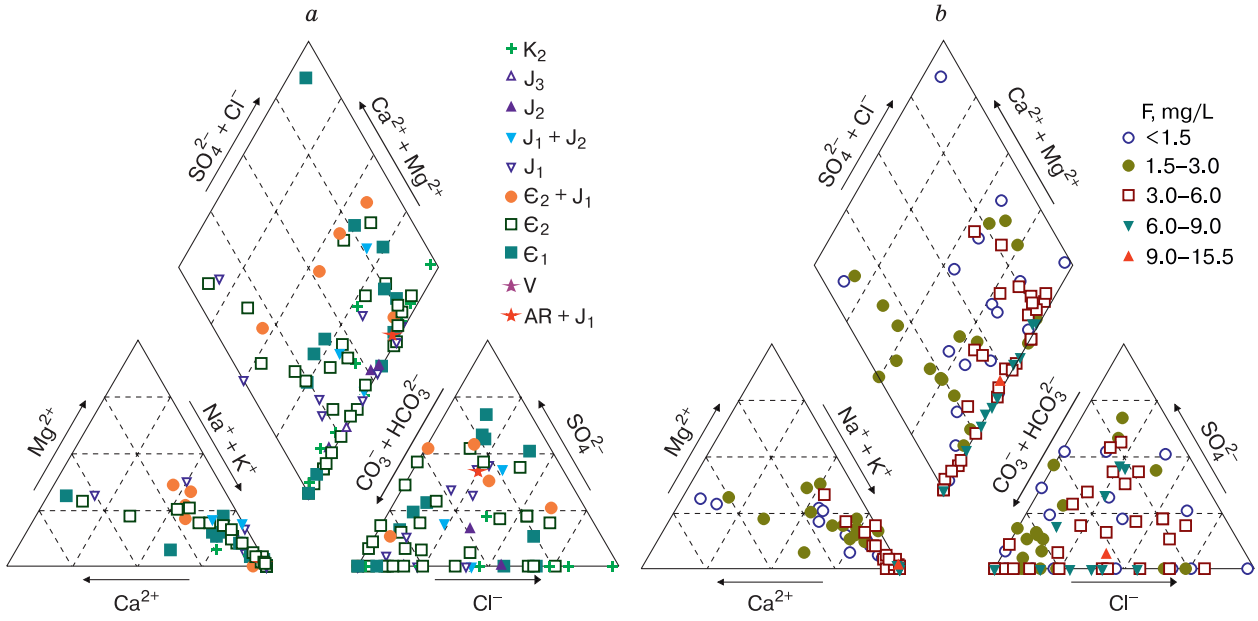

Fig. 2. Piper diagrams of the macrocomponent composition of groundwater (*a*) and fluoride concentrations (*b*) in different aquifers of the Lena–Aldan interfluve.

K_2 – Lower Cretaceous aquifer, J_3 – Upper Jurassic aquifer, J_2 – Middle Jurassic aquifer, $J_1 + J_2$ – jointly sampled Middle and Lower Jurassic aquifers, J_1 – Lower Jurassic aquifer, $Є_2 + J_1$ – jointly sampled Lower Jurassic and Middle Cambrian aquifers, $Є_2$ – Middle Cambrian aquifer, $Є_1$ – Lower Cambrian aquifer, V – Vendian aquifer, $AR + J_1$ – jointly sampled Lower Jurassic and Archean aquifers.

tively well [*Balobaev et al., 2003; Shepelev and Makogonova, 2010; Pavlova and Fedorova, 2020*]. Scarce data on these aquifers are available for the Lena–Amga and Lena–Vilyui interfluves. At the base of the Lower Jurassic section, there are basal conglomerates overlain by quartz and feldspar–quartz sandstones with siliceous and ferruginous cement. This layer is overlain by marine deposits (sandstones interbedded

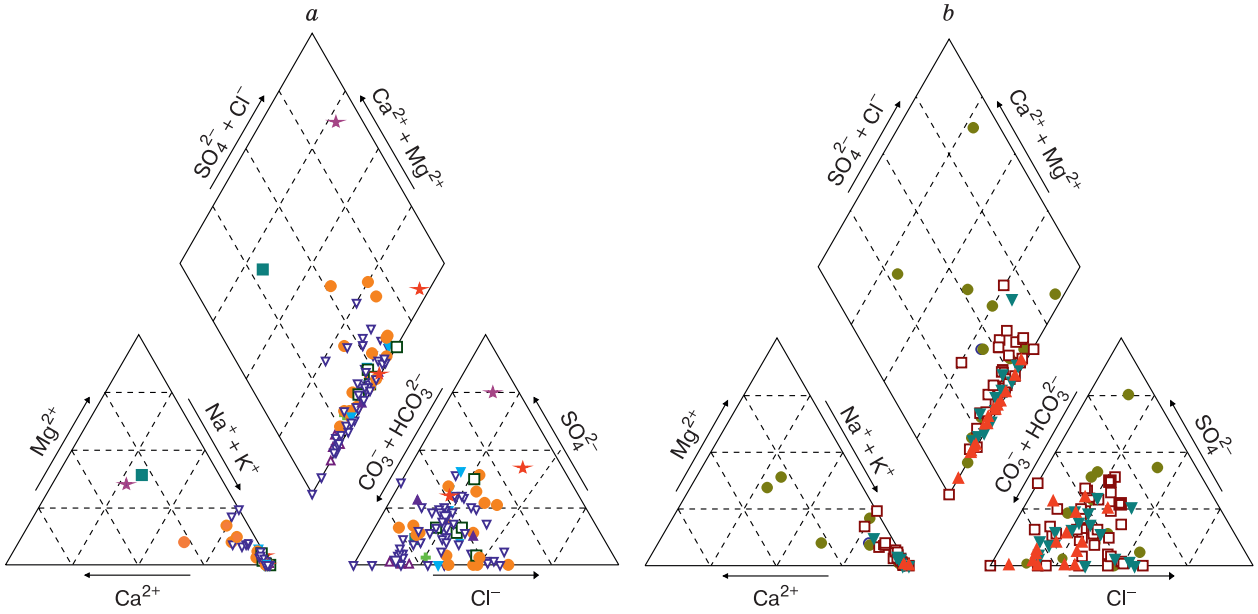

Fig. 3. Piper diagrams of the macrocomponent composition of groundwater (*a*) and fluoride concentrations (*b*) in different aquifers of the Lena–Vilyui interfluve.

For legend, see capture to Fig. 2.

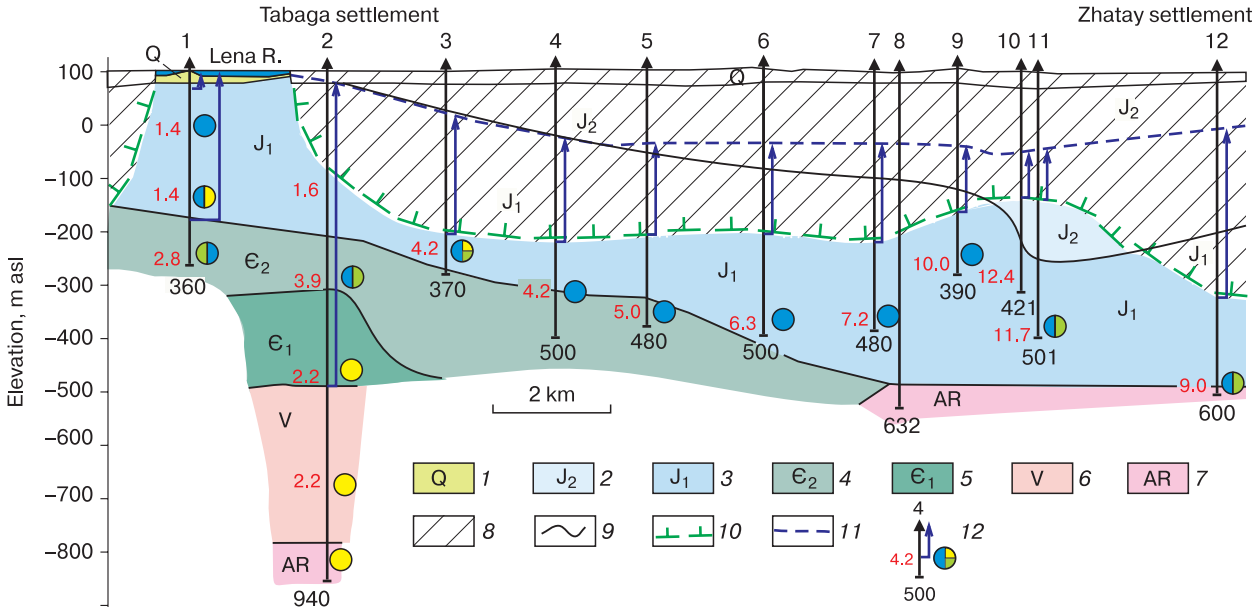

Fig. 4. Hydrogeological section along the line between Tabaga and Zhatay settlements (drawn according to legacy data of the Melnikov Permafrost Institute, Siberian Branch of the Russian Academy of Sciences).

Aquifers: (*1*) Quaternary alluvial, (*2*) Middle Jurassic terrigenous, (*3*) Lower Jurassic terrigenous, (*4*) Middle Cambrian carbonate, (*5*) Lower Cambrian carbonate, (*6*) Upper Proterozoic terrigenous-carbonate, (*7*) locally aquiferous fractured zone of the Archean crystalline basement; (*8*) cryogenic aquiclude; (*9*) boundaries between deposits of different ages; (*10*) permafrost boundary; (*11*) piezometric level of subpermafrost water; (*12*) hydrogeological borehole (figure at the top is its id number, figure at the bottom is the borehole depth, m; on the left, fluoride concentration in water (mg/L) is indicated). The color corresponds to the dominating anions in the water: blue – bicarbonate, yellow – sulfate, green – chloride. Arrows indicate groundwater pressure.

with siltstones and rare lenses of limestones and shell rocks). In the Lena–Amga interfluve, the Lower Jurassic aquifer lies at a depth of 563 m, while in the

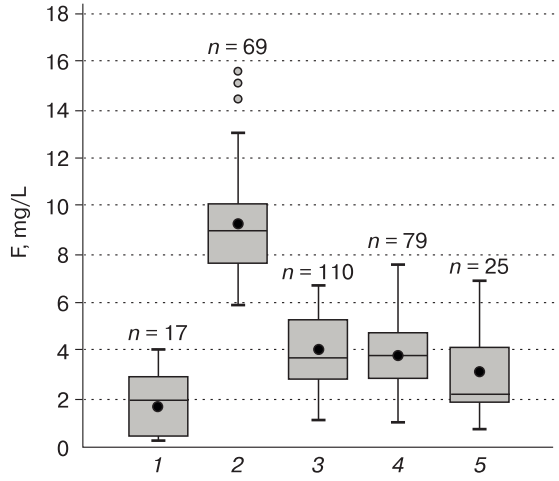

Fig. 5. Boxplots of fluoride concentration in subpermafrost water of Central Yakutia (*n* – sample size).

1 – Cretaceous and Upper Jurassic aquifers; *2*, *3* – Lower Jurassic aquifer complex (*2* – over crystalline basement rocks in the area of the Yakutsk arch, *3* – over Cambrian deposits); *4* – jointly sampled Lower Jurassic and Middle Cambrian aquifers; *5* – Middle Cambrian aquifer.

area of Yakutsk, at 173–420 m. In a larger part of the city, the subpermafrost water of this aquifer is hydraulically connected with the Middle Cambrian aquifer; together, they represent a single pressure system of formation water in pores and fractures [*Balobaev et al., 2003*].

Water-saturated Middle Jurassic formations were studied in the north of Yakutsk. These formations consist of sands interbedded with siltstones, silt, and quartz fine-grained sandstones; clays and shales are often found in the section. The top of this aquifer lies at a depth of 380–500 m [*Shepelev and Makogonova, 2010*]. The Upper Jurassic aquifer is found to the north of Kangalass Promontory latitude . It consists of continental formations (sands and sandstones with interlayers and lenses of coal) at depths of 200–540 m. It's top descends to depths 1800–2496 m within the Lungkhinskaya and Nizhnealdanskaya depressions, where the Lower Cretaceous subpermafrost aquifer composed of interbedded sands, sandstones, mudstones, and clays is the closest to the surface. In the Nizhnealdanskaya depression, water-saturated Lower Cretaceous deposits lie under the permafrost with a thickness varying from 270 to 415–610 m.

In general, the concentration of fluoride varies within the range of 4.1–11.7 mg/L in subpermafrost waters confined to the Lower and Middle Jurassic de-

posits. Local rise in its concentration (9.0–15.5 mg/L) is observed in the area of Yakutsk arched uplift (Fig. 4). This uplift can be traced in a series of boreholes on the left bank of the Lena River in the northern part of Yakutsk (Lake Beloe, Zhatay, and Markha settlements), and on the right bank in the Tekhturskaya borehole (in the mouth of the Suola River). Here, Cretaceous deposits overlie the Archean rocks (depths ~560–600 m), whereas Cambrian aquifers are absent. The TDS content in water of Jurassic aquifer is 0.9–1.5 g/L; sodium bicarbonates predominate (Figs. 2 and 3). This water has a somewhat increased alkalinity (slightly to moderately alkaline reaction). The proportion of calcium, which could form secondary minerals with fluorine, can rarely reach 2 % (mg-eq/L).

Subpermafrost groundwater of the slightly lithified Cretaceous and Upper Jurassic rocks has the TDS content of 0.5–1.2 g/L; it is of the sodium chloride–bicarbonate or bicarbonate composition and has the fluoride concentration of 1.6–4 mg/L.

DISCUSSION

Fluoride concentration in subpermafrost water of Central Yakutia varies in the range of several tenths to 15 mg/L. There is no evident direct relationship between the fluoride concentration and the aquifer depth, as well as the modern thickness of overlying cryogenic aquiclude. However, the influence of long-term freezing on the accumulation of fluoride in the subpermafrost groundwater cannot be excluded. It is known that the dissolution of fluorine minerals increases under alkaline conditions in water with the TDS content of 0.7–1.7 g/L [*Saxena and Ahmed, 2001*]. Cryogenic transformation of subpermafrost water in Central Yakutia–precipitation of difficultly soluble calcium carbonates during freezing of aquifers, desulfatization (sulfate reduction) of water under anaerobic conditions in the presence of organic matter – is the main control of increased alkalinity and low calcium concentration [*Kononova, 1973; Anisimova, 1981; Fotiev, 2009*]. The desulfatization process is possible under both degradation and aggradation of permafrost [*Anisimova, 1981*]. The fluoride source is the aquifer rock. The concentration of fluoride in subpermafrost water considerably increases under conditions of impeded water exchange and changes in the base of the cryogenic aquiclude within the Yakut arch uplift, where terrigenous sandstones of the Lower Jurassic aquifer are in contact with fluorine-rich granitic rocks (Fig. 5). According to V.T. Balobaev [*1991*], the modern (~10 000 years) uplift rate of permafrost base around Yakutsk can be estimated at 1.7 cm/yr and is due to lower values of heat flux in the frozen zone compared to the thawed subpermafrost zone. While permafrost is degrading, alkaline confined aquifer water migrates into the thawed rock layers and mixes with the low-mineralized water [*Kononova, 1973; Anisimova, 1981*]. As a result of the interaction between the desalinated solution and fluorine-containing minerals, the fluoride transfer from rocks and its concentration in subpermafrost water is possible.

According to [*Shvartsev, 2017*], fluoride concentration directly reflects the time of evolution of the water–rock system: the longer this time, the higher the fluoride concentration. Anomalously low hydrostatic pressure in subpermafrost complexes attests to the long interaction between subpermafrost water and host rock and to significantly worse water exchange conditions in the central and northern parts of the study area. In the area of the Yakutsk arch uplift and the Nizhnealdanskaya depression, the piezometric level of groundwater is close close to zero or even below sea level. Such hydrodynamic situation is formed under conditions of continuous permafrost degradation, when the emerging due to phase transitions free volume is not compensated by the water inflow.

The relatively low concentration of fluoride is characteristic for the subpermafrost water within the right bank of Lena River to the south of Yakutsk latitude. The geological and hydrogeological structure of this territory has the following features: (1) intrapermafrost aquifers (taliks) with fresh groundwater depleted in fluoride are widely distributed within the sandy deposits of medium-altitude terraces of the Lena River; (2) there are open taliks under large lakes that serve as pathways between surface, intrapermafrost and subpermafrost waters; (3) there is a reduction in the thickness of the cryogenic aquiclude to 60–100 m in areas disturbed by tectonic faults, and both vertical and lateral water flows take place along systems of cracks and karst cavities in calcareous rocks; (4) up to the latitude of Tabaga Promontory, free water outflow from boreholes penetrating subpermafrost aquifers takes place. These four controls determine the possibility of subpermafrost water exchange with the surface and atmospheric water and lead to the formation of a more diverse chemical composition of subpermafrost water with a relatively low concentration of fluoride compared to that in aquifers on the left bank of the Lena River.

Minimal fluoride concentrations are measured in groundwater sampled in boreholes close to the main Lena channel regardless of the lithological composition of water-bearing rocks. Thus, fluoride concentrations in subpermafrost water average 2–3 mg/L in areas of the Tabaga and Kangalass promontories, do not exceed d 1.6 mg/L around the Sangary settlement and decline to 0.4–0.8 mg/L around the Kytyl-Dura and Oktemtsy settlements. Such a low fluoride concentration is due to the presence of open talik zones that probably cause the recharge of subpermafrost water through infiltration of river water. This

assumption is confirmed by synchronicity of fluctuations in the water levels of the Lena River and subpermafrost water under the Lena River floodplain in the area of the Tabaga settlement [*Shepelev et al., 2002*].

CONCLUSIONS

Fluoride concentrations in subpermafrost aquifers of Central Yakutia almost everywhere exceed the norms for drinking water. Fluoride concentrations in subpermafrost water are largely controlled by hydrodynamic and geocryological processes near the bottom of the cryogenic aquiclude. A specific geochemical environment favoring fluorine extraction from water-bearing rocks and its accumulation in the solution is formed under their influence. The groundwater of bicarbonate–sodium composition with high alkalinity is maximally enriched with fluorine. Changes in the permafrost thickness under conditions of impeded water exchange are the reason for unstable equilibrium between groundwater and enclosing rocks, which ultimately contributes to the accumulation of reactive chemical elements, including fluorine, in the water.

Such geological conditions were formed within the Yakutsk uplift of the crystalline basement, where the Archean formations are overlain by the Lower and Middle Jurassic terrigenous aquifers. Here, there is a high probability to observe the considerable fluoride concentrations in subpermafrost water.

Optimal fluoride concentrations are only observed in areas, where aquifers are hydraulically connected with the Lena River through open taliks.

The identified distribution pattern of fluoride should be taken into account while setting up prospecting and evaluation of subpermafrost water to eliminate problems with the drinking water supply for the population and planning appropriate water treatment measures.

Acknowledgments. *This study has partially been funded by the Russian Foundation for Basic Research, project No. 18-45-140065.*

References

Anichkina, N.V., 2016. Studies of fluorine biogeochemistry in geosystem components. Nauchn. Oborenie. Biol. Nauki, No. 3, 5–23 (in Russian).

Anisimova, N.P., 1958. Fluorine in drinking waters of Central Yakutia. In: Tr. Severo-Vostochn. Otd. Inst. Merzlotovedeniya, Yakutsk, **1**, 125–133 (in Russian).

Anisimova, N.P., 1981. Cryohydrogeochemical Features of Permafrost. Novosibirsk: Nauka, 153 p. (in Russian).

Anisimova, N.P., Golovanova, T.V., 1972. Fluorine content in subpermafrost waters of Central Yakutia and methods for reducing its concentration. In: Geocryological and Hydrogeological Studies of Siberia. Yakutsk: Yakutsk. Kn. Izd., p. 158–163 (in Russian).

Anisimova, N.P., Pavlova, N.A., 2014. Hydrogeoghemical Studies of Permafrost in Central Yakutia. Novosibirsk: Geo Publ. House, 189 p. (in Russian).

Balobaev, V.T., 1991. Geothermic Features of Permafrost in Northern Asia. Novosibirsk: Nauka, 193 p. (in Russian).

Balobaev, V.T., Ivanova, L.D., Nikitina, N.M. et al., 2003. Groundwater in Central Yakutia and Prospects for Its Use. Novosibirsk: Geo Publ. House, 137 p. (in Russian).

Beshentsev, V.A., 2013. Groundwater resources of the Yamal–Nenets oil and gas province and problems of their use. Izvest. Ural'sk. Gos. Gornogo Univ., No. 2 (30), 15–20 (in Russian).

Bordovskiy, O.K., Ivanenkov, V.N. (Eds.), 1979. Oceanology. Ocean chemistry. Vol. 1. Chemistry of Ocean Water. Moscow: Nauka, 518 p. (in Russian).

Brindha, K., Elango, L., 2011. Fluoride in groundwater: causes, implications and mitigation measures. In: Monroy S.D. (Ed.). Fluoride Properties, Applications and Environmental Management. New York: Nova Publ., p. 111–136.

Donskikh, I.V., 2013. The influence of fluorine and its compounds on people's health (literature review). Byull. Vost.-Sib. Nauchn. Tsentra Ross. Akad. Meditsinskikh Nauk, No. 3 (91), 179–185 (in Russian).

Dzhamalov, R.G., Krichevets, G.N., Safronova, T.I., 2012. Current changes in water resources in Lena River basin. Water Resources **39** (2), 147–160.

Efimova, A.I., Zaitsev, I.K. (Eds.), 1970. Hydrogeology of the USSR. Vol. XX. Yakut ASSR. Moscow: Nedra, 384 p. (in Russian).

Filimonova, L.G., 1977. Fluorine Geochemistry in the Supergene Zone of Permafrost Regions. Moscow: Nauka, 152 p. (in Russian).

Fordyce, F.M., Vrana, K., Zhovinsky, E. et al., 2007. A health risk assessment for fluoride in Central Europe. Environ. Geochem. Health **29**, 83–102. doi: 10.1007/s10653-006-9076-7.

Fotiyev S.M., 2009. Cryogenic Metamorphism of Rocks and Groundwater (Conditions and Results). Novosibirsk: Geo Publ. House, 279 p. (in Russian).

Gordeev, V.V., 1981. A new estimate of the surface runoff of dissolved substances into the ocean. Dokl. Akad. Nauk SSSR, **261** (5), 1227–1230 (in Russian).

Gordeev, V.V., 1983. River Discharge into the Ocean and Features of Its Geochemistry. Moscow: Nauka, 160 p. (in Russian).

Grigoriev, N.A., 2009. Distribution of Chemical Elements in the Upper Part of the Continental Crust. Ekaterinburg: Izd. Ural. Otd. Ross. Akad. Nauk, 382 p. (in Russian).

Kononova, R.S., 1973. Hydrochemical zoning of groundwater as one of the indicators of paleo-permafrost conditions. In: Second Intern. Permafrost Conf. Reports. Yakutsk: Yakutsk. Kn. Izd-vo, vol. 5, p. 90–94 (in Russian).

Krauskopf, K.B., Bird, D.K., 1995. Introduction to Geochemistry. New York: McGraw-Hill, 647 p.

Kraynov, S.R., Shvets, V.M., 1987. Geochemistry of groundwater for household and drinking purposes. Moscow: Nedra, 237 p. (in Russian).

Malago, J., Makoba, E., Muzuka, A.N.N., 2017. Fluoride levels in surface and groundwater in Africa: a review. Am. J. Water Sci. Engin. **3** (1), 1–17. doi: 10.11648/j.ajwse.20170301.11.

Melnikov, P.I., Tolstikhin, O.N. (Eds.), 1983. Map of Permafrost-Hydrogeological Zoning of Eastern Siberia, 1:2.5 M scale.

Compiled by Ivanova L.D., Lomovtseva N.S., Nikitina N.M., Piguzova V.M. Moscow: GUGK. 4 sh. (in Russian).

Ozsvath, D.L., 2009. Fluoride and environmental health: a review. Rev. Environ. Sci. Biotechnol. **8**, 59–79. doi: 10.1007/s11157-008-9136-9.

Pavlova, N.A, Fedorova, S.V., 2020. Fluoride levels in fresh and slightly saline waters of permafrost zone (Central Yakutia). In: Proc. Fourth All-Russia Sci. Conf. Water–Rock Interaction: Geological Evolution. Ulan-Ude: Izd. Buryat. Nauchn. Ts. Sib. Otd. Ross. Akad. Nauk, p. 171–174 (in Russian). doi: 10.31554/978-5-7925-0584-1-2020-171-174.

Romanovskii, N.N., 1983. Groundwater of the Permafrost Zone. Moscow: Izd. Mosk. Gos. Univ., 231 p. (in Russian).

Saxena, V., Ahmed, S., 2001. Dissolution of fluoride in groundwater: a water-rock interaction study. Environ. Geol. **40**, 1084–1087. doi: 10.1007/s002540100290.

Semenov, V.P., Zheleznyak, M.N., 2018. Specific features of geothermal field and permafrost bedding in the Vilyui syneclise. Prirodn. Res. Arktiki Subarktiki **26** (4), 45–54 (in Russian). doi: 10.31242/2618-9712-2018-26-4-45-54.

Shepelev, N.G., Makogonova, O.V., 2010. Modeling of hydrogeological conditions of subpermafrost aquifer for the territory of Yakutsk. Nauka i Obrazovan. No. 2 (58), 21–26 (in Russian).

Shepelev, V.V., Boytsov, A.B., Oberman, N.G. et al., 2002. Monitoring of Groundwater in the Permafrost Zone. Yakutsk: Izd. Inst. Merzlotoved. Sib. Otd. Ross. Akad. Nauk, 172 p. (in Russian).

Shepelev, V.V., Tolstikhin, O.N., Piguzova, V.M. et al., 1984. Permafrost-Hydrogeological Conditions of Eastern Siberia. Novosibirsk, Nauka, 191 p. (in Russian).

Shvartsev, S.L., 1978. Hydrogeochemistry of the Supergene Zone. Moscow: Nedra, 287 p. (in Russian).

Shvartsev, S.L., 2017. Mechanisms of fluoride accumulation in nitric thermal waters. Izvest. Tomsk. Politekhnich. Univ. Inzhiniring Georesursov **328** (12), 105–115 (in Russian).

Shvartsev, S.L., Ryzhenko, B.N., Alekseev, V.A. et al., 2007. Geological Evolution and Self-Organization of the Water–Rock System. Vol. 2: The Water–Rock System under Conditions of Supergenesis. Novosibirsk: Izd. Sib. Otd. Ross. Akad. Nauk, 389 p. (in Russian).

Subba, Rao N., 2017. Controlling factors of fluoride in groundwater in a part of South India. Arab. J. Geosci. **10** (524). doi: 10.1007/s12517-017-3291-7.

Turekian, K.K., 1972. Chemistry of the Earth. USA, New York: Holf Rinehart & Winston Inc., 136 p.

Vernadsky, V.I., 1955. Selected Works. Vol. 2. Moscow: Izd. Akad. Nauk SSSR, 615 p. (in Russian).

Wedepohl, K.H., 1969. Handbook of Geochemistry. Vol. II-1. Berlin: Springer-Verlag, 442 p.

WHO (World Health Organization), 2017. Guidelines for Drinking-Water Quality: Fourth edition Incorporating the First Addendum. Switzerland, Geneva, World Health Organization, 631 p.

Yanin, E.P., 2007. Fluorine in the environment (distribution, behavior, technogenic pollution). Ekologich. Ekspertiza (Moscow), No. 4, 2–98 (in Russian).

Yousefi, M., Ghalehaskar, S., Asghari, F.B. et al., 2019. Distribution of fluoride contamination in drinking water resources and health risk assessment using geographic information system, northwest Iran. Regulatory Toxicol. Pharmacol. **107**, 104408. doi: 10.1016/j.yrtph.2019.104408.

Zamana, L.V., Usmanova, L.I., Usmanov, M.T., 2011. Ecologic-geochemical assessment of ground waters in Chita city used for decentralized water-supply. Voda: Khimiya i Ekologiya, No. 12 (**42**), 105–109 (in Russian).

Received April 30, 2021
Revised January 31, 2022
Accepted February 6, 2022

Translated by Yu.A. Dvornikov

EARTH'S CRYOSPHERE
SCIENTIFIC JOURNAL

Earth's Cryosphere, 2022, vol. XXVI, No. 2, pp. 42–50

METHODS OF CRYOSPHERIC RESEARCH

SHALLOW-DEPTH TRANSIENT ELECTROMAGNETIC SOUNDINGS FOR IDENTIFICATION OF GAS-HYDRATE ACCUMULATIONS IN THE CRYOLITHOZONE OF THE NORTHERN REGIONS OF WESTERN SIBERIA

E.V. Murzina[1,3], A.V. Pospeev[1,2], I.V. Buddo[1–3], M.V. Sharlov[3], I.K. Seminskiy[1,3], N.V. Misyurkeeva[1,3], I.A. Shelohov[1,3]

[1] *Institute of the Earth's Crust, Siberian Branch of the Russian Academy of Sciences, Lermontova str. 128, Irkutsk, 664033 Russia*
[2] *Irkutsk National Research Technical University, Lermontova str. 83, Irkutsk, 664074 Russia*
[3] *SIGMA-GEO LLC, Zvezdinskaya str. 6, Irkutsk, 664039 Russia; mkv@sigma-geo.ru*

The territory of the north of Western Siberia is known as one of the promising regions of the Russian Arctic in terms of reserves of alternative fuel sources, in particular, gas hydrates. According to the results of interpretation of the data of 3D areal near-field transient electromagnetic sounding (NTES) in the permafrost zone, performed in Nadym district of the Yamalo-Nenets Autonomous okrug at depths of 100–220 m, geoelectric anomalies of increased electrical resistivity values were revealed, accompanied by the manifestation of double induced polarization. The authors associate the mentioned anomalies with the possible accumulations of gas hydrates in the permafrost thickness. To justify the applicability of the sounding method by the formation of the field in the near zone in a shallow modification for mapping subpermafrost geoelectric anomalies in the permafrost zone, a description of a mathematical experiment is presented. The experiment is based on empirical electromagnetic data. As a result of mathematical modeling, it is shown that the use of electromagnetic soundings by the formation of the field in the near zone makes it possible to estimate the conductivity and polarizability of the upper part of the section of the study area and to identify anomalies in the permafrost zone, which are probably associated with hydrate-bearing deposits.

Keywords: *frozen ground, permafrost zone, gas hydrate, near-field transient electromagnetic sounding (NTES), double-induced polarization, electrical resistivity*

INTRODUCTION

In recent decades, an active search and exploration of hydrocarbon deposits has been carried out in the Russian Arctic. A significant role is played by electromagnetic studies, including near-field transient electromagnetic sounding (NTES) aimed at studying the reservoir properties of the target intervals in both the upper and lower stages of the geological section [*Van'yan, 1965*]. The most important feature of the north of Western Siberia is the widespread distribution of permafrost–the upper layer of the earth's crust characterized by subzero temperatures of soils and rocks, regardless of the phase state of water in it [*Shvetsov, 1955; Romanovsky, 1993*]. Permafrost includes frozen (with ice), dry cryotic, and cryotic rocks. Cryotic rocks are saline or saturated with saline waters and brines with temperatures below 0 °C.

Another promising object of the study is represented by gas hydrates associated with permafrost. Gas hydrates are ice-like crystalline compounds that form at certain temperatures and pressures from water molecules and low-molecular-weight gas (CH_4, C_2H_6, CO_2, N_2, etc.) [*Istomin and Yakushev, 1992*].

The search, exploration, and development of hydrate-bearing accumulations in the Russian Arctic is limited by the inaccessibility of the region and the lack of a well-developed set of geophysical methods comparable in efficiency to marine research. In particular, marine electrical exploration CSEM (controlled source electromagnetic method) in combination with seismic exploration by the common depth point method (CDP) has become popular abroad to search for deposits of gas hydrates in the shelf zone [*Vorob'ev and Malyukov, 2009*]. A prerequisite for the successful application of shallow near-field transient electromagnetic sounding (shallow NTES) for solving geocryological problems is the differentiation of the geoelectric characteristics of sedimentary rocks depending on their moisture content and ice content [*Stogniy, 2003; Kozhevnikov et al., 2014; Ageev, 2019*]. The efficiency of the shallow NTES method for studying both the upper part of the section and the deep (up to 3–4 km) layers in the geological conditions of Western Siberia is also reflected in [*Buddo et al., 2017, 2018, 2021; Sharlov et al., 2017; Misyurkeeva et al., 2017, 2019, 2020, 2021; Shelokhov et al., 2018;*

Dolgikh et al., 2019; Rybalchenko et al., 2020]. However, there is practically no confirmation of the results of interpretation of geophysical data indicating the detection of gas hydrate accumulations in the permafrost by direct field methods (drilling of the wells).

In this article, the authors present and discuss the results of the work carried out by the shallow NTES method on the Tazovsky Peninsula (Nadym district). According to the results of electrical surveys, there are high-resistivity anomalies of specific electrical resistance (SER) accompanied by anomalies of doubled induced polarization (DIP) in the permafrost [*Murzina et al., 2016; Misyurkeeva et al., 2017, 2021*]. Geoelectric structures of this kind were also found by other researchers [*Kozhevnikov and Antonov, 2010; Afanasenkov et al., 2015*] based on the results of electromagnetic survey in the Russian Arctic.

ON GAS HYDRATES IN PERMAFROST OF THE NORTH OF WESTERN SIBERIA

Though most of the gas hydrate deposits discovered to date are confined to sea areas, the first indication of the existence of continental gas hydrate deposits in the permafrost zone were discovered in the early 1950s in Eastern Siberia [*Chersky and Tsarev, 1973*]. Large accumulations of gas hydrates are known in frozen deposits of the Mackenzie River delta in Canada and in northern Alaska within large oil and gas fields [*Aregbe, 2017; Uchida et al., 2000*]. The existence of layers with gas hydrates in permafrost of northern areas of Western Siberia identified mainly by indirect evidence within the Messoyakha, Yamburg, and Bovanenkovo fields was mentioned in a number of recent studies [*Yakushev and Chuvilin, 2000; Chuvilin et al., 2000, 2007; Yakushev et al., 2003; Yakushev, 2009; Leonov, 2010*].

When analyzing the conditions for the existence of gas hydrate formations in the north of Western Siberia, many researchers use such concepts as zones of stability [*Istomin and Yakushev, 1992*] and metastability of gas hydrates [*Perlova, 2001; Yakushev et al., 2003*]. The term "gas hydrate stability zone" (GHSZ) is currently understood as "a part of the lithosphere and hydrosphere of the Earth, the thermobaric and geochemical regimes of which correspond to the conditions for the stable existence of natural gas hydrates of a certain composition" [*Istomin and Yakushev, 1992, p. 175*].

The gas hydrate metastability zone (GHMZ) is a part of the permafrost section above the top of GHSZ, where the temperature regime of the rocks suggests the possibility of self-preservation of gas hydrates at subzero temperatures [*Perlova, 2001*]. In particular, according to the latest data, gas hydrates can form and exist for a long time in frozen sandy sediments with a low degree of salinity [*Chuvilin et al., 2018, 2019*].

Not much is known about the distribution of gas hydrates within terrestrial paleobasins. Thus, in the Mackenzie River delta, their presence in is possible in permafrost areas, because the GHSZ on land is only formed in association with permafrost [*Uchida, et al., 2000*]. Favorable conditions for the formation of subpermafrost and intrapermafrost gas hydrate deposits exist in the northern part of the West Siberian basin with a continuous permafrost of 200–400 m in thickness [*Ershov, 1989; Leonov, 2010*].

As a rule, large accumulations of gases in the clathrate form are confined to areas of oil and gas fields [*Yakushev et al., 2003; Chuvilin et al., 2007; Yakushev, 2009*] and may consist of not only catagenic gas but also biogenic gas formed during the microbial decomposition of organic matter in sedimentary deposits [*Yakushev and Chuvilin, 2000; Yakushev, 2009; Leonov, 2010*]. Most often, such accumulations are located in the GHSZ, but there are exceptions, in particular, the Yamburg gas condensate field on the Tazovsky Peninsula, 60 km north of the study area. The presence of metastable gas hydrates in the permafrost strata was noted here based on active gas manifestations and the determination of gas content in core samples at depths of 70–120 m [*Istomin and Yakushev, 1992*].

On the example of the Bovanenkovo field, V.L. Bondarev showed the presence of traces of fluid migration in the form of gas shows in the intervals of supra-Cenomanian deposits. Most of the gas shows are confined to the interval of 38–120 m [*Bondarev et al., 2008*]. Methane in the composition of gases is of predominantly biogenic origin. In some cases, the ^{13}C isotope is present in the gases, which may indicate the presence of some amounts of epigenetic (migratory) gases in their composition [*Bondarev et al., 2004*].

In addition, heaving mounds (bulgunnyakhs) are widespread in the north of Western Siberia in the basins of drained thermokarst lakes (khasyreys). Some heaving mounds are considered traces of hydrovolcanic processes [*Nezhdanov et al., 2011; Bogoyavlensky et al., 2019*]. This indicates the possibility of methane entering with the upward flows of formation waters; this gas may be a "building material" for the formation of subpermafrost accumulations of gas hydrates.

From the foregoing, it follows that the existence of stable gas hydrate formations associated with a thick permafrost and metastable relict accumulations of gas hydrates associated with incompletely thawed frozen strata of the past is possible in the north of Western Siberia. Metastable gas hydrates are not only a potential source of hydrocarbons located close to the surface; they are also an extremely unstable and explosive substance [*Perlova et al., 2017*], the position of which in the section must be taken into account when drilling and spudding deep wells.

Mapping of sediments with possible hydrate content according to data of shallow near-field transient electromagnetic sounding in the north of Western Siberia

The studied, data from which are presented in this article and form the basis for further synthetic modeling, is located in the Tazovsky Peninsula, on the interfluve between the Khadutte and Tabyakha rivers in the upper reaches, on the schematic map of permafrost zoning [*Baulin et al., 1967*], it belongs to the northern zone, subzone of predominantly epigenetically frozen deposits (Fig. 1). Alluvial, lacustrine-alluvial, and alluvial-estuary deposits of river terraces are epigenetically frozen; their freezing occurred from top to bottom after sedimentation.

The study area is located in the area of disjunct occurrence of modern and relict frozen strata separated by taliks. The total thickness of the cryogenic strata reaches 400 m and more. There are also numerous open and closed taliks under riverbeds and lakes, as well as areas of a sharp increase in the thickness of frozen strata [*Baulin et al., 1967; Shpolyanskaya, 1981*].

The measurements were carried out using a Fast-Snap digital telemetry station for shallow-depth surveys over a dense network of observations (100 observation points per 1 km^2). A coaxial array with a 100 × 100 m generator loop and two 10 × 10 m receiving loops at a distance of 0 and 100 m from the array center was used as a probing array.

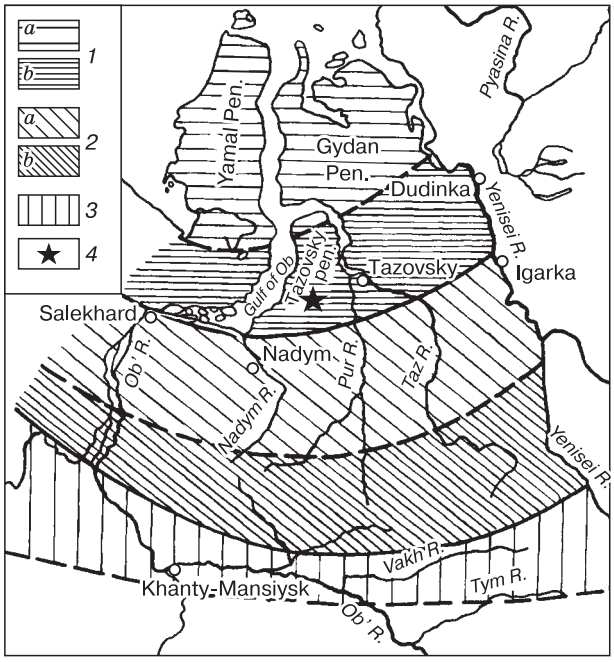

Fig. 1. Schematic map of permafrost zones and subzones [*Baulin et al., 1967*].

1 – northern zone (*a*, subzone of polygenetically frozen sediments; *b*, subzone of predominantly epigenetically frozen sediments); *2* – central zone (*a*, subzone of frozen mineral soils and peat bogs; *b*, subzone of frozen peat bogs); *3* – southern zone of deep-lying relic frozen strata; *4* – area of field work with shallow-depth NTES.

Figure 2 displays a section along the 13,500-m-long shallow NTES profile oriented from south to north. The upper layer of modern permafrost with increased electrical resistivity values (from 500 to 2000 Ω·m) reaches a depth of about 80–100 meters. This layer is characterized by a sharp increase in resistivity values compared to the underlying strata. It is represented by lacustrine-alluvial, alluvial-marine, and glacial-marine deposits of the Quaternary age [*Shatsky, 1978*]. Taking into account the geocryological conditions of the study area [*Ershov, 1989*], the high-resistivity horizon identified in the upper part of the section is associated with the area of permafrost development and is characterized by the increased ice content and temperatures of about –5 °C.

On the profile built according to the shallow NTES data (Fig. 2), within intervals of 2.0–11.6, 12.2–13.1 km, the modern layer of frozen rocks (resistivity 500–2000 Ω·m) is underlain by a heterogeneous layer with the lower boundary in the form of high-resistivity "pockets". The resistivity of rocks in this interval decreases to 20–80 Ω·m with local peaks up to 150–300 Ω·m. The thickness of this layer is also quite variable, from 50 to 160 m. This interval is mainly represented by the Korlikovskaya sequence (Oligocene) of whitish and light gray sands, poorly sorted, with lenses of gravelstones. The abundance of kaolin in the form of nest filler, lenticular layers, and pellets is typical [*Shatsky, 1978*]. On the graph of temperature distribution over depth [*Ershov, 1989*], the permafrost temperature in this layer (at depths from 100 to 200 m) increases with depth from –4 to –2 °C. A significant decrease in resistivity relative to the overlying high-resistivity horizon can also be associated with a decrease in the ice content with depth.

Below this parts of the section, there are taliks mainly lying under a layer of modern frozen strata. According to the shallow NTES data, they correspond to resistivity values from 5 to 10 Ω·m.

The lower layer of relic permafrost is located in the thickness of the Eocene-Paleocene deposits [*Shatsky, 1978*]. According to the shallow NTES data (Fig. 2), it corresponds to lower resistivity values, from 25 to 65 Ω×m, and its thickness presumably reaches 200 m. The deposits are represented by alternating layers of fine- and medium-grained sands, diatomite and opoka-like clays. Temperatures of –2...0 °C are typical for this depth interval [*Ershov, 1989*]. With depth, the temperature of the rocks relatively quickly rises to values at which phase transitions of water begin. However, due to the zero curtain effect, the rocks can remain in a frozen state for quite a long time [*Baulin et al., 1967; Shpolyanskaya, 1981; Ershov, 1989*].

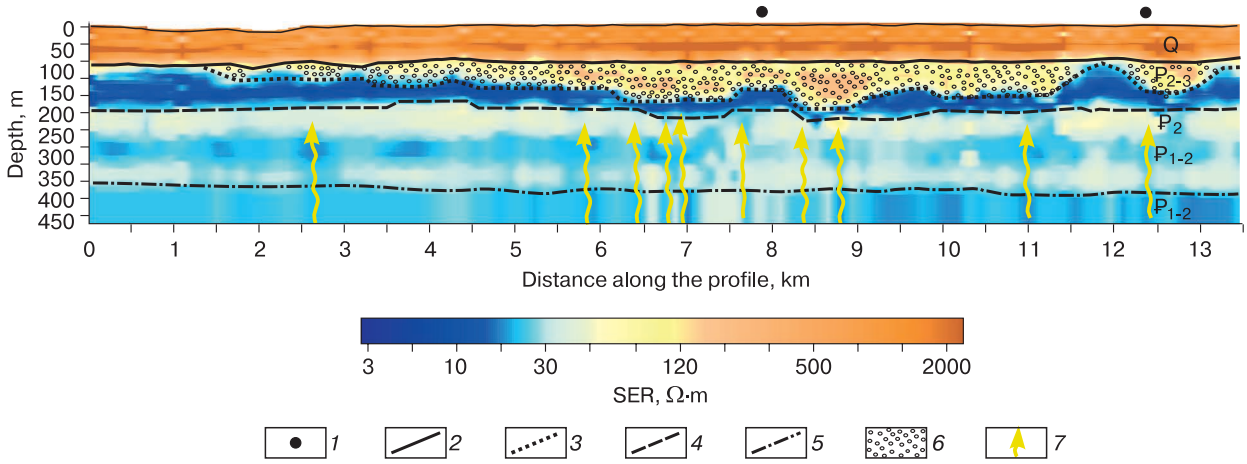

Fig. 2. Geoelectric section along the profile surveyed by the shallow NTES method on the interfluve between Khadutte and Tabykha rivers in their upper reaches.

1 – heaving mound; *2* – supposed bottom of the upper layer of modern permafrost; *3* – supposed bottom of the layer of frozen hydrate-bearing strata in the near-bottom part of modern permafrost; *4* – supposed base of the interpermafrost talik and the roof of the relict frozen rock; *5* – bottom of the lower relic layer of frozen rock; *6* – supposed accumulations of hydrate-bearing deposits; *7* – supposed channels of fluid migration. Q – Quaternary deposits, $P_{2–3}$ – Oligocene deposits, P_2 – Eocene deposits, and $P_{1–2}$ – Paleocene–Eocene deposits.

The anomalies in the form of high-resistivity pockets in the bottom part of the modern permafrost stratum identified according to the NTES data can probably be associated with both a local increase in the thickness of modern permafrost and the possible presence of hydrate-bearing deposits in the section [*Misyurkeeva et al., 2017*].

In accordance with the zoning map of the West Siberian oil and gas province [*Kontorovich, 2008*], the study area belongs to the Urengoy oil and gas field of the Nadym–Pur oil and gas region (OGR). At the same time, it is known that in the study area, at depths of 1100–1500 m, in the Cenomanian sediments, stage, there is a giant gas deposit. The Cenomanian productive stratum is characterized by significant heterogeneity. The most common in the section are fine-grained sandstones (sands) and siltstones (siltstones). Sandy-silty rocks are characterized by weak cementation. Sandstones and coarse-grained silts with kaolinite cement have good reservoir properties. The thickness of oil and gas reservoirs within the territory under consideration varies and is about 600–650 m. Spatial coincidence of the anomalies identified in the permafrost with the area of the predicted gas deposit in the Cenomanian strata (Fig. 3, *d*) is noted [*Misyurkeeva et al., 2017*].

Under the high-resistivity anomalies, in the underlying Eocene–Paleocene deposits (in the relic permafrost), subvertical anomalies of low resistivity relative to the host deposits are observed, which can probably be associated with gas migration channels (Fig. 2). A spatial coincidence of the areas of anomalies with the position of heaving mounds on the earth's surface was noted (Figs. 3, *a*, *b*, *d*), which may be indicative of the deep nature of the formation of these heaving mounds [*Nezhdanov et al., 2011; Bogoyavlensky et al., 2019*].

According to the totality of facts established during the shallow NTES work, namely: (1) the presence of high-resistivity "pockets" in the near-bottom part of the modern permafrost; (2) the presence of low resistivity anomalies on geoelectric sections under the identified high-resistivity anomalies in the cryogenic stratum, interpreted as traces of fluid migration [*Murzina et al., 2016; Misyurkeeva et al., 2017, 2021*]; (3) the presence of heaving mounds on the surface associated with traces of deep fluid migration [*Nezhdanov et al., 2011; Misyurkeeva et al., 2017, 2021; Bogoyavlensky et al., 2019*] over the identified resistivity anomalies; and (4) the coincidence of geoelectric anomalies and the areas of the predicted gas deposit in the Cenomanian sediments [*Misyurkeeva et al., 2017*], we can assume that the high-resistivity anomalies identified in the permafrost are associated with probable hydrate-containing deposits.

Evaluation of sensitivity of shallow NTES signals to identification of subpermafrost anomalies using mathematical modeling

To assess the sensitivity of nonstationary soundings to variations in the geoelectric characteristics of permafrost (electrical resistivity and inductively induced polarization of rocks) and layers below it, mathematical modeling of induction transient characteristics was carried out. Its essence was to calculate the shallow NTES curves for the selected physi-

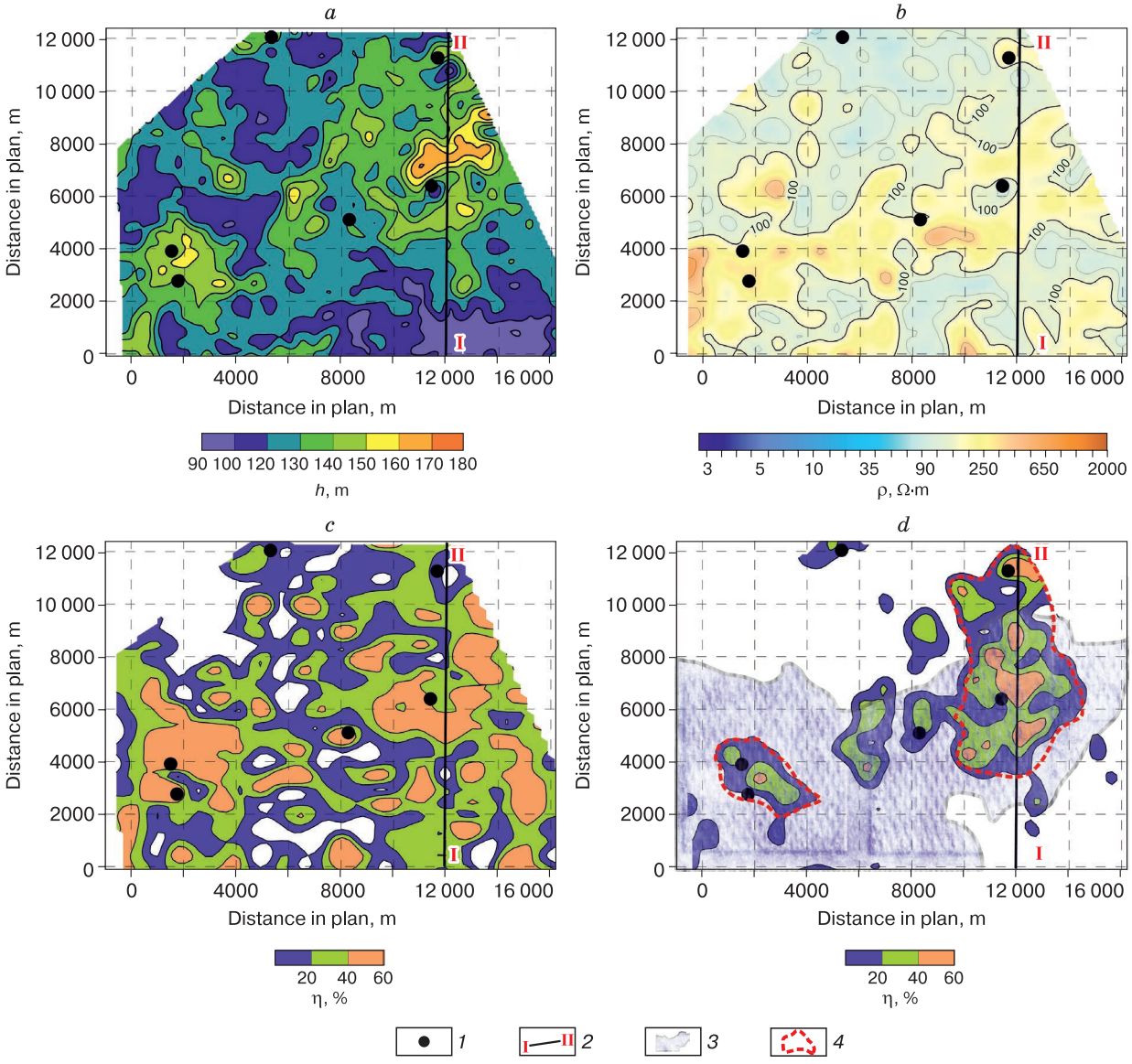

Fig. 3. Results of shallow NTES data interpretation for the interfluve between the Khadutte and Tabyakha rivers in their upper reaches.

a – thickness map (*h*) of the upper modern permafrost, including the assumed layer of hydrate-bearing deposits (0–200 m); *b* – map of the normalized resistivity (ρ) of the upper permafrost, including the assumed layer of hydrate-bearing deposits (0–200 m); *c* – map of the polarizability coefficient (η) of the upper modern permafrost (0–90 m); *d* – map of the polarizability coefficient of the high-resistivity layer (η) in the near-bottom part of the upper permafrost (90–200 m). *1* – heaving mound; *2* – position of the geoelectric profile; *3* – predicted area of gas field in the Cenomanian deposits; *4* – predicted area of hydrate-bearing deposits in the interpermafrost talik zone.

cal-geological model, apply electromagnetic (EM) interference characteristic of the area under study to them, and then solve the inverse problem of electrical exploration. When conducting a numerical experiment, calculations were carried out for an areal observation network using the shallow NTES method applied in the study.

Based on the results of interpretation of the shallow NTES data, simplified models M_1 and M_2 have been developed. Model M_1 is a standard model of permafrost, and model M_2 is a model of permafrost with a lens of supposed hydrate-bearing deposits under the permafrost layer. These models formed the basis for further modeling (Table 1).

In the study area, layer 1 (the upper layer of modern permafrost) of a depth of 100 m is represented by ice-rich rocks with temperatures of about –5 °C and a resistivity of ρ = 2000 Ω·m. Permafrost polar-

ization parameters according to Kozhevnikov: $\eta \approx 70$ %, $\tau = 3 \cdot 10^{-5}$ s, $C = 0.9$ [*Kozhevnikov and Antonov, 2010*].

Layer 2 lying directly below the icy frozen rocks, in which the existence of gas hydrates is assumed, is represented by sands with interlayers of siltstones, silty, micaceous and opoka-like clays. It is characterized by rather low resistivity values from 30 to 50 Ω·m. Temperatures of −4...−2 °C are typical for this depth interval, and the presence of pore ice is assumed, which is favorable conditions for both accumulation of gas hydrates and preservation of relict gas hydrates [*Chuvilin et al., 2019*].

If there are hydrate-containing deposits in the permafrost, then due to the absence of dissociation of crystallization water in gas hydrate molecules, their accumulation should have high resistivity. According to laboratory studies, the resistivity of gas hydrates is about 150 Ω·m [*Permyakov et al., 2017*]. Taking into account the heterogeneity of the studied geological objects, for a lens of hydrate-bearing deposits, the resistivity can be about 110–300 Ω·m. The manifestation of the FTI effect in the high-resistivity layer in the near-bottom part indicates the presence of ice in the lens. It is possible to assume that the polarization parameters of gas hydrates are similar to the properties of frozen rocks: $\eta \approx 80$ %, $\tau = 2 \cdot 10^{-4}$ s, $C = 0.9$. In the plantar part of the first and second layers, there is layer 3 (talik layer) with the average resistivity is 9 Ω·m. Below the taliks, there is a relic frozen strata (layer 4) characterized by low resistivity values of about 30 Ω·m. Its thickness is about 200 m.

The solution of direct and inverse problems within the framework of the accepted models M_1 and M_2 was carried out using the *Model 3* software [*Agafonov et al., 2006*]. The synthetic transient responses obtained in the framework of the model experiment were calculated up to a time of 10 ms. The duration of the synthetic transient characteristics calculated in the framework of the model experiment was chosen based on the required depth of frozen strata (at least 400 m) and the geoelectric parameters of the given models. The first type of curve (Fig. 4) is characteristic of permafrost (Table 1, M_1). The second type of curve (Fig. 4) is characteristic of permafrost in the presence of a high-resistivity body in the near-bottom part associated with a lens of hydrate-bearing deposits (Table 1, M_2).

Several hundred responses were calculated, which were complicated by the addition of EM noise, in accordance with the noise parameters of real field data.

The area-averaged noise parameters were determined using the TEM-Processing software by processing a set of real noise records obtained with the FastSnap equipment [*Sharlov et al., 2010*] at one of the shallow NTES survey sites in Western Siberia [*Sharlov et al., 2017*]. Each noise record was a series of measured background values of electromagnetic noise (noise oscillogram with arithmetic time step) with the current turned off in the generator loop. To determine the maximum amplitude of the scatter of noise values (noise level), the noise record was recalculated into a logarithmic time grid corresponding to the time step of reading the synthetic curve. Next, the noise level was scaled to the level of the actually measured signal, i.e. normalization was performed for the value of current in the generator loop (I ~ 17–20 A) and $\sqrt[2]{N}$ where N is the number of accumulations performed when measuring real curves (N ~ 1600–2400 accumulations). Figure 4 shows examples of synthetic responses calculated for different geoelec-

Table 1. **Reference Models**

Layer No.	h, m	ρ, Ω·m	η, %	τ, s	C
	M_1, *geoelectric model of permafrost*				
1	100	2000	70	$3 \cdot 10^{-5}$	0.9
2	50	30	0	0	0
3	20	9	0	0	0
4	200	30	0	0	0
	M_2, *geoelectric model with a lens of hydrate-bearing sediments under the permafrost*				
1	100	2000	70	$3 \cdot 10^{-5}$	0.9
2	100	200	80	$2 \cdot 10^{-4}$	0.9
3	20	9	0	0	0
4	200	30	0	0	0

Note: h is layer thickness, ρ is the electrical resistivity, η is the polarizability coefficient, τ is the relaxation time, and C is the degree of polarization.

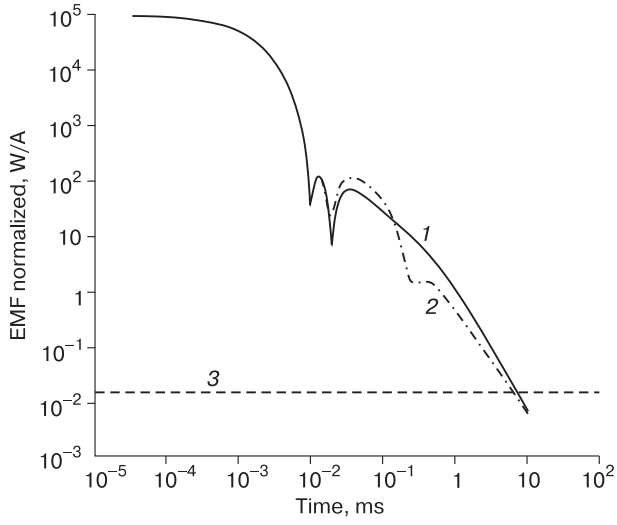

Fig. 4. Electromotive force (EMF) of the NTES signal vs time for models M_1 and M_2.

1 – EMF curve for a coaxial loop over a polarized section of the frozen strata ($Qq(M_1)$); *2* – EMF curve for a coaxial loop over a polarized section of the frozen strata with a lens of hydrate-bearing deposits ($Qq(M_2)$); *3* – noise level.

Table 2. **Models of subpermafrost anomaly associated with hydrate-containing deposits**

No.	ρ, %	η, %	*h*, m
1	10	20	35
2	20	30	40
3	30	40	45
4	40	50	50
5	50	55	60
6	60	60	70
7	70	65	75
8	80	70	85
9	90	80	90

Note: ρ – specific electrical resistance, η – polarizability coefficient, *h* – thickness.

tric conditions with a plotted noise level that does not exceed 0.015 μV/A.

By interpolating the previously described reference models (Table 1), a three-dimensional geoelectric model of the geological section was formed with the presence of a gas hydrate deposit under the upper permafrost layer. The interpolation of the model took place in such a way that with each step, the analyzed subpermafrost layer was added 10 % of the resistivity parameters, η and *h* of the desired object (Table 2). The polarizability parameters were set for the first two horizons and for a subpermafrost high-resistivity object associated with gas hydrate accumulations. The relaxation time and the degree of polarization were fixed in accordance with the permafrost polarization indices according to N.O. Kozhevnikov [*Kozhevnikov and Antonov, 2010*].

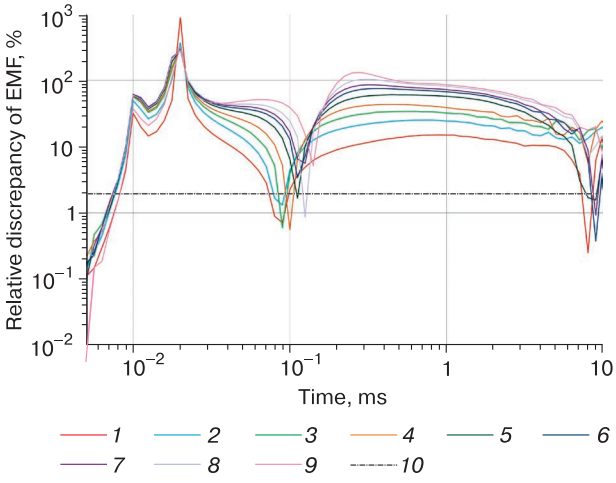

Fig. 5. Plot of relative discrepancy (%) between synthetic noisy EMF signals from the background model and the model with a successive increase in the anomalous contribution vs the relaxation time (Table 2).

1 to *9* – discrepancies between the synthetic curves of the shallow NTES in accordance with Table 2; *10* – the level of electromagnetic noise according to the actual field data.

On the graph of the percentage discrepancy (Fig. 5) between the coaxial shallow NTES curves calculated from the models obtained by changing the parameters (resistivity, η, and *h*) of the subpermafrost layer, it can be seen that the amplitude of the anomaly is more than 100 % and repeatedly exceeds the noise level (2 %). This fact testifies to the high sensitivity of the NTES curves to changes in the subpermafrost conductive half-space.

Data inversion was carried out automatically using algorithms for solving poorly conditioned problems according to A.N. Tikhonov [*Tikhonov and Arsenin, 1986*]. A priori information was taken into account by fixing the number of layers in accordance with the geological model and the parameters of the first polarized permafrost layer. In the process of solving the inverse problem, it was necessary to establish the fact of a change in the geoelectric situation when a lens of hydrate-bearing deposits appeared under the permafrost.

Several cycles of inversion took place. Initially, the resistivity model and the thickness of the subpermafrost anomaly were determined. Then, the resistivity model and the anomaly thickness were refined with the selection of polarizability parameters. The logarithmic root-mean-square discrepancy between the practical and theoretical curves was used as the minimization functional, which tends to zero in the process of solving the inverse problem.

When the discrepancy was less than 3 %, the sensitivity of the sounding curves to the electromagnetic anomaly was estimated. To do this, the root-mean-square error δ, % (Table 3) of the desired parameters was calculated for the groups of curves formed in accordance with Table 2.

Table 3. **Results of synthetic modeling of shallow NTES signals**

No.	Root-mean-square error of reconstruction of an anomalous object parameters		
	δ_{SER}, %	δ_η,%	Δ_h,%
1	31	43	9
2	27	40	9
3	22	30	5
4	16	20	5
5	10	25	10
6	11	17	13
7	11	7	13
8	6	5	2
9	10	1	5

Note: δ_{SER} is the rms error in determining the electrical resistivity, δ_η is the rms error in determining the polarizability coefficient, Δ_h is the rms error in determining the thickness.

Based on the results of modeling the shallow NTES curves for the southern part of the Tazovsky Peninsula (the area between the Khadutte and Tabyakha rivers), it is possible to confidently identify high-resistivity anomalies with a relative value of 40 % with accompanying anomalies η ~ 50 % and the anomaly thickness increase by more than 50 m.

CONCLUSIONS

The features of the geoelectric section of permafrost identified from data of near-field transient electromagnetic sounding at the key site in Nadym district of the Yamalo-Nenets Autonomous okrug, on the interfluve between the Khadutte and Tabyakha rivers in their upper reaches, allow us to draw the following conclusions:

– high-resistivity resistivity SER anomalies obtained from the NTES field experiment and accompanied by DIP anomalies can be associated with changes in the permafrost structure, as well as with the possibility of the existence of gas hydrates in the cryogenic layer;

– the coincidence of the spatial position of gas fields in the deposits of the Cenomanian stage and the anomalies identified according to the NTES data in the near-surface part of the section may indicate the possible deep nature of the formation of gas hydrate accumulations in the permafrost;

– subvertical anomalies of low SER under high-resistivity anomalies can characterize manifestations of deep fluid migration;

– according to NTES, in the geological section of the northern part of Western Siberia, one can confidently identify subpermafrost anomalies of increased SER with a relative value of 40 % accompanied by anomalies η ~ 50 % with an increase in the thickness by more than 50 m;

– it is advisable to recommend a drilling study of the identified geophysical anomalies to clarify their nature and assess their possible connection with gas hydrate deposits.

Acknowledgments. *The authors are grateful to the General Director of SIGMA-GEO LLC, Cand. Sci. Yu.A. Agafonov for the opportunity to use the materials. The authors are grateful to Prof. Dr. Sci. N.O. Kozhevnikov for help in shaping the structure of the article and constructive suggestions. We also thank Cand. Sci. V.E. Tumskoy and Cand. Sci. E.M. Chuvilin for their invaluable help in the preparation of the final version of the article and highly appreciate fair criticism of the reviewers, which made it possible to significantly improve the final text.*

References

Agafonov, Yu.A., Pospeyev, A.V., Surov, L.V., 2006. The system of data interpretation and main directions of application of the results of nonstationary electromagnetic sounding to the south of Siberian Craton. Pribory Sistemy Razvedochn. Geofiziki, No. 1, 33–36 (in Russian).

Ageev, D.V., 2019. Application of nonstationary electromagnetic sounding for solving hydrogeological problems in the permafrost zone of the Novyi Urengoy oil and gas field. Inzhenern. Izyskaniya XIII (3), 40–47 (in Russian).

Afanasenkov, A.P., Volkov, R.P., Yakovlev, D.V., 2015. Increased electric resistivity anomaly under permafrost sediments layer as a new indicator for prospecting hydrocarbon deposit. Geol. Nefti Gaza, No. 6, 40–51 (in Russian).

Aregbe, A.G., 2017. Gas hydrate – properties, formation and benefit. Open J. Yangtze Oil and Gas, **2** (1), 27–44.

Baulin, V.V., Belopukhova, E.B., Dubikov, G.I., Shmelev, L.M., 1967. Geocryological Conditions of the West Siberian Lowland. Moscow: Nauka, 213 p. (in Russian).

Bogoyavlensky, V.I., Sizov, O.S., Mazharov, A.. et al., 2019. Earth degassing in the Arctic: remote and field studies of the Seyakha catastrophic gas blowout on the Yamal Peninsula. Arktika: Ekologiya Ekonomika, No. 1 **(33)**, 88–105 (in Russian). doi: 10.25283/2223-4594-2019-1-88-105.

Bondarev, V.L., Mirotvorskii, M.Yu., Shaidullin, R.M., Gudzenko, V.T., 2004. Conditions for the Formation of Nonindustrial Hydrocarbon Gas Accumulations in the Supraproductive Deposits of the Yamal Peninsula and Geochemical Methods for Diagnosing Their Nature. Moskva: NPC "Geokhimiya"– Nadymgazprom, 182 p. (in Russian).

Bondarev, V.L., Mirotvorsky, M.Yu., Zvereva, V.B. et al., 2008. Gas geochemical characteristics of the supra-Cenomanian deposits of the Yamal Peninsula (on the example of the Bovanenkovo oil condensate field). Geol. Geofizika Razrabotka Neftyan. Gazovykh Mestorozhdenii, No. 5, 22–34 (in Russian).

Buddo, I.V., Misurkeeva, N.V., Shelohov, I.A. et al., 2017. Experience of 3D transient electromagnetics application for shallow and hydrocarbon exploration within Western Siberia. In: Proc. 79th EAGE Conf. Exhibition 2017 (Paris, France, 12–15 June 2017). doi: 10.3997/2214-4609.201700667.

Buddo, I.V., Smirnov, A.S., Misyurkeeva, N.V. et al., 2018. Integration of electromagnetic and seismic survey data at all stages of geological exploration: from the prospecting stage to the development of hydrocarbon fields. Ekspozitsiya Neft' Gaz October, No. 6 (66), 24–28 (in Russian).

Buddo, I.V., Seminskij, I.K., Shelohov, I.A. et al., 2021. Electromagnetic studies for cryolithozone investigation in the Arctic settings: background of application and experimental data. In: Proc. Conf. "Modern Studies of Cryosphere Transformation and Issues of Geotechnical Safety of Structures in the Arctic". V.P. Melnikov and M.R. Sadurtdinov (Eds.). Salekhard, p. 71–74 (in Russian).

Chersky, N.V., Tsarev, V.P., 1973. Prospects for the Development of Gas Hydrate Deposits. Research and Recommendations for Improving Mining in the Northern and Eastern Regions of the USSR, Part 1. Yakutsk: Izd. Yakutskogo Filiala Sib. Otd. Akad. Nauk SSSR, 121 p. (in Russian).

Chuvilin, E., Bukhanov, B., Davletshina, D. et al., 2018. Dissociation and self-preservation of gas hydrates in permafrost. Geosciences **8**, 431 p. doi: 10.3390/geosciences8120431.

Chuvilin, E.M., Davletshina, D.A., Lupachik, M.V., 2019. Hydrate formation in frozen and thawing methane-saturated sediments. Earth's Cryosphere, XXIII (2), 44–52.

Chuvilin, E.M., Perlova, E.V., Baranov, Yu.B. et al., 2007. Structure and Properties of Permafrost in the Southern Part of the Bovanenkovo Gas Condensate Field. Moscow: GEOS, 135 p. (in Russian).

Chuvilin, E.M., Yakushev, V.S., Perlova, E.V., 2000. Gas and gas hydrates in the permafrost of Bovanenkovo gas field, Yamal Peninsula, West Siberia. Polarforschung **68**, 215–219.

Dolgikh, Y., Sanin, S., Buddo, I. et al., 2019. Improving the efficiency of geophysical research based on the integration of seismic and modern electrical exploration. In: Proc. Conf. Tyumen 2019 (March 2019). Vol. 1, p. 1–5. doi: https://doi.org/10.3997/2214-4609.201900577.

Ershov, E.D., 1989. Geocryology of the USSR. Western Siberia. Moscow: Nedra, 454 p. (in Russian).

Istomin, V.A., Yakushev, V.S., 1992. Gas Hydrates in Natural Conditions. Moscow: Nedra, 236 p. (in Russian).

Kontorovich, A.E., 2008. Geology of Oil and Gas. Selected Works. Vol. 1. Geology of Oil and Gas in Siberia. Novosibirsk: Izd. SNIIGTiMS, 540 p. (in Russian).

Kozhevnikov, N.O., Antonov, E.Yu., 2010. Inversion of IP-affected NTES responses of a two-layer earth. Russian Geology and Geophysics **51** (6), 905–918.

Kozhevnikov, N.O., Antonov, E.Yu., Zaharkin, M.A. et al., 2014. NTES surveys for search of taliks in areas of strong fast-decaying IP effects. Russian Geol. Geophysics **55** (12), 1815–1827.

Leonov, S.A., 2010. Prospects for the hydration potential of the supra-Cenomanian deposits in the north of Western Siberia. Author's abstract Cand. Sci. diss. Moscow, 24 p. (in Russian)

Misyurkeeva, N.V., Buddo, I.V., Agafonov, Yu.A. et al., 2017. Shallow NTES and NTES electromagnetic studies application in geological settings of Arctic zone of Western Siberia. In: Proc. Conf. Geomodel 2017 (Gelendzhik, Russia, Sept. 11–14, 2017) (in Russian). doi: 10.3997/2214-4609.201702225.

Misyurkeeva, N.V., Buddo, I.V., Sholokhov, I.A. et al., 2021. Permafrost structure in the north of Western Siberia from modern geophysical studies. In: Proc. Int. Conf. "Modern Studies of Cryosphere Transformation and Issues of Geotechnical Safety of Structures in the Arctic". V.P. Melnikov and M.R. Sadurtdinov (Eds.). Salekhard, p. 297–300 (in Russian).

Misyurkeeva, N.V., Buddo, I.V., Shelohov, I.A. et al., 2019. New data on fluid dynamic processes in the Arctic Zone of Western Siberia based on the results of TEM, STEM electromagnetic studies and seismic CDP studies. In: Proc. Conf. Tyumen 2019 (March 2019), p. 1–6. doi: 10.3997/2214-4609.201900574

Misyurkeeva, N.V., Buddo, I.V., Smirnov, A.S. et al., 2020. Shallow transient electromagnetic method application to study the Yamal Peninsula permafrost zone. In: Proc. Conf. Geomodel 2020 (Gelendzhik, Russia, Sept. 2020). Vol. 2020, p. 1–6. doi: 10.3997/2214-4609.202050105

Murzina, E.V., Misyurkeeva, N.V., Buddo, I.V. et al., 2016. The result of the application of automatic inversion for permafrost studies using high-density NTES soundings. In: Proc. 13th Sci. Practical Seminar "Application of Modern Electric Exploration Technology in Prospecting Mineral Deposits" (Saint Petersburg, Nov., 2016), p. 119–122 (in Russian).

Nezhdanov, A.A., Novopashin, V.F., Ogibenin, V.V. et al., 2011. Mud volcanism in the north of Western Siberia. Tr. Inst. TyumenNIIgiprogaz: Geolog. Geologorazvedka. Tyumen: Flat, p. 73–79 (in Russian).

Perlova, E.V., 2001. Features of Gas Content in Permafrost by the Example of the Northwestern Part of Yamal Peninsula. Cand. Sci. (Geol.-Mineral.) diss., Moscow, 174 p. (in Russian).

Perlova, E.V., Miklyaeva, E.S., Leonov, S.A. et al., 2017. Gas hydrates of the Yamal Peninsula and adjacent shelf of the Kara Sea as a complicating factor in the development of the region. Problemy Resursn. Obespecheniya Gazodobyv. Raionov Rossii, No. 3 (**31**), 255–262 (in Russian).

Permyakov, M.E., Manchenko, N.A., Duchkov, A.D. et al., 2017. Laboratory modeling and measurement of the electrical resistivity of hydrate-bearing sand samples. Geol. Geophysics **58** (5), 792–800.

Romanovskiy, N.N., 1993. Foundations of Lithosphere Cryogenesis. Moscow: Izd. Mosk. Gos. Univ., 336 p. (in Russian).

Rybalchenko, V.V., Trusov, A.I., Buddo, I.V., et al., 2020. A complex of auxiliary studies at the stages of exploration and development of oil and gas fields: from mapping permafrost to prospecting for groundwater to ensure drilling and operation. Gazovaya Promyshlennost, No. 11 (808), 20-28 (in Russian).

Sharlov, M.V., Agafonov, Yu.A., Stefanenko, S.M., 2010. The modern telemetric electric exploration stations "SGS-TEM" and "FastSnap". Efficiency and experience of use. Pribory i Sistemy Razvedochnoi Geofiziki (Saratov), No. 1 (31), 20–24 (in Russian).

Sharlov, M.V., Buddo, I.V., Misyurkeeva, N.V. et al., 2017. Transient electromagnetic surveys for high resolution near-surface exploration: basics and case studies. First Break **35** (9), 63–71.

Shatsky, S.B., 1978. Paleogene and Neogene of Siberia. Novosibirsk: Nauka, 168 p. (in Russian).

Shelokhov, I.A., Buddo, I.V., Smirnov, A.S. et al., 2018. Inversion of TEM responses to create a near surface velocity structure. First Break **36** (10), 47–51. doi: 10.3997/1365-2397.n0125.

Shpolyanskaya, N.A., 1981. Frozen zone of the Lithosphere of Western Siberia and Tendency of Its Development. Moscow: Izd. Mosk. Gos. Univ., 167 p. (in Russian).

Stogniy, V.V., 2003. Pulsed Inductive Electrical Exploration of Permafrost Taliks in Central Yakutia. Yakutsk, 124 p. (in Russian).

Tikhonov, A.N., Arsenin, V.Ya., 1986. Methods for Solving Ill-Posed Problems. Moscow: Nauka, 286 p. (in Russian).

Uchida, T., Dallimire, S., Mikati, J., 2000. Occurrences of natural gas hydrates beneath permafrost zone in Mackenzie delta: visual and X-ray imaginary. Ann. New York Acad. Sci. **912**, 1021–1033.

Vanyan, L.L., 1965. Fundamentals of Electromagnetic Sounding. Moscow: Nedra, 109 p. (in Russian).

Vorob'ev, A.E., Malyukov, V.P., 2009. Gas Hydrates. The impact of Technology on Unconventional Hydrocarbons. Moscow: Izd. RUDN, 289 p. (in Russian).

Yakushev, V.S., 2009. Natural Gas and Gas Hydrates in the Cryolithozone. Moscow: VNIIGAZ, 192 p. (in Russian).

Yakushev, V.S., Chuvilin, E.M., 2000. Natural gas and hydrate accumulation within permafrost in Russia. Cold Reg. Sci. Technol. **31**, 189–197.

Yakushev, V.S., Perlova, E.V., Makhonina, N.A. et al., 2003. Gas hydrates in sediments of continents and islands. Ross. Khimich. Zh. **XLVII** (3), 80–90 (in Russian).

Received September 16, 2019
Revised December 17, 2021
Accepted February 28, 2022

Translated by A.V. Muravyov

EARTH'S CRYOSPHERE
SCIENTIFIC JOURNAL

Earth's Cryosphere, 2022, vol. XXVI, No. 2, pp. 51–55

REVIEW

"KURUMS: A PHENOMENON OF THE CRYOSPHERE" (review of the monograph by V.R. Alekseev)

A.A. Galanin

Melnikov Permafrost Institute, Siberian Branch of the Russian Academy of Sciences, Merzlotnaya str. 36, Yakutsk, 677010 Russia; agalanin@gmail.com

An analytical review of the recently published monograph by Vladimir Romanovich Alekseev is presented. This monograph is devoted to kurums, a specific type of the covering coarse clastic formations that are widespread in the mountainous permafrost of northern Asia.

Keywords: *kurums, coarse clastic formations, mountainous permafrost, frost weathering, deserption, frost creep, heave, solifluction, rock glaciers, congelation ice, cryogenic processes, cryomorphogenesis*

A popular science monograph by V.R. Alekseev "Kurums: A Phenomenon of the Cryosphere" (Fig. 1) is devoted to kurums, which are one of the least studied phenomena in the cold regions of the world. This is a voluminous (348 pages) book with a long (more than 600 titles) list of references. The monograph is well illustrated with photographs, figures, and tables.

The extremely widespread occurrence of kurums in the mountains of the cold regions in the world, and, in particular, in Russia–from Karelia to Chukotka and from Taimyr to Altai Mountains–allows us to consider kurums as the key type of the covering deposits in the mountain permafrost. Kurums are very complex and dynamic systems. Some of their facies are affected by very rapid vertical and horizontal displacements, others are intensively watered. Therefore, disturbance of the natural regime of these formations by technical measures is often accompanied by unpredictable consequences (suffosion, creep, appearance of slope icings, etc.).

However, despite the extremely widespread occurrence of kurums, very few modern researchers specialize in this field. Much less monographic summaries with a holistic view on kurums have been published.

One of the reasons for the poor study is technical difficulties of mining in kurums composed of large blocks cemented by ice and soil. Hence, the drilling in

Fig. 1. Vladimir Romanovich Alekseev (*a*) and his monograph "Kurums: A Phenomenon of the Cryosphere" (*b*).

kurums is associated with large financial expenses and requires of powerful equipment. As a rule, such works cannot be afforded within the framework of small modern scientific projects.

In the 1970s and 1980s, large infrastructure facilities were extensively built in the Soviet Union. The study of kurums and evaluation of their impact on technical structures became the most urgent during the lying of the Baikal-Amur Mainline in permafrost areas of the Patom and Stanovoy highlands. Many experts in geocryology, geomorphology, and engineering geology from the leading scientific institutions (Moscow State University; Institute of Geography, Russian Academy of Sciences; Melnikov Permafrost Institute, Siberian Branch of the Russian Academy of Sciences; etc.) were involved in solving this project. Dozens of articles considering various issues of this versatile problem were published.

It turned out that the difficulty of the study of kurums is caused by not only technical but also methodological problems. Even estimation of the grain size composition of these formations appears to be a challenge because of a large size and weight of debris. Perhaps, that is why most of data on kurums obtained during that period fit into a few small monographs. The most important of them are the works [*Tyurin et al., 1982; Govorushko, 1986; Romanovsky et al., 1989*].

Unfortunately, even in our time, journal papers and annual collections of scientific conferences demonstrate that interest in the study of kurums and mountain permafrost as a whole has almost waned in the national science.

In this context, the monograph by V.R. Alekseev [*2021*] is very relevant, useful, and timely. According to the reviewer, it solves two important problems. Firstly, the monograph is a kind of summary–quintessence, generalizing a lot of scattered publications for the last 30 years, directly or indirectly relating to the key aspects of the kurum formation. At the same time, it states the fundamental issues associated with kurums and related phenomena in a popular form, making the results of their study accessible to a wide range of readers.

In the first chapter, the author acquaints a reader with the main features of the morphology of kurums, analyzes the origin of the term "kurum", and gives various definitions of this phenomenon proposed by different authors and different scientific schools. It turns out that, in spite of the physical apparentness of this phenomenon, there is no unambiguous definition of it.

Further, the author considers different types and feeding mechanisms of kurums, focusing on the fact that a necessary condition for their occurrence is the presence of cold climate and permafrost. Whereas, in warm regions, the coarse clastic slope formations are essentially different and are not kurums. Therefore, kurums are a distinctive feature of the permafrost and are formed as a result of the complex combination of frost weathering, freezing, solifluction, deserption, etc. Kurums arise and develop in close paragenesis with rock slides, avalanches, snowfields, and glaciers.

In the following paragraphs of the first chapter, V.R. Alekseev attempts to typify and classify kurums according to some features. For example, the author distinguishes valley, slope, and watershed kurums on the basis of the underlying relief, which seems appropriate. However, like all previous researchers, the author faces classification problems of kurums, both due to insufficient data on their internal structure and origin, and due to the continual nature of this formation and the lack of clear boundaries with other types of the coarse clastic formations of the mountain permafrost.

The author concludes that, at present, it is impossible to create the detailed genetic classification of kurums, which is probably conditioned by their polygenetic origin. Therefore, it seems very rational to use the algorithm proposed by the author for their typification according to 14 morphological features. This algorithm can be very useful in the field description of kurums and their large-scale mapping.

In the following paragraphs of Chapter 1, the author considers some natural and technogenic formations morphologically similar to kurums, such as stone glaciers, stone mounds (*obo*), and ancient megalithic structures within the cold regions. In terms of the cryogenic origin, discussion of the megaliths seems very timely and relevant. Some modern "alternative-scientists" continuously broadcast about numerous traces of ancient civilizations in Siberia and Arctic in their numerous monographs, TV programs, and Internet-resources. They describe the "strangely" stacked giant megaliths or oddly shaped rocks with obvious signs of the artificial origin.

All these statements are a direct result of the modernization of the Russian educational system according to the "western principle", which began more than 30 years ago and continues to this day. As a result, specialization of individual researchers has narrowed in so much that the obvious and well-studied 30 years ago natural phenomena are now considered as mysterious incomprehensible ones and even become cargo cults! Therefore, the paragraphs of the monograph by V.R. Alekseev devoted to the debunking of such cargo cults are extremely topical.

At the same time, indeed, many structures, created by man in the ancient times in the cold regions, are often composed of material from kurums and have their properties. Such formations are some stone mounds, slab graves in the highlands, and others. The author tries to deal with these phenomena in more detail in Chapter 2.

In the last paragraph of Chapter 1, the author analyzes the geographical distribution of kurums and their role among other rock formations, analyzes the

altitudinal zoning, latitudinal and longitudinal zoning, association with slope aspect, climate, etc., and gives the examples of different scale maps and diagrams.

The second chapter of the monograph is devoted to the discussion of the very border issues and completely unresolved questions of the origin of some natural phenomena, as well as the artificial objects related to crushing, freezing, and dynamics of the coarse clastic rock material in the cold regions.

The author discusses the formation of stone pillars of an aerodynamic shape, which are widespread in Eastern Siberia, in the Polar Urals, and in Subarctic. In spite of the obvious manifestation of the kurum-forming processes here, a mushroom-like shape of residual rock columns – tors of the Northern Verkhoyaniye cannot yet be explained solely in terms of the kurum-forming. Although, according to the reviewer, the distinct mushroom-like aerodynamic shape of many objects and the absence of weathering products at their base clearly indicate their aeolian origin as a result of wind corrasion and do not cause questions for geomorphologists familiar with the classical German [*Penck, 1961; Davis, 1962*] and Russian [*Chichagov, 2010; etc.*] works on arid geomorphology.

In other paragraphs of Chapter 2, the author considers such phenomena as spherical nodules on the islands of the Franz Josef Land, the Vottovaara quarry in Karelia, rocky steppe mounds, etc. In the next paragraph of Chapter 2, the author discusses the hypothesis of the specific water bearing capacity of kurums in the cold regions related to intensive condensation of the atmospheric moisture in their bodies.

The author finds parallels with some, now lost, ancient technologies of the water obtaining in arid regions directly from atmospheric vapor, discusses interesting details of various experiments, including scientific ones, which were set up by different researchers in different years in order to obtain water by condensation. Some of the experiments have been successful, others not so much. In general, in this section, full of detail and quite specific data, there are more questions than answers on physics of the condensation processes in kurums and similar artificial stone structures. The author's thoughts about a possible role of ancient megalithic structures with numerous water channels serving as water reservoirs also seem to be interesting.

In the last paragraph of Chapter 2, the author returns to natural kurums in terms of their recreational and aesthetic value as the objects for testing various types of cross-country vehicles, as well as physical training and endurance. Indeed, kurums are the natural heavy-going landscape for any type of modern machinery. On the other hand, this makes kurums a good testing site for new models. Every year, kurums attract more and more attention of extreme hiking and auto-tourism.

The third chapter of V.R. Alekseev's monograph is devoted to the discussion of cryogenesis in kurums, the role of snow cover and ground ice, which give kurums their phenomenal specificity. Many of the issues considered in this chapter are devoted to physics of the ice formation and heat exchange in kurums related to their specific radiation balance, to the processes of seasonal phase transitions of water, etc. The chapter contains rare photographs of congelation, basal, and other types of ice in kurums.

One of the paragraphs of this chapter is devoted to the analysis of the thermal regime. The conclusions are supported by the interesting schematic geological models, results of observations in geothermal wells, and temperature graphs indicating that the daily temperature variations in the summer period do not spread deeper than 2–3 m. However, in winter, the higher thermal conductivity of kurums leads to greater cooling of underlying rocks. In general, the author concludes that it is the frozen state that gives kurums their specific properties. Moreover, in regions with discontinuous permafrost, kurums contribute to its more active formation.

The next paragraph is devoted to the analysis of dynamics of kurums and to mechanisms of their movement. Like many of his predecessors, the author comes to the conclusion about the polygenetic character of the kurum movement results from heave, deserption, solifluction, suffusion, etc. The author comments on different ways, which were used by different authors in qualitative and quantitative estimations of the rates of kurum movement.

A logical continuation of the discussion is the consideration (in the next paragraph) of the interaction of kurums with different types of sediments and their transformation during the natural evolution. Here, the author operates with the data on the grain size composition and roundness of fragments under weathering. The author assures a reader that, during this evolution, well-rounded boulders and pebbles, morphologically very similar to the formations of a fluvial series, may arise in some facies of kurums.

In the next paragraph, the author analyzes the few data on the relative and absolute age of kurums, rightfully associating their extensive formation with the cold epochs of the Quaternary period and with the main stages of the formation of permafrost as a whole.

In the next very important section, the author characterizes a facies structure of kurums following the most developed and thorough scheme of A.I. Tyurin et al. [*1982*]. This scheme divides kurums into more than 30 facial varieties, being very logical within the framework of theoretical considerations. At the same time, this scheme is extremely difficult to use in practice, because the boundaries between most facies are conditional and unclear. Moreover, there are no strict boundaries in nature. The boundaries exist only

in the classifications invented by man. They do not reflect the depth of knowledge of a particular phenomenon; rather, they illustrate the deterministic way of thinking and the methodology of a researcher.

Probably, for this reason, this and other schemes of the facies analysis of kurums remained not too much in demand and stopped their development after 1980. They were no longer used in the monograph by N.N. Romanovsky et al. [*1989*]. Nevertheless, it is the scheme of the facial separation of kurums by A.I. Tyurin et al. [*1982*] that most thoroughly describes their morphogenetic diversity. This allows us to proceed to the ideas of the continual series of the coarse clastic formations in the cold regions, including stone glaciers, kurums, talus, deserption, and other groups of slope processes and sediments in the permafrost.

The last paragraph of the chapter is devoted to the analysis of the engineering hazard of kurums as the bases of engineering structures, as well as hazardous secondary processes, which are common within the kurum fields and the formations related to them. Here, the author considers to a greater extent the results of technogenic activity, which have led to the formation of technogenic stone glaciers and associated ice-rock slides. The Rasvumchor Plateau in Khibiny Mountains, technogenic glaciers of the Rudnaya Mountain on the Putorana Plateau are well known areas of such phenomena.

In the fourth chapter, the author discusses the unique and extremely diverse flora and fauna of kurums. The description of this world is accompanied by specific folkloric passages, the metaphorical language of which emphasizes and reinforces the phenomenal appearance of kurums and even consolidates the diverse material given in the previous chapters. It should be noted that most of the taxa given by the author characterize the entire ecosystem, in which kurums are perhaps not a major element. However, some rare species, which the author describes in more detail, are definitely associated with kurums. One of them is the black-capped marmot. The point is that, for many small animals, kurums provide an opportunity to locate their dwelling as deep as possible, several meters below the surface, where annual and mean winter temperatures are close to zero.

The description of the vegetation world of kurums should be noted separately. The author considers the colorful and the richest world of epilithic lichens. Indeed, while most other plants only try to survive in the harsh conditions of kurums, for lichens kurums are the main biotope and, in some areas, the only type of substrate suitable for habitation.

Another large section, which completes Chapter 4, is devoted to not the happiest pages of the history of the human interaction with kurums. Here, the author provides interesting historical information about the extremely harsh conditions of the development of some deposits in the high-altitude areas of the cold regions. The history of the development of the northeast of Russia during the years of the existence of the Central Administration of Prison Camps deserves special attention. This period involves the development of tin-uranium concentrate at the Budugychag deposit in Magadan oblast, the Vostochny uranium deposit in Chukotka, etc. It is interesting that most of the residential structures in the areas beyond the forest boundary were built from the coarse clastic material of kurums. Many structures have survived to the present day.

The fifth chapter is devoted to a discussion of technogenic kurums. The author refers them to refuse large-block dumps of mining deposits, which are frozen and saturated with ground ice. In general, of course, there are common features between the technogenic and natural kurums, especially in terms of the thermal physics, grain size composition, and climatic conditions in the course of their formation. However, the origin of these formations is principally different. Mining enterprises annually store millions of tons of coarse clastic rocks in the form of dumps. The author considers unique and single results of the observations over the temperature dynamics of some dumps, within which the specific thermal structures have been formed for several years, gives the results of assessment and forecast of the dynamics of some dumps in the near future.

In the following sections of Chapter 5, the author considers the advantage of coarse fractions of clastic material for construction purposes, gives the properties of rock fill for road construction in permafrost areas, and many other practically useful data, directly or indirectly derived from the "theory of kurum-forming". The kurum material can be used to protect certain structures from excessive thawing as a natural accumulator of cold and thermal regulator, as filtering material in the construction of hydraulic structures, and many others.

In the final, sixth chapter, the author decided to present the results of the analysis of the published literature in the field of the study of kurums and related phenomena. The results of this analysis are disappointing. The publication activity in Russia declined over the past 30 years. Over the past 10 years, only 27 works have been published including only 11 articles and 0 monographs. While from 1970 to 1980, 100 works were published, including 24 articles and 7 monographs.

In this chapter, the author also analyzes the most important publications from his point of view, peculiarities of the authors' methodology, and even provides some of their biographical data and photographs. In general, this section seems useful, especially for the most inquisitive young researchers, who need to know "by sight" their predecessors and, perhaps, their opponents or theoretical contradictors.

In conclusion of Chapter 6, V.R. Alekseev discusses the reasons to distinguish the separate relevant direction – kurum science. The reviewer fully agrees with the author, because, being engaged for many years in stone glaciers, simultaneously had to study a wide range of phenomena of cryogenic-gravitational series. The point of the latter is fully covered by the term kurums in the understanding of the author of the monograph. Moreover, following the continual concept subsequent to a number of domestic and foreign specialists, the reviewer believes that the objective cognition of kurums is impossible separately from the gravitational-slope and glacial processes of morpholithogenesis and cryolithogenesis.

In conclusion of the monograph, the author again returns to the definition of kurums, but with the consideration of the performed data analysis. Analyzing the morphogenetic diversity of kurums and their facies, the author convinces of the necessity to combine them under the general term "kurumium". It seems original and logical in the descending lithodynamic series (eluvium, colluvium, deluvium, proluvium, alluvium, limnium, etc.). However, in the opinion of the reviewer, this requires special discussion. In addition, the reviewer completely agrees with the author that improvement (completion) of the kurum classification is long overdue, because the classifications, which have been published earlier, as time shows, appear not quite functional and remain almost unused in the modern literature.

Thus, the content of the monograph and the style of presentation used by V.R. Alekseev allow us to consider this work as the well-illustrated popular summary, which gives a broad idea of the modern study of kurums and paragenetic phenomena. The language of the presentation is amazingly balanced and easy to understand without losing the essence. The author often touches on very deep and almost philosophical issues of synergy and self-organization of matter in the cold regions. He does it in the implicit form, without formulas and strict definitions, but through thinking, posing questions, lyrical digressions and even metaphors, thus encouraging a reader to find his own solution.

It is difficult for the reviewer to formulate any serious comments on this monograph, even though he cannot fully agree with some of the author's conclusions. However, the monograph is of the highest rating for the popular science genre. It involves almost the entire volume of key fundamental knowledge about kurums and related phenomena at the current time, except for some narrow issues. In addition, the monograph contains a very extensive list of citations, including the most modern ones. The list of references is the comprehensive compilation of domestic and foreign literature on kurums and related phenomena.

It is necessary to note once again the brightness of the language used by the author, which makes this book a unique and colorful edition. Undoubtedly, this monograph will be useful to a wide range of readers from schoolchildren to professionals in the field of the Quaternary geology, permafrost science, geomorphology, and geography. The monograph can be recommended as additional educational literature for students of natural sciences of higher and special educational institutions. It will be extremely useful for biologists, soil scientists, and archaeologists working in cold regions and permafrost environments. Some sections will undoubtedly be of interest to many travelers, romantics and other adventurers.

References

Alekseev, V.R., 2021. Kurums: A Phenomenon of the Cryosphere. Novosibirsk: Academic Publishing House "Geo", 348 p. (in Russian).

Chichagov, V.P., 2010. Arid Geomorphology. Platform Anthropogenic Plains. Moscow: Novy Mir, 520 p. (in Russian).

Davis, W.M., 1962. Geomorphological Essays. Translated from: Davis W.M., 1951. Geographical Essays. Part II. Physiographic Essays (New York, 1951). S.Yu. Geller, Yu.A. Meshcheryakov, and O.K. Parchevsky (Eds.). Moscow: Izd. Inostrannoi Literatury, 455 p. (in Russian).

Govorushko, S.M., 1986. Kurum Morpholithogenesis. Vladivostok: Inst. Geogr. Dal'nevost. Nauch. Ts. Ross. Akad. Nauk, 120 p. (in Russian)

Penck, W., 1961. Morphological analysis. Translated from German: Penck, W., 1924. Die Morphologische Analyse. Ein Kapitel Der Physikalischen Geologie (Stuttgart: Verlag von J. Engelhorns Nachf). M.V. Piotrovsky (Ed.). Moscow: Geografgiz, 369 p. (in Russian).

Romanovsky, N.N., Tyurin, A.I., Sergeev, D.O. et al., 1989. Kurums of the Bald Zone of Mountains. Novosibirsk: Nauka, 152 p. (in Russian).

Tyurin, A.I., Romanovsky, N.N., Poltev, N.F., 1982. Permafrost-Facies Analysis of Kurums. Moscow: Nauka, 150 p. (in Russian).

Received December 16, 2021
Revised January 5, 2022
Accepted January 7, 2022

Translated by V.A. Krutikova